Universidade de Lisboa

Faculdade de Farmácia

Development of polymeric platforms loaded with minocycline targeting bone regeneration and tissue healing

Victor Zacharias Martin

Dissertation supervised by Professor Ana Francisca De Campos Simão Bettencourt and co-supervised by Professor Isabel Alexandra Caldeira Ribeiro.

Biopharmaceutical Sciences

2018

Universidade de Lisboa

Faculdade de Farmácia

Development of polymeric platforms loaded with minocycline targeting bone regeneration and tissue healing

Victor Zacharias Martin

Dissertation supervised by Professor Ana Francisca De Campos Simão Bettencourt and co-supervised by Professor Isabel Alexandra Caldeira Ribeiro.

Biopharmaceutical Sciences

2018

Abstract

Bone is a mineralized conjunctive tissue with an unique trauma healing capability, however satisfactory regeneration becomes more difficult with wider bone defects. In addition, pandemic aging and obesity are increasing the request of surgical procedures, which demand grafts. Moreover, infections and inflammation-based diseases as periodontitis can cause bone matrix destruction, leading to tooth loss and ultimately to the need of bone grafts for further rehabilitation. Minocycline, a tetracycline derivative antibiotic, presents non-antimicrobial effects including interactions with matrix metalloproteinase enzymes, growth factors and cytokines, resulting in anti-inflammatory activities, collagen type 1 synthesis and upregulation of Wnt signaling, preventing bone loss and increasing bone formation.

In this context, we conjectured that minocycline could be applied in three different polymeric drug-delivery platforms aiming osteoinduction, anti-inflammatory and antimicrobial activity, targeting periodontal disease with chitosan nanoparticles and bone regeneration using two different polylactide (PLA) scaffolds. Nanoparticles were produced by an ionic gelation technique and presented a rounded morphology, nanometric size and positive zeta potential. In addition, nanoparticles provided a controlled release and significant improved results regarding metabolic activity of human gingival fibroblasts. Furthermore, nanoparticles were identified within membrane-bounded vesicles inside the cytosol and presented a significant downregulation of IL-1β, TNF-α, CXCL-8 and NFKB1 inflammatory genes expression. Polylactide scaffolds loaded with minocycline were produced using two techniques, solvent casting/particulate leaching containing bioglass and 3D printing containing hydroxyapatite nanoparticles. Scaffolds were treated by alkali hydrolysis and coated with collagen. Results from both scaffolds showed controlled antibiotic release, antimicrobial activity and biofilm formation inhibition against *Staphylococcus aureus*. Also, presented improved cellular metabolic activity and differentiation parameters using human mesenchymal stem cells. In this work, novel chitosan nanoparticles and PLA scaffolds loaded with minocycline were successfully produced and characterized. Further *in vivo* studies need to be assessed to corroborate the biological benefits of these materials.

Key words: Chitosan-nanoparticles, polylactide-scaffolds, 3D-printing, tissue engineering, bone infection.

Resumo

O tecido ósseo é um tecido conjuntivo mineralizado com uma capacidade singular de reparação, porém, uma regeneração satisfatória torna-se mais difícil em defeitos ósseos consideráveis, justificando-se nestas situações o uso de enxertos para garantir uma regeneração apropriada. Além disso, o envelhecimento pandêmico e as altas taxas de obesidade da população vêm aumentando a necessidade de procedimentos cirúrgicos em que os enxertos são necessários. Ainda, intervenções orais e maxilofaciais como a colocação de implantes, necessitam frequentemente de enxertia para alcançar uma reabilitação protética adequada, com resultados biomecânicos e estéticos apropriados. Além do que infeções e doenças inflamatórias como periodontite podem causar a destruição da matriz óssea, conduzindo a perda dentária, a qual muitas vezes necessita de enxertos prévios à reabilitação do espaço protético.

O enxerto autógeno é considerado atualmente como o enxerto padrão, uma vez que possui fatores de crescimento que promovem a osteoindução, células e uma estrutura que permite a proliferação celular e a angiogénese. Porém, este tipo de enxertos apresenta uma remodelação rápida, requer uma área dadora e está associado a morbidade e riscos para os pacientes. Como alternativa, investigadores têm vindo a desenvolver enxertos sintéticos tais como estruturas tridimensionais que tentam mimetizar a composição e a estrutura natural do osso em biomateriais cerâmicos ou poliméricos. Estes ainda podem conter fatores de crescimento ou mesmo fármacos que visam alcançar elevadas concentrações locais com menores efeitos colaterais, conseguindo-se uma melhor e mais rápida substituição do biomaterial por uma nova matriz óssea. Estes novos materiais permitem ainda reduzir o tempo cirúrgico e a morbidade do paciente, uma vez que não são necessárias áreas dadoras.

No âmbito da regeneração tecidual guiada, a impressão 3D tem vindo a ser explorada, pois pode controlar com precisão as características morfológicas dos materiais e ainda produzir peças baseadas em exames de imagiologia médica. Paralelamente, sistemas nanoparticulados têm mostrado um grande potencial na veiculação localizada de fármacos, sendo usados no tratamento de cancro, infeções e regeneração tecidual, trazendo vantagens como libertação controlada de fármacos e a possibilidade de serem embebidos em polímeros e géis. O diminuto tamanho dos sistemas de partículas permite a sua penetração na matriz óssea e a internalização pelas células. Outro aspeto interessante é que alguns antibióticos apresentam efeitos no metabolismo ósseo para além da sua atividade antibacteriana. Por exemplo, a minociclina, antibiótico do grupo das tetraciclinas, apresenta vários efeitos não antimicrobianos, entre os quais, inibição de enzimas metaloproteinases, interações com citocinas e fatores de crescimento, reduzindo a inflamação, prevenindo a perda óssea e aumentando a formação de matriz óssea. Além disso, infeções relacionadas com dispositivos

ortopédicos aumentam a incidência de osteomielite, a qual pode levar a perda do enxerto e a necrose tecidual.

Neste contexto, foram projetadas três plataformas poliméricas distintas destinadas à veiculação localizada de minociclina visando a osteoindução, a atividade anti-inflamatória e antimicrobiana. Assim, as plataformas destinadas ao tratamento periodontal ou à regeneração óssea incluíram a formulação de nanopartículas de quitosano e de dois *scaffolds* à base de ácido poliláctico (PLA).

As nanopartículas de quitosano foram idealizadas para utilização *in situ* em bolsas periodontais como auxiliar terapêutico, combinando a atividade do quitosano com a da minociclina, visando a prevenção da destruição dos tecidos de suporte dentários. As nanopartículas foram produzidas por uma técnica de gelificação iónica, utilizando-se um tensioativo para melhorar a eficiência de encapsulação do fármaco. Foram realizadas várias experiências para seleccionar a formulação mais adequada à prossecução dos estudos.

Os melhores resultados foram alcançados com a formulação que apresentava uma proporção de quitosano e tripolifosfato de 3:1 e pH igual a 5,5, obtendo-se uma distribuição de tamanho nanométrico (372 ± 55 nm) e uma carga superficial positiva (potencial zeta igual a + 23 ± 1 mV). A libertação total do fármaco foi alcançada ao fim de 24 horas, atingindo-se concentrações iguais a 1 µg/mL nos primeiros 30 minutos e 4 µg/mL após 24 horas, ambos valores superiores à concentração mínima inibitória da maioria dos patógenos periodontais.

Os ensaios celulares foram realizados utilizando fibroblastos gengivais humanos (HGFs) e foi possível observar que as nanopartículas apresentaram um aumento significativo da atividade metabólica em comparação com uma solução de minociclina de concentração idêntica. Não foram detetadas alterações na morfologia celular, área de contato e organização do citoesqueleto de actina. Ainda, foi possível observar nanopartículas internalizadas em vesículas no citosol celular por imunofluorescência usando nanopartículas fluorescentes e por imagens de microscopia eletrónica de transmissão (TEM). Este fenómeno pode resultar num aumento da concentração do fármaco intracelular, sendo importante, uma vez que os principais patógenos podem invadir células hospedeiras ficando protegidos de alguns antibióticos e das células do sistema imunitário.

Relativamente às propriedades anti-inflamatórias das nanopartículas estas foram avaliadas através de PCR quantitativo, usando HGFs tratados com lipopolissacarídeos. Os resultados permitiram concluir que as nanopartículas com minociclina reduziram significativamente a expressão gênica dos genes IL-1β, TNF-α, CXCL-8 e NFKB1 em comparação com uma solução de minociclina e com nanopartículas sem fármaco, sugerindo que a encapsulação do antibiótico nas nanoparticulas de quitosano amplifica o efeito anti-inflamatório do fármaco.

Paralelamente desenvolveram-se *scaffolds* poliméricos com derivados de PLA para veiculação localizada de minociclina, visando a regeneração de defeitos ósseos.

Primeiramente produziram-se *scaffolds* através da técnica de moldagem por solvente e lixiviação de partículas. O esteroisómero poli (D,L ácido láctico) (PDLLA) foi escolhido pela melhor osteoindução e degradação mais rápida em comparação com os outros isómeros. Os *scaffolds* foram preparados misturando vidro bioativo e cloreto de sódio no polímero dissolvido. Após a remoção do sal, as amostras foram tratadas por hidrólise alcalina e funcionalizadas pela adsorção de minociclina e colagénio. Imagens obtidas através de microscopia eletrónica de varrimento (SEM) permitiram a observação de poros de tamanhos variados e interconexões entre estes. As partículas do vidro bioativo foram identificadas por espectroscopia de raios X por dispersão em energia (EDS). As interações químicas entre o antibiótico e o polímero foram evidenciadas através de espetroscopia de infra-vermelho com transformada de Fourier (FTIR-ATR) e de dispersão de raios X (XRD), o que pode explicar a não libertação do antibiótico em pH igual a 7,4. Por outro lado, a pH igual a 5, observou-se uma libertação controlada até às 72 horas.

A atividade antimicrobiana dos *scaffolds* foi avaliada com uma estirpe de *Staphylococcus aureus* através do ensaio de difusão em agar, tendo-se observado um halo de inibição de diâmetro igual a 28 ± 2 mm. Os sobrenadantes obtidos por incubação dos *scaffolds* contendo minociclina também apresentaram atividade antimicrobiana, obtendo-se uma concentração inibitória mínima (MIC) igual a 0,0625 µg/mL. Foi ainda observada uma inibição na produção de biofilme nas amostras com antibiótico através de imagens de SEM. O efeito dos *scaffolds* na atividade metabólica celular foi avaliado usando osteoblastos humanos e os resultados revelaram que o tamanho da amostra influenciou a resposta celular, evidenciando a toxicidade associada á concentração do antibiótico no meio de cultura. Com pequenos pedaços, foram obtidos resultados positivos de viabilidade celular, enquanto que, com amostras maiores, houve uma importante redução na viabilidade dos osteoblastos.

Outro tipo de *scaffold* foi produzido através de técnica de modelagem por deposição fundida e impressão tridimensional. Subsequentemente a superfície foi modificada por hidrólise alcalina. Nanopartículas de hidroxiapatite (HA), colagénio e minociclina foram adicionados por adsorção visando a biofuncionalização destes *scaffolds*. A análise da superfície por SEM mostrou um aumento na rugosidade superficial, uma camada de colagénio envolvendo o material e partículas de HA. A hidrólise alcalina modificou o grau de cristalização do polímero, demonstrado por XRD. Observou-se também um aumento na molhabilidade da superfície, avaliada através da determinação dos ângulos de contato em água. Os estudos de libertação do fármaco evidenciaram uma completa eluição do antibiótico até 24 horas em pH igual a 5 e a 7,4, sendo a velocidade superior a pH ácido. Os *scaffolds* revelaram atividade antimicrobiana contra *S. aureus*, originando um halo de inibição igual a 31 ± 0,4 mm de diâmetro e apresentaram uma MIC de 0,0625 µg/mL relativamente ao sobrenadante obtido por incubação dos *scaffolds*. A inibição da formação de biofilme foi também observada por

SEM, tendo os *scaffolds* com minociclina revelado uma redução considerável. Para os ensaios de citocompatibilidade foram testadas células mesequimais humanas (hMSCs) e os resultados da redução da resazurina mostraram que os scaffolds com HA e minociclina apresentaram um aumento da viabilidade celular em comparação á amostras controle. A análise microscópicas revelaram que as células proliferaram ativamente sobre os *scaffolds*, com uma morfologia alongada e plana e uma distribuição dispersa.

Globalmente os resultados obtidos permitem concluir que é possível desenvolver diferentes estratégias para veiculação localizada de minociclina. Conclui-se que as nanopartículas de quitosano apresentam potencial como alternativa viável na aplicação terapêutica subgengival de minociclina e que os seus efeitos anti-inflamatórios e proliferativos podem complementar o tratamento de periodontite e reduzir a destruição tecidual.

Por último, observou-se que a adição de minociclina e bio-cerâmicas aos *scaffolds* poliméricos pode ser alcançada com métodos simples de produção e que apresentaram resultados favoráveis em relação à resposta celular e à inflamação, mantendo a atividade antimicrobiana. Novos estudos precisam ser realizados para um melhor entendimento da interação destes materiais num ambiente biológico, para assegurar sua segurança numa futura aplicação biomédica.

Palavras-chave: Quitosano-nanopartículas, ácido poliláctico-*scaffolds*, impressão-3D, engenharia tecidual, infeção óssea.

Acknowledgements

I would like to express my sincere and profound appreciation to my supervisors Professor Ana Bettencourt and Professor Isabel Ribeiro from Faculdade de Farmácia da Universidade de Lisboa, for accepting me, a stranger from dentistry, in the best possible way and the trust that they have put in me, making decisions about the project together, the concern about my wills and even the possibility to represent them and the group at Bilbao and Sevilla. Thank you for all the support, advises, teaching, availability and help along this year, which without them none of this would be possible.

Also a special acknowledgement to my non-official mentors Professor Lídia Gonçalves, Professor Catarina Santos, Professor Ester Zuza and Professor Pedro Gomes who taught me and guided in the best possible way through topics that were completely away from my knowledge, and who's also availability, patience and helpfulness contributed to several parts and the success of this thesis.

To Professor Cecília Rodrigues for accepting me as a late student.

To Doctor Nuno Monge for the scaffold drawings.

To Marta Alves from Corrosion Science and Surface Engineering (CSSE), Instituto Superior Técnico for the contact angle readings.

To company Microsense - metrologia industrial for the X-Ray microtomography of the scaffolds.

To Naroa Sadaba for the silicon molds and friendship.

To all the colleagues from Lab 112 and friends from the master classes for the integration and the countless good times.

To the institutions, Faculdade de Farmácia da Universidade de Lisboa, Faculdade de Medicina Dentária da Universidade do Porto, Instituto Superior Técnico de Lisboa and Faculty of Engineering in Bilbao, University of the Basque Country.

To the new friends and the very old ones.

To my mother, father, grandmother and sister for the unconditional love, supporting this crazy adventure overseas and for always being present.

To my beloved Fernanda Margarida, the best company anytime, anywhere. For all the support, advices and companionship during this adventure.

To my family from São Paulo, Conchas, Pres. Prudente, Sevilla and Abrantes.

Financial support:

Portuguese government, Fundação para a Ciência e Tecnologia (FCT), (Pest-UID/DTP/04138/2014).

European Commission (Cost Action TD1305, IPROMEDAI): COST-STSM-TD1305-38384.

Index

Index of Figures

Index of Tables

List of Abbreviations

3D - Three-Dimensional
ACN - Acetonitrile
ACS - Absorbable Collagen Sponge
ALB - Albumin
ALN - Alendronate
ALP - Alkaline Phosphatase
ATB - Antibiotic
ATCC - American Type Culture Collection
ATR - Attenuated total Reflectance
BCIP - 5-Bromo-4-Chloro-3-Indoyl Phosphate
Bcl-2 - B-Cell Lymphoma 2
BCP - Biphasic Calcium Phosphate
BCPC - Biphasic Calcium Phosphate Composite
BG - Bioglass
BHI - Brain and Heart Infusion Broth
BMA - Bone Marrow Aspirate
BMP - Bone Morphogenetic Protein
BMPr - Bone Morphogenetic Protein Receptor
Cat-k - Cathepsin K
CFU - Colony Forming Unit
Chi - Chitosan
CLSI - Clinical and Laboratory Standards Institute
CLT - Clarithromycin
Col - Collagen
COOH - Carboxylic Acid
CXCL-8 - Interleukin 8
DCM - Dichloromethane
DL% - Drug Loading
DLX-5 - Distal-Less Homeobox 5
DMSO - Dimethyl Sulfoxide
DSPC - 1,2-Distearoyl-sn-Glycero-3-Phosphocholine
E2 - 17β-Estradiol
EDS - Energy Dispersive Spectrometer
ER - Estrogen Receptor
F-actin - Filamentous Actin
FBS - Fetal Bovine Serum
FDA - Food and Drug Administration
FTIR - Fourier-Transform Infrared Spectroscopy
HA - Hydroxyapatite
HAc - Hyaluronic Acid
HGFs - Human Gingival Fibroblasts
HPMC - Hydroxypropyl Methylcellulose
HTCC - N-(2-hydroxyl)Propyl-3-Trimethyl Ammonium Chitosan Chloride
IC50 - Half-Maximal Inhibitory Concentration
IL-1 – Interleukin 1
IL-6 - Interleukin 6
LPS - Lipopolysaccharide
MAPK - Mitogen-Activated Protein Kinase
MH - Minocycline Hydrochloride
MIC - Minimal Inhibitory Concentration
Micro-CT - Microtomography
MKK/ERK - Mitogen Activated Protein Kinase
MMP – Matrix Metalloproteinase

MSCs – Mesenchymal Stem Cell
MTT - 3-(4,5-Dimethyl-2-Thiazolyl)-2,5-Diphenyl-2H-Tetrazolium Bromide
NFkB - Nuclear Factor kappa-B
NPs - Nanoparticles
OCN - Osteocalcin
OPG – Osteoprotegerin
OPN – Osteopontin
OSX - Osterix
PA - Polyanhydride
PAA – Poly-Acrylic Acid
PARP-1 - Poly [ADP-ribose] Polymerase 1
PBS – Phosphate Buffered Saline
PD - Periodontal Disease
PDGF Platelet-Derived Growth Factor
PDI - Polydispersity Index
PDLA - Poly(D-lactic Acid**)**
PDLLA - Poly(D,L-lactic Acid)
PEG - Polyethylene Glycol
Pi - Phosphorylation
PLA - Polylactide
PLC - Poly-Caprolactone
PLGA - Poly(Lactic-co-glycolic Acid)
PlGF - Placental Growth Factor
PLLA - Poly(L-lactic Acid)
PPF poly(Propylene Fumarate)
PRP - Platelet Rich Plasma
PTH - Parathyroid Hormone
RAL - Raloxifene
RANKL - Receptor Activator of Nuclear Factor κB Ligand
ROS - Reactive Oxygen Species
Runx2 - Runt-related Transcription Factor 2
SD - Standard Deviation
SDS - Sodium Dodecyl Sulfate
SEM - Scanning Electron Microscopy
SEMA 4D - Semaphorin-4D
SERM - Selective Estrogen Receptor Modulator
Smad - Similar Mothers Against Decapentaplegic
SV - Simvastatin
Tab/tak - Transforming Growth Factor Beta Activated Kinase
TCP - Tricalcium Phosphate
TCs - Tetracyclines
TEM - Transmission Electron Microscope
TGF-β - Transforming Growth Factor Beta
TNF-α - Tumor Necrosis Factor Alpha
TPP - Tripolyphosphate Pentasodium
TSA - Trypto-Casein Soy Agar
VEGF - Vascular Endothelial Growth Factor
XRD - X-ray Diffraction
Z-Ave – Average Size
ZP – Zeta Potential
α-MEM - α-Minimal Essential Medium

Chapter 1. General introduction

1.1. Bone cells, physiology, turn over and defects

Bone is a mineralized conjunctive tissue, with an unique trauma healing capability [1]. Osteoblasts, osteocytes and osteoclasts are the specialized bone cells (Fig. 1.1). When a bone defect occurs due to injury, cells are supplied from the periosteum and the regeneration occurs [1,2]. However, satisfactory regeneration becomes more difficult the wider the bone defect. That is why even with this property of healing in many situations bone graft is necessary [3]. Orthopedic procedures, like pseudo-arthrosis chirurgical treatment, hip or knee arthroplasty, arthrodesis and tumor removal commonly require bone graft [4]. Furthermore, oral and maxillofacial procedures often demand replacing the missing bone (Fig. 1.2). An example is to allow the correct implant insertion based on the prosthesis ideal position when the residual bone is not enough, aiming the optimization of functional/biomechanics results and the improve gingival and facial aesthetic [3].

Moreover, infections and inflammation-based diseases as periodontitis can cause bone matrix destruction by the activation of matrix metalloproteinases [5], leading to tooth loss and ultimately might lead to the need of bone grafts for the further rehabilitation [6].

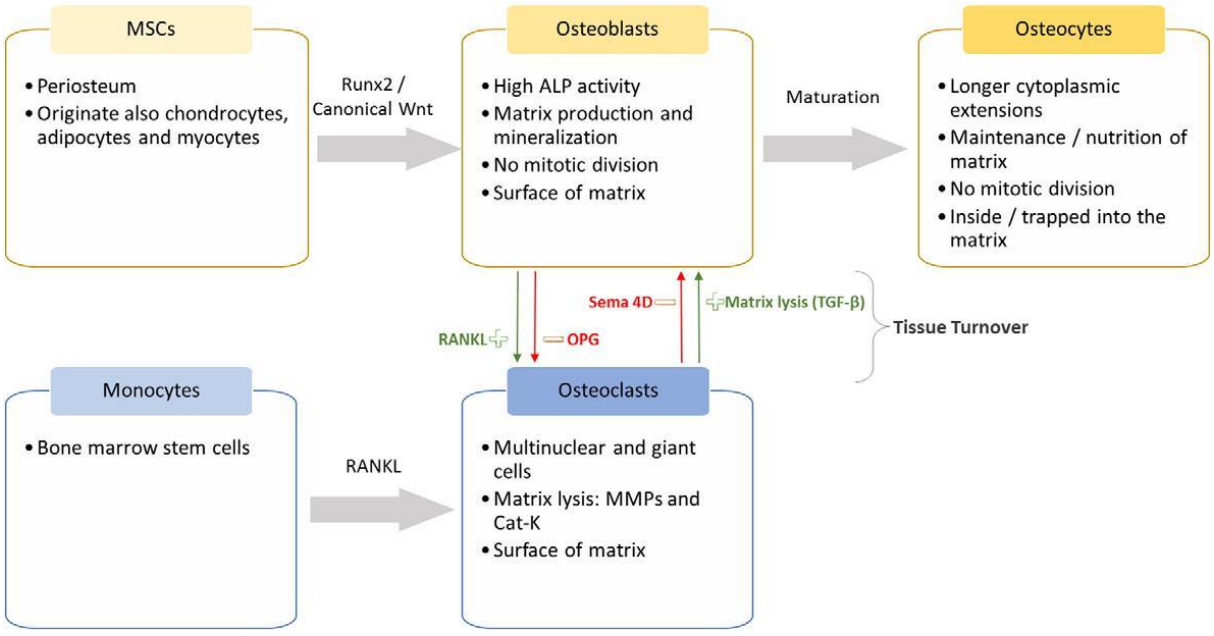

Figure 1.1. The specialized bone tissue cells: origin and characteristics (adapted from [94]). Abbreviations: alkaline phosphatase – ALP, cathepsin K – Cat-k, matrix metalloproteinase – MMP, mesenchymal stem cell – MSCs, osteoprotegerin – OPG, receptor activator of nuclear factor κB ligand – RANKL, Runt-related transcription factor 2 - RUNX2, semaphorin-4D – SEMA 4D and transforming growth factor beta - TGF-β.

Moreover, bone grafts substitute sales are expected to rise, reaching almost three billion dollars per year across the 10 major markets, with a compound annual growth rate of 3.8%

and the key drivers for this accentuate growth are pandemic aging and obesity, increasing the demand of chirurgical procedures as spinal fusion, trauma fixation and craniomaxillofacial needs [7].

To date, the main approach for replacing missing bone is by using grafts. Bone grafts can be autogenous, homogenous, heterogeneous or synthetic. Autogenous means that the bone is removed from the patient's own body, often from the iliac crest, skullcap, mandible or tibia [3]. To the present it is considered the gold standard (Fig. 1.3) once it contains growth factors for osteoinduction (i.e. to promote the differentiation of cells into active osteoblasts), cells for the osteogenesis and the framework for osteoconduction (meaning bone growth on the surface) [8]. However, it presents fast remodelation and limited source, once a donator area is required. In addition, autogenous grafts are often associated with high surgical risks and morbidity [3].

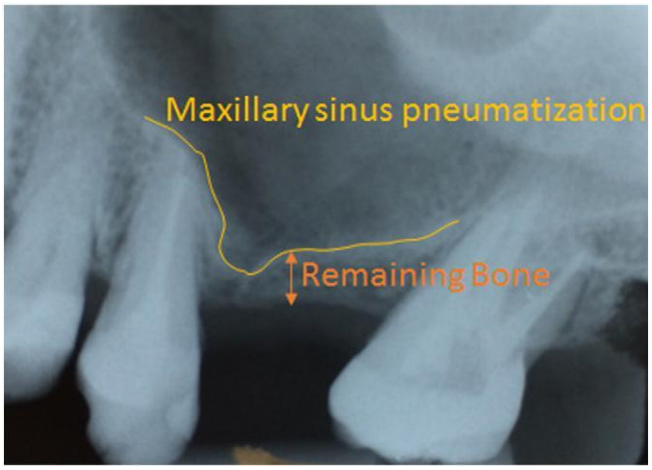

Figure 1.2. Example of bone draft demand in oral surgery. Maxillary sinus pneumatization caused by loss of tooth, where the installation of dental implant is not possible by the lack of bone height. Radiograph assigned by Victor Z Martin DDs. (Adapted from [13]).

The second most common type of bone grafts is homogenous or allograft, which is a graft removed from human cadavers and available in bone banks [8]. Heterogeneous or xenograft is a graft obtained from species other than human, as bovine bone [3]. This type of bone graft often requires sterilization and deactivation of proteins, remaining only the mineral matrix. Homogenous or heterogeneous grafts are only osteoconductive, meaning that these grafts are often combined with patient's own stem cells (also named mesenchymal stem cells) or growth factors [9]. Therefore, osteogenic as bone marrow aspirate (BMA) [10] or osteoinductive compounds as bone morphogenetic proteins (BMPs) or platelet rich plasma (PRP) [11,12] must be also used in the procedures (Fig. 1.3).

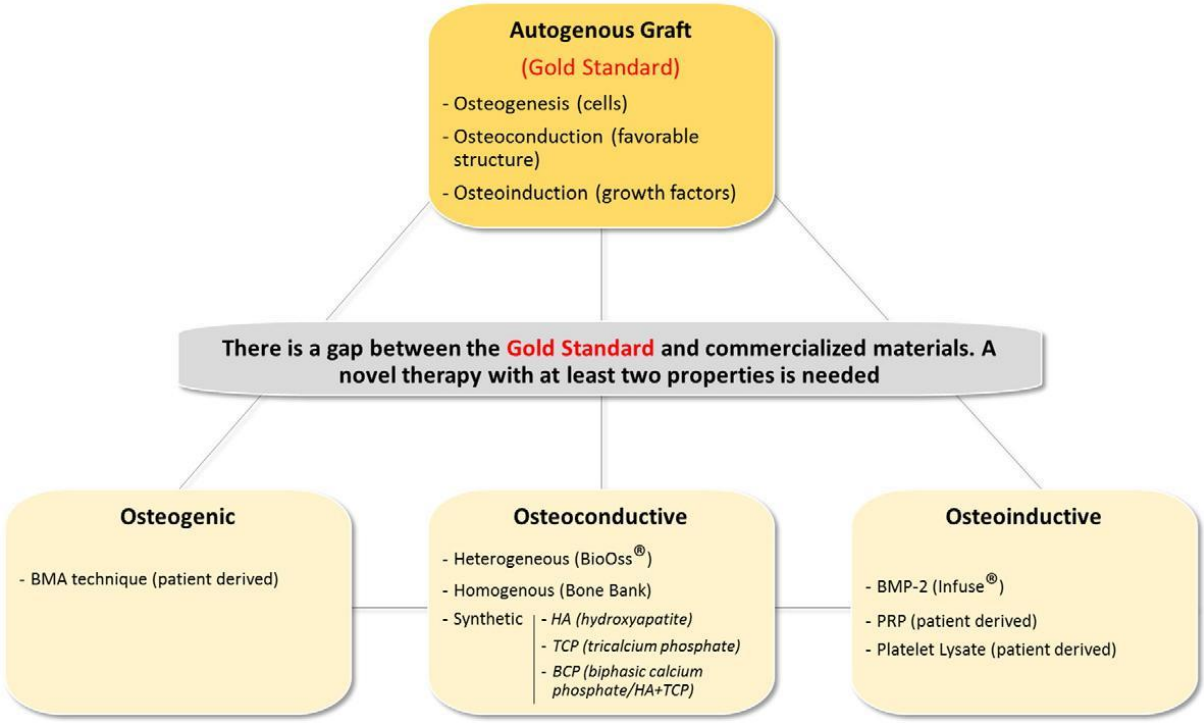

Figure 1.3. The most used current therapies for bone repair and regeneration. The big gap between the gold standard and the current graft alternatives, presenting only one of three capabilities of the autogenous type. Osteoinduction is the stimulation of osteoprogenitor cells to differentiate into osteoblasts; Osteoconduction is the ability of the material to act as a scaffold for the cells and blood capillary; Osteogenesis represents vital osteoblasts that contribute to the growth of new bone along with bone formation. Abbreviations: Bone morphogenetic protein 2 – BMP-2, bone marrow aspirate – BMA and platelet rich plasma – PRP. (Adapted from [13]).

Alternatively, research has been focused on finding, safer, less expensive and easier to use synthetic bone grafts. These bone substitutes can be produced from biomaterials as hydroxyapatite (HA), tricalcium phosphate (TCP), bioactive glass and polymers [8]. To date, those types of grafts can provide only osteoconduction, limiting its usage in bone reconstruction [3].

To improve biomaterials clinical outcome as bone grafts, researchers are trying to combine different compounds as hormones, growth factors and drugs with the materials. Synthetic scaffolds made with polymers or ceramics based composites are being developed to deliver different bioactive compounds in the target area, aiming to achieve a high local concentration with minimum side effects (Fig. 1.4), maintaining the space, so that defects can be adequately replaced by newly formed bone. These grafts provide osteoinduction in an osteoconductive material and can facilitate the chirurgical procedure, reduce the time of the surgery, as well as the morbidity and provide an unlimited source [4].

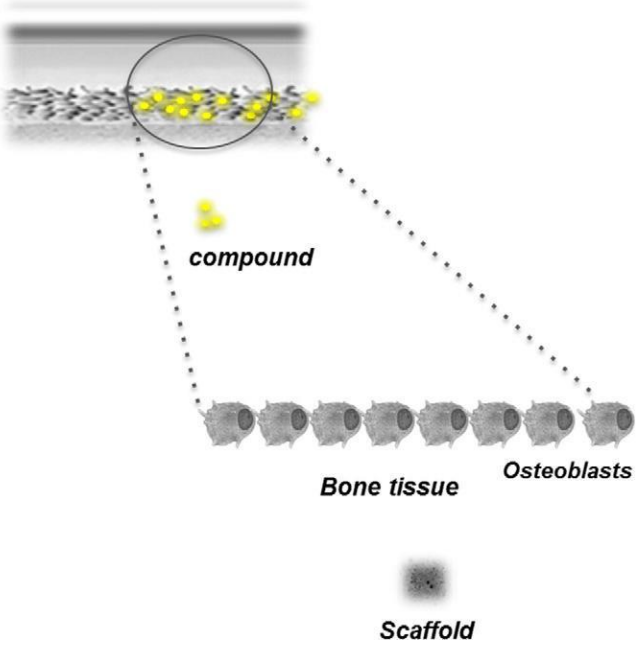

Figure 1.4. Biomaterials as local drug delivery systems. The released compounds from scaffolds are in close contact with the osteoblasts. (Adapted from Martin et al., 2017 [13]).

1.2. Research on synthetic grafts and nanotechnology for bone regeneration

Current studies are exploring different types of biomaterials (metallic, polymeric, ceramic or composites) loaded with biological compounds (growth factors, platelet lysates, hormones, phytohormones) or different types of drugs (i.e. antibiotics, alendronate, simvastatin, raloxifene) aiming the *in situ* delivery of osteoinductive compounds to improve bone regeneration.

Different types of drug delivery platforms are being under evaluation including grafts as well as nanoparticulate forms. Among grafts, scaffolds are three-dimensional structures principally made from polymers or ceramics, mimicking the composition and structure of natural bone [14].

Several techniques are used to create porous scaffolds, such as phase separation method and solvent-casting/salt-leaching method, one of the most used techniques to produce scaffolds [15]. This method allows the production of biodegradable sponge structures with more than 93% porosity and pore size until 1000 µm [15]. The advantages are the possibility to create complex geometries such as cylinder structures and the easiness to control porosity and geometry of the scaffolds. However, the disadvantages are the loss of water-soluble biomolecules or cytokines during porogen leaching and the possibility of remaining the porogen as salt that can harmfully affect the cells. [15].

One of the current growth leader technique involving tissue regeneration created to overcome these limitations is 3D printed scaffolds - a process than can precisely control architecture,

shape, porosity, pore size and interconnectivity and can be utilized to formulate implantable materials based on medical imaging and computer-aid design [16]. Besides, it is known as an easy, quick, and reproducible technique [16,17].

In parallel another strategy that shows great potential in local drug delivery for bone regeneration is the use of biodegradable nano/microparticles (NPs). These systems have been developed rapidly over the past few years and gained significant importance in the medical field due to the new possibilities regarding the treatment of several pathological conditions, including cancer, infections, respiratory diseases and tissue regeneration [6,18]. As advantages, NPs can offer sustained release of drugs, be absorbed into polymer gels, adhere to diseased tissues and maintain local drug concentration for a long time [18]. Due to the small particle size, NPs are able to penetrate into bone matrix and be internalized by cells [19].

Examples of different bioactive compounds and drugs under investigation in the field of bone regeneration will be next detailed.

1.2.1. Growth factors

BMP is a generic name given for specific proteins extracted from bone matrix [3]. These proteins are members of the transforming growth factor-beta (TGF-β) superfamily and the most studied are BMP-2, BMP-3, BMP-4 and BMP-7 [20]. As function mechanism, BMP-2 binds to BMP receptor (BMPr) and participates in the regulation of Runx2 gene expression resulting in osteoblastogenesis activity [21]. Other independent pathways are also reported, involving P38/MAPK pathway and miRNAs, as the enhancement of alkaline phosphatase (ALP) activity [22], as illustrated in Fig. 1.5. However, BMP-2 usage is associated with severe edemas, undesired ectopic bone formation, delayed bone formation and possibly increased cancer risk [23]. One of the possible reasons for these undesirable side effects is the overdoses of the compound or a burst release, related with the loaded vehicle, as observed with an absorbable collagen sponge (ACS) carrier [24]. Current studies are trying to reach a minimal dosage and a controlled delivery system capable of avoiding the initial high release related to the over-doses side effects, using different biomaterials as BMP carriers, cited in Table 1.1.

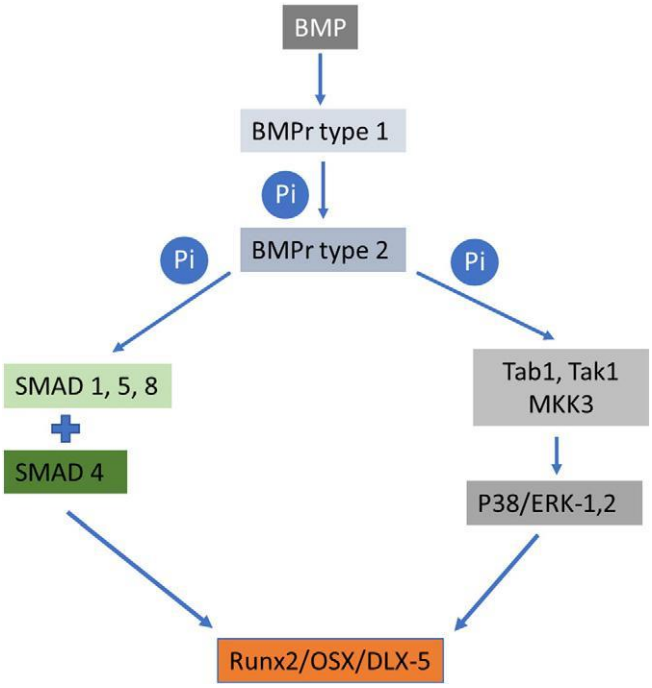

Figure 1.5. Simplified BMP-2 signaling pathways, via SMADs and p38. miRNAs can be associated with the BMP signaling. BMP-2 binds to BMP receptor (BMPr) type 1, which phosphorylates the BMPr type 2, consequently phosphorylates the receptor-regulated SMADs. SMADs act as transcription factors and participate in the upregulation of Runx2 gene expression. SMADs independent pathways are also reported, involving P38/MAPK pathway and miRNAs (Adapted from [13]).

Abbreviations: Bone morphogenic protein – BMP, Bone morphogenic.protein receptor – BMPr, distal-less homeobox 5 – DLX-5, mitogen activated protein kinase – MKK/ERK, Osterix – OSX, Runt-related transcription factor 2 – Runx2, phosphorylation – Pi, similar Mothers against Decapentaplegic – Smad, TGF beta activated kinase – Tab/tak.

Table 1.1. Overview of growth factors compounds and carriers for bone regeneration. (Adapted from [13]).

Type	Active Compound	Carrier	Signaling	Limitations/Systemic side effects	Reference
Growth Factors	BMP-2	Scaffolds: BCPC/BCP Honeycomb + β-TCP PLC + HA + Silk PPF + PLGA Graft: BCP Sponge: DSPC + ACS Nanocomplexe: HTCC	Smads and P38/MAPK pathways	- High cost - Edema - Cancer risks	[25] [26] [29] [28] [27] [22] [31]
	BMP-7	Microparticles: Chitosan		- Less efective than BMP-2 with the same side effects	[30]
	TGF-β	Scafffold: PLC + HA + Silk		- Inflammation - ROS - Cancer risks	[29]
	VEGF	Scaffold: β-TCP + PLGA	VEGF and BMP-2 pathways	- Unwanted Vascularization - Tumor Growth	[32]
	PIGF-2	Nanocomplexe: HTCC	VEGF and Hypoxia pathways	- Expressed by cancer cells - Osteoclast recruitment and	[31]

Abbreviations:1,2-distearoyl-sn-glycero-3-phosphocholine – DSPC, Absorbable collagen sponge – ACS, Biphasic calcium phosphate – BCP, Biphasic calcium phosphate composite – BCPC, Bone morphogenetic protein – BMP,

hydroxyapatite – HA, Hyaluronic acid – HAc, N-(2-hydroxyl)propyl-3-trimethyl ammonium chitosan chloride – HTCC, Placental growth factor – PlGF, platelet-derived growth factor – PDGF, poly-caprolactone – PLC, poly(propylene fumarate) – PPF, poly(lactic-co-glycolic acid) - PLGA, reactive oxygen species – ROS, Transforming growth factor beta - TGF-β, Tricalcium phosphate – TCP and vascular endothelial growth factor – VEGF.

1.2.2. Hormones and phytohormones

One of the several functions of hormones in the organism is to control the blood levels of calcium and its homeostasis. Estrogens, growth hormones and thyroid hormones, as calcitonin and parathyroid hormone (PTH) are some examples of hormones directly linked to bone metabolism. Current studies are trying to use some of these hormones to improve local bone regeneration (Table 1.2).

PTH is well known to stimulate bone remodeling; its usage is approved by The Food and Drug Administration (FDA) in the treatment of osteoporosis since 2002. Intermittent administration can lead to bone formation, with an increase of osteoblasts activity by stimulating Wnt signaling pathway and the production of pro-angiogenesis growth factors like VEGF and angiopoetin-1 [33]. However, in a continuous exposure the osteoclasts activity increases [34].

Estrogens, especially 17β-estradiol (E2), are responsible for the maintenance of bone homeostasis in mammals. For instance, lack of E2 results in bone resorption and the increase of fat tissue in bone marrow. E2 can increases the differentiation of MSCs in osteoblasts instead of adipocytes, by activating MAPK and Erk1/2 and increase their activity [35]. E2 can also inhibits osteoclasts resorption function [35], however estrogens were related with increased risks of breast cancer, cardiovascular diseases and thromboembolisms [36].

Another important molecule is resveratrol, a phytoestrogen extracted from grapevine, peanut and other plants when in contact with certain microorganisms. Resveratrol can be use in the prevention of osteoporosis and regarding the prevention of alveolar bone loss, it is known that resveratrol can inhibit the loss of this type of bone, reducing interleukin-17 in gingival tissue, activating Nrf2 pathway and decreasing oxidative stress and pro-inflammatory cytokine production [37]. However, resveratrol has low solubility and it is quickly metabolized in human body, presenting an extremely short plasma half-life and low bioavailability [38].

Table 1.2. Overview of hormones with interest in local delivery applications. (Adapted from [13]).

Type	Active Compound	Carrier	Signaling	Limitations/Systemic side effects	Reference
Hormones	PTH	Scaffold: PLLA + PA	Wnt signaling, VEGF Pathways and PTHr	- High blood calcium levels - Inhibition of bone regeneration - Cancer risks	[39]
	Resveratrol	Scaffold: PLC + COOH PAA PLC + ALB Systemic: Subcutaneous injection	ER, Wnt and Sirtuin 1 signaling	- Low solubility - Short plasma half-life - Low bioavailability	[40] [41] [42] [37]

Abbreviations: albumin – ALB, carboxylic acid – COOH, estrogen receptor – ER, Parathyroid hormone – PTH, poly(l-lactic acid) – PLLA, poly-acrylic acid – PAA, polyanhydride – PA, poly-caprolactone – PLC, and vascular endothelial growth factor – VEGF.

1.2.3. Alendronate

Alendronate (ALN) is a drug that belongs to nitrogenous bisphosphonate class. It is used in the treatment of cancer, bone disorders such as osteoporosis, fibrous dysplasia, and others diseases [43]. ALN acts in osteoclast cells, altering the cytoskeleton, thus inhibiting its interaction with bone matrix. ALN prevents osteoclast recruitment, their differentiation and causes apoptosis of these cells [44]. ALN also promotes the upregulation of BMP-2, ALP, collagen type I (COL1) and osteocalcin (OCN) gene expression, osteoblast precursor's formation and the inhibition of osteoclast bone resorption [45,46,47]. As side effects, hypocalcemia, atrial fibrillation and jaw necrosis are the most serious problems related with the usage of ALN, mainly with high IV dose application [48]. As examples, the study of Park et al. [49], a biphasic calcium phosphate (BCP) scaffold was developed containing 5 mg ALN and presented an increase of ALP activity and calcium content, as well as mRNA expression of OCN and Osteopontin (OPN). The *in vivo* assay showed gain of bone volume and revealed abundant mature bone formation.

Going further, Hur et al. [50] modified a clinically approved metallic bone plate with 4-azidobenzoic acid-modified chitosan, loaded with ALN and tested *in vivo*. The plate with ALN presented significant more bone formation with an ALN release up to 60 days with no significant cytotoxicity and no alterations in mechanical properties.

1.2.4. Simvastatin

Simvastatin (SV) is a small molecule drug that belongs to the statins group. It is known as a coenzyme A reductase inhibitor that is mainly used to decrease serum cholesterol levels and recently showed effects on new bone formation through increasing the expression of the BMP-2 gene in bone cells [51]. However, less than 5% of the drug reaches the systemic circulation due to extensive first-pass metabolism in the liver as SV presents high liposolubility [52]. In the study of Yue et al. [53] nanostructured lipid carriers loaded with SV were tested *in vivo* with BioOss® and the results showed that more new bone area, neovascularization and increased the ALP activity were found in the presence of SV nanoparticles group.

1.2.5. Raloxifene

Raloxifene (RAL) is a nonsteroidal benzothiophen derivative that acts as selective estrogen receptor modulator (SERM). It has estrogenic actions on bone and anti-estrogenic actions on

the uterus and breast [54]. It is approved by FDA since 1997 for the treatment and prevention of osteoporosis, and for reduction of breast cancer risks [54]. In the study of Zhang et al. [55] a scaffold made with chitosan, collagen, and β-TCP and loaded with poly (lactic-co-glycolic) acid (PLGA) microspheres containing RAL was tested *in vitro* and the results showed a superior cell viability, significantly enhanced cell proliferation, higher mineralization capacity and ALP activity.

1.2.6. Antibiotics

Interestingly some antibiotics may have an effect on bone metabolism along with their antimicrobial activity (Table 1.3). One example is clarithromycin (CLT), the use of this macrolide has been suggested to accelerate bone remodeling through antibacterial and anti-inflammatory properties [56,57]. Alenezi et al. [58] presented a study investigating the controlled release of CLT using PLGA microspheres and BCP as a carrier. *In vivo* results suggested that CLT group presented highest amount of bone formation, however only 12 weeks after the procedure.

Another example are the tetracyclines (TCs) and their derivatives, produced by the *Streptomyces* genus of *Actinobacteria*, which present non-antimicrobial effects including the direct interaction with matrix metalloproteinase enzymes (MMPs), tissue inhibitors of MMPs, growth factors and cytokines [59,60], resulting in antioxidant, anti-inflammatory and anti-apoptotic activities [61]. TCs bone effects are also related with the increase of collagen type 1 synthesis and upregulation of Wnt signaling [62], preventing bone loss and increasing bone formation [63]. Their anti-inflammatory activity is based on MMPs inhibition and the anti-apoptotic effect, with inhibition of caspase-1 and caspase-3 activation and the enhancement of Bcl-2-derived effects [61]. TCs also displays a high affinity towards mineralized tissues, being able to form bioactive tetracycline-calcium orthophosphate complexes [64] and its antimicrobial effect is related with the inhibition of bacterial protein synthesis by binding to the 30S bacterial ribosome [60].

Among tetracyclines, minocycline and doxycycline are the second-generation of semi-synthetic antibiotics, presenting better pharmacokinetic profile, broader spectrum of activity, longer half-life and improved lipid solubility resulting in improved tissue penetration, in comparison with others from the same class [65]. Moreover, minocycline has recently been considered beneficial for diseases with an inflammatory basis, as dermatitis, rheumatoid arthritis, periodontal disease, atherosclerosis and central nervous system pathologies [61].

The study of Yoshinari et al. [66] demonstrated the effects of local minocycline applications associated with guided tissue regeneration using a non-absorbable membrane in maxillary and mandibular bone defects in humans and presented remarkable results by the antibiotic activity

of the compound. Gomes et al. [67] as well as Dou et al. [68] demonstrated the *in vitro* ability of minocycline in increasing bone marrow stem cells differentiation in osteoblasts, proliferation and mineral deposition. In 2016, Ma et al. [69] developed an absorbable membrane containing minocycline nanoparticles and tested by *in vivo* models, with exceptional results regarding bone regeneration. Additionally, Matos et al. [70] developed a novel formulation of acrylic bone cements composed with 2.5 (wt.%) of minocycline capable of antibacterial activity against *Staphylococcus aureus*, with a drug release up to 7 days.

Table 1.3 - Overview of antibiotic compounds and carriers with interest in local delivery applications. (Adapted from [13]).

Type	Active Compound	Carrier	Signaling	Limitations/Systemic side effects	Reference
Macrolides	Clarithromycin	Microspheres: PLGA + BCP	**Anti-inflammatory** (Bind to 50S ribosomal subunit, reduction of IL-6 and CXCL-8 production) resulting in bone formation;	- Normal ATB side effects (upset stomach, allergic reactions,diarrhea) - Antimicrobial Resistance	[58]
Tetracyclines	Tetracycline	Nanocomposite: HAP + β-TCP Nanoparticles: PLGA + Chi	**Inhibition of MMPs** (cation quelation); **Anti-inflammatory** (attenuation of mRNA gene expression of IL-6, IL-1, reduction of MAPK phosphorylation,caspases activation and PARP-1 activity); **Anti-apoptotic** (increasing Bcl-2 signaling); **Antioxidant** (quenching hydrogen peroxide); -**Bone formation** (stimulating Wnt pathway).	- Normal ATB side effects (upset stomach, allergic reactions,diarrhea) - Problems during tooth development - Dizziness - Antimicrobial Resistance	[71] [72]
	Doxicycline	Gel (Atridox®) Microspheres: HPMC			[67] [73]
	Minocycline	Nanocomposite: Gelatin + HA Membrane: COL + Chi Cement: Acrylic + Lactose Gel (Dentomycin®) Microspheres (Periocline®, Arestin®) Nanoparticles: PLGA + PEG, Microgranules: HPMC			[67] [68] [69] [70] [19] [74]

Abbreviations: Antibiotic – ATB, Biphasic calcium phosphate – BCP, calcium hydroxyapatite – HAP, collagen – COL, Hydroxyapatite – HA, poly (lactic-co-glycolic) acid – PLGA, Tricalcium phosphate – TCP, Hydroxypropyl methylcellulose – HPMC, Chitosan – Chi, Polyethylene glycol – PEG, B-cell lymphoma 2 – Bcl-2, Poly [ADP-ribose] polymerase 1 - PARP-1, Mitogen-activated protein kinase – MAPK, Matrix metalloproteinases – MMPs, Interleukins 1,6 and 8 – IL-1, IL-6 and CXCL-8.

1.3. Current scenario and aims of the thesis

Until today, the autogenous graft is still the gold standard to any procedure, only in some specific cases with precise indication or small defects, biomaterials can be use with safety and efficiency.

Improvement of the osteoconductive properties of the biomaterials associated with the controlled release of osteoinductive compounds might replace the autogenous grafts in several clinical situations, diminishing its usage that will result in faster, costly and easier surgeries, with less side effects (as edemas) and morbidity. It is also important to mention that, biomaterials can present two important functions: one as scaffolds for osteoprogenitor cells, providing an interface for cells to attach, proliferate and differentiate, and other as drug delivery systems of substances with positive effects on bone regeneration. In addition, the ability of

preventing infections can be important once oral surgeries are conceptually clean-contaminated and the relevant bacteria of osteomyelitis can be present in the patient's skin or medical care providers (e.g. surgeons) [75]. Furthermore, orthopedic device-related infections increase the incidence of osteomyelitis, which can lead to a second chirurgical intervention for the removal of initially inserted bone graft and necrotic tissue, raising the costs of the treatment, risks and discomfort for the patient [76].

An important feature is the development of three-dimensional (3D) printing technology that is changing the scaffold designs in regenerative medicine, offering improved speed, low cost, and availability of a wide range of printing materials, accuracy, and reproducibility [77]. Additionally, this new technique can produce structures based on imaging techniques and scaffolds composed with components in the extracellular matrix to deliver bio-compounds and drugs [78,79]. Among the materials frequently used regarding medical needs, polymers and ceramics are good options [14]. Medical synthetic polymers are known by their biocompatibility and biodegradability, presenting advantages over ceramic materials as controllable degradation rate, predictable and reproducible mechanical properties [14].

With that in mind, we conjectured that minocycline, an antibiotic with multiple biological activities, could be applied in three different polymeric platforms aiming osteoinduction, anti-inflammatory and antimicrobial activity.

The first hypothesis involved the biopolymer chitosan as nanoparticles carrying minocycline, idealized to be used *in situ* against periodontal disease, combining the chitosan effects with the antibiotic activity, once antibiotics are frequently prescribed as adjuvant for the treatment [6]. Moreover, the anti-inflammatory effects of minocycline and chitosan could be useful against periodontitis, which is known as an inflammation-related disease caused by the presence of bacteria in the gingival crevice [80]. Periodontitis is most prevalent chronic inflammatory condition in humans and is considered the major cause of tooth loss in adults by the destruction of tooth-supporting tissues and absorption of alveolar bone [60].

The other two hypothesis involved 3D polylactide (PLA) scaffolds targeting bone regeneration as a graft loaded with minocycline, with differences regarding the scaffold production technique, where one was produced by the solvent casting technique, using salt as porogen and silicon molds and the other was printed using the additive technique. PLA stands out due to its mechanical properties, biocompatibility and biodegradability, successfully used as orthopedic implants for tissue engineering. Its degradation products are non-toxic and is approved for direct contacting with biological fluid by FDA [81,82]. A scaffold designed for a controlled release of minocycline could improve and accelerate the bone regeneration, providing osteoconductive framework with osteoinductive, anti-inflammatory and antimicrobial effect.

A multidisciplinary approach involving the production, physical-chemistry characterization as well as *in vitro* assays regarding drug release, microbiological and cell culture evaluation was followed aiming the development of three novel polymeric platforms with potential application regarding bone regeneration and periodontal healing.

Chapter 2. Enhanced anti-inflammatory effects of chitosan nanoparticles carrying minocycline aiming periodontal disease treatment

2.1. Introduction

Periodontal disease (PD) is the most prevalent chronic inflammatory condition in humans worldwide [1,2], triggered by bacteria toxins which stimulates the host inflammatory response, causing the destruction of periodontal tissue and tooth loss [2,3]. Additionally, several systemic diseases as cardiovascular illnesses, diabetes mellitus and rheumatoid arthritis are associated with PD by sharing biochemical risk markers with these inflammation-related diseases [1,4,5]. The etiology of the PD is related with the presence of several bacterial species surrounding natural teeth, including *Porphyromonas gingivalis* [6,7] and *Aggregatibacter actinomycetemcomitans*. The lipopolysaccharide (LPS) of their membrane can activate the host immuno-inflammatory response leading to the release of inflammatory cytokines such as interleukins IL-1, CXCL-8, nuclear factor kappa-B (NFkB), tumor necrosis factor alpha (TNF-α), and matrix metalloproteinases (MMPs) produced by fibroblasts, epithelial cells and defense cells [8-10] generating an immune-mediated destruction of the periodontal supporting tissues, including alveolar bone [5].

Besides, these bacteria are known by the capability of invade periodontal cells, such as gingival epithelial cells and osteoblasts, inhibiting their maturation [8,9,11]. In addition, internalized bacteria are considered protected from host immune surveillance and regular antibiotic treatment, leading to intracellular persistence, development and dissemination to adjacent tissues, resulting in the disease recurrence and ineffective treatments [12].

Among the possible antibiotics available for PD treatment, minocycline can be a good choice due to its antimicrobial effect, intracellular internalization, including in gingival fibroblasts along with its anti-inflammatory role [13,14]. Minocycline is a broad spectrum semi-synthetic tetracycline derivative that has been proved effective against *P. gingivalis* and *A. actinomycetemcomitans* [15], inhibiting bacterial protein synthesis by binding to bacterial 30S ribosomal subunits10 [16]. Moreover, tetracycline is one of the few antibacterial class with effects on the preservation of pro-anabolic and anti-catabolic activity over tissue cells, inhibiting the osteoclast-mediated bone resorption and MMPs activity, presenting anti-inflammatory and antioxidant effects [13,16,17]. The signaling of its anti-inflammatory effects are based on the attenuation of mRNA gene expression of interleukins IL-6, IL-1, inhibition of caspases activation, reduction of p38 mitogen-activated protein kinase (MAPK) phosphorylation and poly [ADP-ribose] polymerase 1 (PARP-1) activity [13].

Being a disorder originated due to microbial biofilms, PD treatment is based on mechanical root debridement, aiming the root planning and the reduction of subgingival bacteria [1,11,18].

However, instrumental debridement cannot completely remove pathogens from some anatomical areas and bacteria that invaded tissue cells, which can result in non-effective treatments and recurrence [1], justifying the need of antimicrobial therapy as adjuvant [3]. Systemic antibiotic therapy can be effective against periodontal pathogens, however large doses must be administered to achieve an effective inhibitory concentration in gingival crevicular fluid, which may lead to side effects and bacterial resistance [19]. Furthermore, the infection around PD is associated with the triggering of the inflammation process [2]. Until today, there is no consolidated protocol aiming the reduction of the disease inflammation itself, the main source of the periodontal tissue destruction [3].

To overcome the limitations regarding the current therapeutic approaches nanoparticulate platforms can be explored as local delivery systems aiming the establishment of a drug reservoir inside the periodontal space that can maintain higher concentrations at the site for prolonged periods with lower plasma concentrations [18,19] and more importantly, reach the intracellular bacteria reservoirs [12,20]. Besides, nanoparticles can protect the drug against *in vivo* degradation and present a more favorable drug pharmacokinetics [21].

With that in mind a study was designed to test the hypothesis that a novel chitosan nanoparticulate system loaded with minocycline could run a viable alternative as a local drug delivery system presenting controlled drug release, modulating inflammatory response and achieve fibroblast internalization, once the main pathogens have the ability of cellular invasion [9,11]. In addition, chitosan, a naturally-derived polymer, has been used in several biomedical devices due to its proper biodegradability and biocompatibility, exhibiting antibacterial activity, along with mucoadhesive, analgesic and anti-inflammatory properties [7,22,23]. To the best of our knowledge, it is the first time that a chitosan nanoparticle is developed carrying minocycline aiming periodontal disease treatment.

2.2. Materials and Methods

2.2.1. Nanoparticles preparation

2.2.1.1. Materials

Chitosan (Low molecular weight - 50 to 190 kDa, deacetylation above 92%, Aldrich), Tween®80 (Ph. European, Merck), acetic acid (Riedel-de Haen), tripolyphosphate pentasodium (Alfa Aesar), minocycline hydrochloride (kindly donated by Atral Cipan, Portugal), sodium hydroxide (Akzo Nobel), acetonitrile (Fisher Scientific), HEPES buffer (VWR Chemicals) and trehalose (AppliChem) were used in the experiments. Purified water was of Milli-RX quality (Merck Millipore, Germany). All other reagents and solvents were of the purest grade available, and generally were used without further treatment.

2.2.1.2. Preparation of Chitosan nanoparticles

Chitosan nanoparticles (NPs) were prepared using an ionic gelation technique previously optimized in the laboratory [24] and modified accordingly with Nagpal et al. [25] in order to increase the drug encapsulation efficiency. The detailed description and characterization regarding the development of the nanoparticle´s formulation is described in Annex 1. Briefly, the selected final formulation was prepared by obtaining a chitosan stock solution of 10 mg/mL that was prepared by dissolving the chitosan polymer in a 1% (V/V) acetic acid aqueous solution and then, diluted to 1 mg/mL with a Tween80 (2% w/V) solution, prepared in ultra-pure water. The pH was adjusted to 5.5 with 0.5 N sodium hydroxide solution.

The FITC-labeled chitosan was produced with a fluorochrome using Oregon Green 488 reactive dye that has a succinimidyl ester moiety that reacts efficiently with primary amines to form stable dye–chitosan conjugates according the instructions of Molecular Probes (ThemoFisher, USA). Briefly, a stock solution of 2 mg/mL of chitosan was prepared in phosphate buffer at pH 6.0 and the dye was added. The mixture was kept at room temperature with slow agitation for 3 h. In order to purify the dye-chitosan conjugated from the non-reacted dye, the solution pH was increased to 8 in order to precipitate the complexes. Samples were washed three times with water and centrifuged at 10000 x g for 15 min (AllegraTM 64R centrifuge, Beckman Coulter).

NPs were formed by adding the tripolyphosphate pentasodium (TPP) solution (10 mg/mL; pH = 9.5), containing minocycline hydrochloride (MH) at 2 mg/mL or ultra-pure water (for blank NPs preparation), slowly drop-wised into the chitosan solution under vigorous magnetic stirring at room temperature for 25 min. The proportion of chitosan and TPP concentration was 3:1. After, the solutions were centrifuged for 10 min, 15000 g at 6°C (Allegra 64R, Beckman Coulter) and the supernatant was discarded. Finally, a cryoprotectant solution was added (trehalose 10%) and the samples were freeze-dried for 12 h (Christ Alpha 1-4, Braun Biotech International).

2.2.2. Nanoparticles physicochemical characterization

Mean particle size and polydispersity index (PDI) of the NPs were assessed by light scattering using a Zetasizer Nano-S (Malvern Instruments). Briefly, 350 µL of the NPs solution were put in a cuvette and their distribution size was obtained from the average of three runs per sample. Zeta potential was measured using a Zetasizer Nano Z (Malvern Instruments) using 60 µL of the samples diluted in 2 mL of filtered purified water. Results were expressed as mean ± standard deviation (SD).

The microstructure and morphological features of blank NPs (b-NPs) and NPs loaded with MH (MH-NPs), were evaluated with a Hitachi H-9000-NA transmission electron microscope (TEM) operating at 200 kV. The particle samples for TEM observation were prepared by dropping an

ethanolic suspension of the particles kept under ultrasonic stirring onto a formvar-coated copper grid. The grid was subsequently air-dried for TEM observation.

Attenuated total reflectance (FT-IR/ATR) was performed to identify the functional groups of b-NPs and MH-NPs, using a Nicolet (Thermo Electron) spectrometer. The ATR spectra were recorded in a transmittance mode in the region of 600–4000 cm^{-1}.

The crystal structure of b-NPs and MH-NPs was analyzed by X-ray diffraction (XRD), using a Bruker D8 ADVANCE Powder Diffractometer equipped with monochromatic CuKα (target) radiation (1.5405 A). Data sets were collected in the 2Θ range of 8-75º, with a step with of 0.02˚/min. The analyses were performed at room temperature.

2.2.3. Drug loading and minocycline release

The drug loading (DL%) corresponds to the quantification of the MH in the lyophilized nanoparticles**.** For that 10 mg of the freeze-dried NPs were re-suspended with 500 µL of acetonitrile (ACN) solution (ACN:H_2O 1:1), vortexed for 1 min and then centrifuged for 12 min, 20000 g at 6 °C. After, the supernatant was collected for MH quantification. DL% is calculated by Equation 1 [26].

$$DL(\%) = \left(\frac{WMH}{WNP}\right) x\ 100 \qquad \text{Equation 1}$$

w_{MH} is the amount (mg) of MH obtained with the dissolution of the NPs and w_{NP} is the weight (mg) of the nanoparticles.

MH release from the NPs was evaluated using a dialysis technique [21]. A 150 mg sample of NPs was placed inside a 100 kDa dialysis bag [27] with 1 mL of HEPES (10mM at pH 7.4) and then put inside a 50 mL Falcon tube, containing 15 mL of the same HEPES solution. Tubes were put in an incubator (Model 100 – 800, Memmert) at 37°C spinning in a tube rotator. At predetermined intervals aliquots of the outside tube supernatant were collected and analyzed in triplicate throughout a 24 h period and the withdrawn aliquots were replaced with equal volumes of fresh HEPES solution. For comparison, the diffusion of a MH solution was also tested at 125 µg/mL, the maximum theoretical concentration of antibiotic release from the MH-NPs.

In all the previous described assays the antibiotic quantification was assessed by spectrophotometry (λ = 350 nm) with a microplate reader (FLUOstar Omega, BMG Labtech). Calibration curves ranging from 0.95 to 125 µg/mL obtained by the microdilution of MH with the same solvent (HEPES or ACN) were used to quantify samples. The reproducibility was analyzed and considered adequate for sample analysis and supernatants from blank (b-NPs) were also analyzed and used as control. Each sample was measured three times.

2.2.4. Cytocompatibility Analysis

The cytocompatibility of b-NPs and MH-NPs was conducted *in vitro* by assessing the functionality of cultured human gingival fibroblasts (HGFs) in the presence of distinct NPs concentrations. Concentrations of b-NP and MH-NP (μg/mL) were equalized in all studies and related to MH solution (free drug) equivalent doses. The fibroblasts were expanded in α - Minimal Essential Medium (α-MEM) containing 10% fetal bovine serum (FBS), 100 IU/mL penicillin, 100 μg/mL streptomycin and 2.5 μg/mL amphotericin B (all Gibco), at 37 °C and 5% CO_2. After reaching confluency, the cells were trypsinized and subcultured at 10 000 cells/cm^2 for further studies.

2.2.4.1. Cell viability/metabolic activity

In vitro cytotoxicity was assessed using the MTT assay which is based on the conversion of a tetrazolium salt (MTT) into formazan crystals in the viable cells [28]. Briefly, 24 h-adhered cells were exposed to b-NPs, MH-NPs and MH solution at the antibiotic equivalent dose of 0.5, 1.0 and 2.0 μg/mL up to 6 days at 37 °C, 5% CO_2. Cells in media alone, devoid of NPs, were used as negative control. At definite time intervals, a 10% MTT solution (5 mg/mL, Sigma-Aldrich) was added to wells followed by 3 h incubation. Then the supernatant was removed and all crystals were dissolved by dimethyl sulfoxide (DMSO). The absorbance of the colored solution was measured at 550 nm with a microplate reader (Synergy HT; BioTek).

2.2.4.2. Cell morphology

The cell morphology characterization was conducted following filamentous actin (F-actin) staining and nucleus counterstaining. Briefly, 24 h adhered cells were exposed to MH solution (2 μg/mL), b-NPs or MH-NPs for 48 h and processed for microscopical analysis as previously described. Six representative fields were digitally registered for further cell surface area measurements and skewness (i.e. the shape of the cells, being the ratio of cell width over cell length) determination, with ImageJ software.

2.2.4.3. Cellular uptake of nanoparticles

Uptake studies were performed using both fluorescent imaging and transmission electron microscopy (TEM). For fluorescent analysis, 24 h adhered HGFs were incubated with FTIC-labelled b-NPs or MH-NPs at the antibiotic equivalent dose of 1.0 μg/mL. Following 6 h, cells were washed with PBS, fixed with 3.7% paraformaldehyde (Sigma-Aldrich) and stained. Briefly, cell membranes were permeated with 0.1% Triton X-100 for 15 min and non-specific proteins were blocked with 1% bovine serum albumin for 30 min (both Sigma-Aldrich). Cell cytoskeleton F-actin was stained with Alexa-Fluor 594 phalloidin conjugated antibody (1:50,

Molecular Probes) during 30 min and cell nuclei labelled with DAPI (1 µg/mL, Sigma-Aldrich) for 10 min. Images of fluorescent-labelled cells and NPs were obtained by using the Selena S digital imaging system (Logos Biosystems).

For TEM analysis, 24 h-cultured HGFs were exposed to b-NPs or MH-NPs, at the antibiotic solution-equivalent dose of 1.0 µg/mL, for a 6 h period. After washing three times with PBS, trypsinized cells were fixed with 2.5% glutaraldehyde for 1 h at 4 °C, washed three times with 0.1 M cacodylate buffer, and then dehydrated using a graded ethanol series and a Spurr's resin series. The cells were placed in a fresh 100% Spurr's resin in molds and polymerized at 60 °C for 8 h. Ultrathin (35–50 nm) sections were cut with a diamond knife, loaded onto nickel-coated TEM grids, and stained with 2% uranyl acetate. The images were acquired by TEM (JEOL 1200 EXII, JEOL, JAPAN) operating at an acceleration voltage of 120 kV.

2.2.4.4. Inflammatory gene expression

HGFs cultures were established in standard conditions for 24 h. Following, cultures were stimulated with 1 µg/mL *P. gingivalis* LPS for 24 h, and subsequently incubated with MH solution, b-NPs or MH-NPs at the antibiotic equivalent dose of 1.0 µg/mL for further 24h.

Total RNA was isolated from established HGFs cultures by Trizol reagent (Invitrogen, Carlsbad, USA), according to the manufacturer's protocol, being its concentration and quality determined with NanoDrop (NanoDrop Technologies). cDNA synthesis was attained with a commercially reverse transcription system (QuantiTect RT Kit, Qiagen) and subsequent quantitative PCR was performed using an iCycler iQ Real-time PCR system (Bio-Rad), with the QuantiTect SYBR green PCR Kit (Qiagen). The relative quantification of each target gene, was normalized to GAPDH levels, and calculated via the $2^{-\Delta\Delta Ct}$ method. Primer sequences of the target genes are presented on Table 2.1.

Table 2.1. Primer sequences of the inflammatory genes. GAPDH was used to the relative quantification of the target genes.

	Foward	Reverse
GAPDH	CGGGAAACTGTGGCGTGAT	GTCGCTGTTGAAGTCAGAGGAG
IL-1β	TGATGGCTTATTACAGTGGC	TGTAGTGGTGGTCGGAGATT
TNF-α	CCTGCCCCAATCCCTTTATT	CCCTAAGCCCCCAATTCTCT
CXCL-8	ACTCCAAACCTTTCCACC	CTTCTCCACAACCCTCTG
NFkB1	AACAGAGAGGATTTCGTTTCCG	TTTGACCTGAGGGTAAGACTTCT

Abbreviations: NFkB1 - Nuclear factor kappa-B p105 subunit; GAPDH - Glyceraldehyde 3-phosphate dehydrogenase; IL-1β - Interleukin 1 beta; IL-6 - Interleukin 6; CXCL-8 - Interleukin 8; TNF-α - Tumor necrosis factor alpha.

2.2.5. Statistical Analysis

Statistical analysis and graphics were conducted with GraphPad Prism 6.01 software. To assess the difference between groups, data normality was determined by the Shapiro-Wilk

test. For normal data sets, one-way ANOVA was performed, followed by multiple comparisons using Turkey's test. For non-parametric data sets, Kruskal-Wallis test was performed, followed by multiple comparisons using Dunn's tests. p values less than 0.05 were considered significant. Data were presented as mean ± standard deviation (SD).

2.3. Results

2.3.1. Nanoparticles characterization

A summary of NPs physico-chemical characterization is shown in Fig. 2.1. NPs within the nanometric size presented a stable positive zeta potential (Fig. 2.1 f). TEM images showed that the size and the shape-rounded morphology of the NPs were not altered in the presence of the MH (Fig. 2.1 a - d).

The XRD profile of b-NPs and MH-NPs showed a pour crystalline hump centered at 20.5◦ (2Ɵ) which are typical finger prints of chitosan. No significant variations are observed between the b-NPs and MH-NPs (Fig. 2.1 e). The diffraction peak off all nanoparticles are broad and poorly defined, suggesting a relatively lower degree of crystallinity and nano-dimensions.

The possible intermolecular interaction between the antibiotic (MH) and the chitosan (NPs) were qualitatively evaluated through FTIR-ATR analysis. Fig. 2.2 shows a typical FTIR-ATR spectrum where the main vibration bands of the chitosan are observed at 1099, 1537, 1649, 2881, 2914, 3436 cm^{-1}[29]. Although characteristic NPs features are observed in MH-NPs spectra, several differences are observed in the 800–1650 cm^{-1} region and 3100-3600 cm^{-1}. The band at 899 cm^{-1} is more intense while the three bands at 1537, 1649 and 3436 cm^{-1} are broader. These features on MH-NPs is result of specific stretching vibration of amine, carboxyl group (C=O) and C–O stretching vibration of MH, at 3040 cm^{-1} 1660 and 870 cm^{-1}, respectively.

Comparing the FTIR-ATR spectra of b-NPs and MH-NPs samples, it can be noticed differences in the intensity of the peaks (Fig. 2.2), confirming the presence of MH into the NPs.

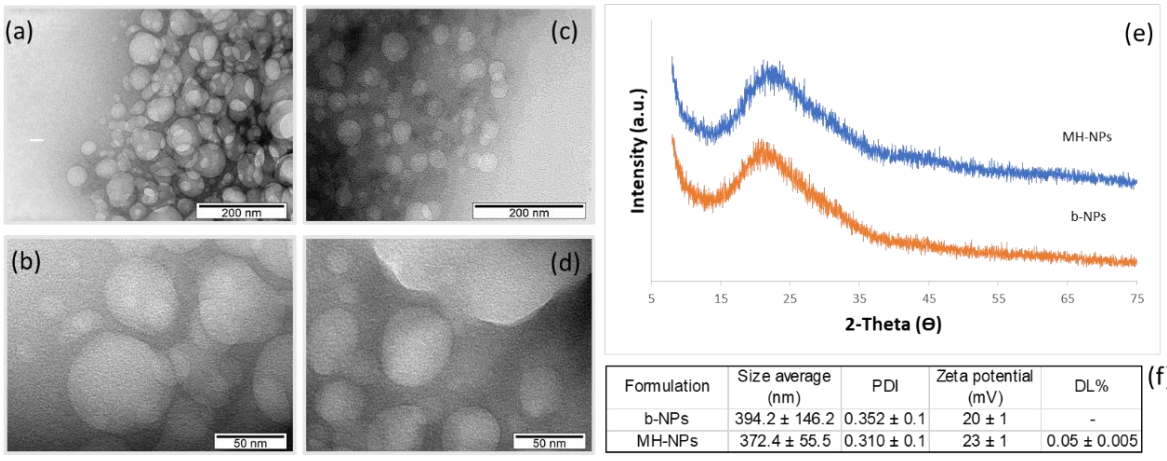

Formulation	Size average (nm)	PDI	Zeta potential (mV)	DL%
b-NPs	394.2 ± 146.2	0.352 ± 0.1	20 ± 1	-
MH-NPs	372.4 ± 55.5	0.310 ± 0.1	23 ± 1	0.05 ± 0.005

(f)

Figure 2.1. (a,b,c,d). TEM images from NPs in different magnifications. (e) XRD analysis, where no significant variations are observed between the b-NPs and MH-NPs (f). Characteristics of b-NPs and MH-NPs. Results are presented as mean ± SD (n = 3).
Abbreviations: PDI – poly dispersion index. DL% - drug loading. b-NPs – blank nanoparticles. MH-NPs – minocycline loaded nanoparticles.

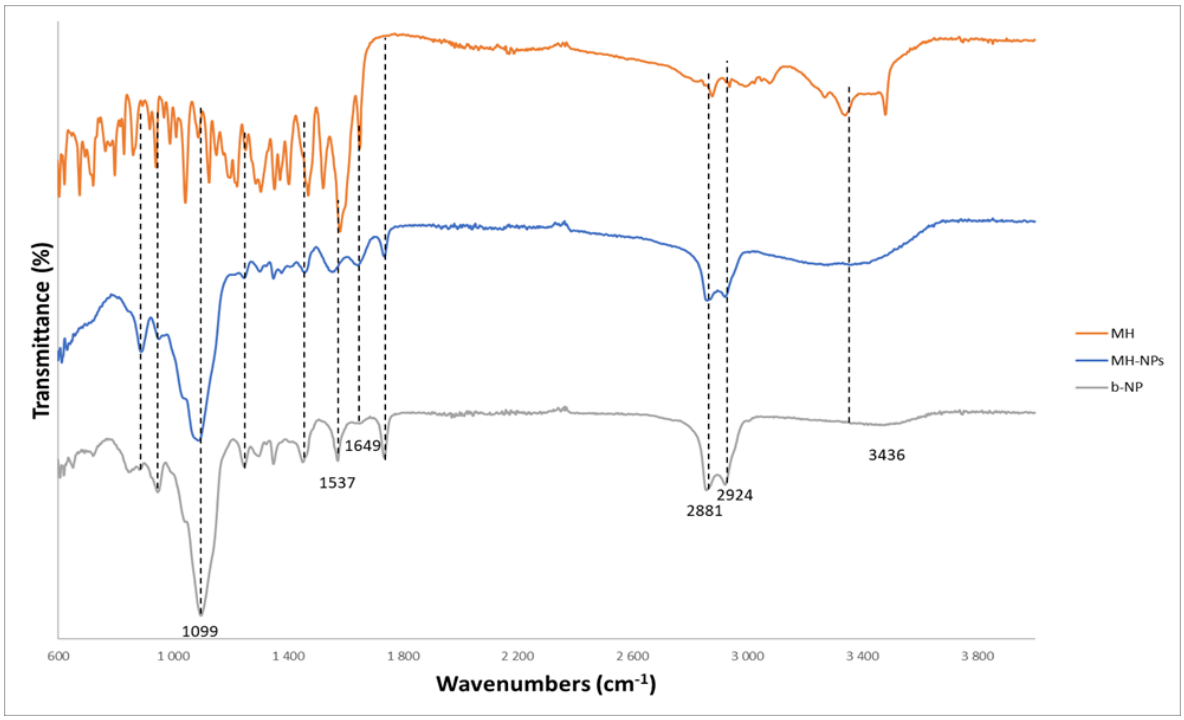

Figure 2.2. FTIR-ATR analysis showed differences among the free drug (MH), b-NPs and MH-NPs, suggesting the presence of the antibiotic within the NPs. Differences are observed between 3100 and 3600 cm^{-1}, 1200 and 1700 cm^{-1} and 600 to 1000 cm^{-1}. (g). Characteristics of b-NPs and MH-NPs.

2.3.2. Minocycline release

The antibiotic release profile of the MH-NPs and the MH solution is illustrated by Fig. 2.3. The total drug diffusion across the dialysis membrane was completed after 400 min for the free drug, presenting an initial burst (80%) at t=0 min, where 50% of the antibiotic of the NPs was released only in approx. 2 h and achieved 100% after 24 h suggesting that the NPs were capable of delaying the antibiotic release.

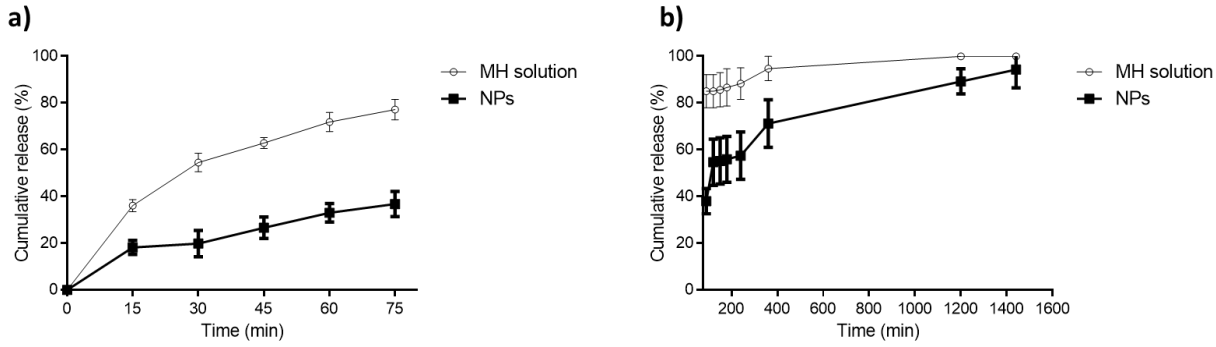

Figure 2.3. The MH cumulative release (%) from the MH-NPs was normalized with the DL% concentration of each sample, where (a), corresponds to 0 to 75 min of release assay and (b) corresponds to 24 h of the release. The MH solution concentration was 125 µg/mL. Mean ± SD (n = 3).

2.3.3. Cytocompatibility Analysis

2.3.3.1. Cell viability/metabolic activity

Cells were found to proliferate actively throughout the assayed culture period, with MTT reduction values increasing from day 1 to day 6 in all experimental conditions (Fig. 2.4). Comparatively, significantly higher values were attained for both b-NPs and MH-NPs (1 and 2 μg/mL) after 1 day of culture.

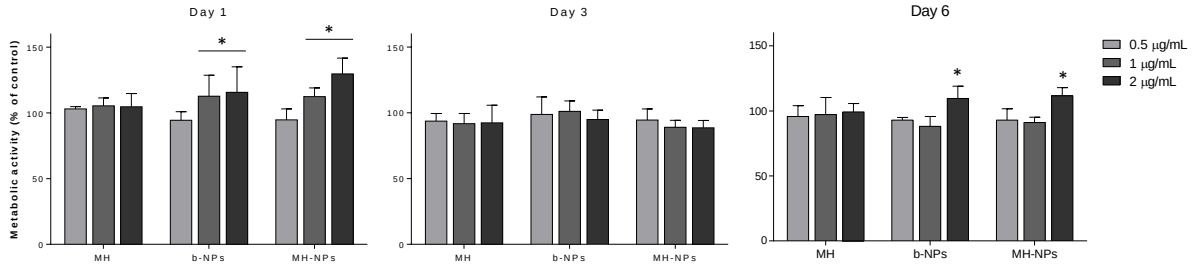

Figure 2.4. Cell viability/proliferation (MTT assay) of HGFs cultures, established up to 6 days, in the absence (control) and presence of MH solution, b-NPs and MH-NPs. Concentrations refer to antibiotic equivalent doses for MH solution and MH-NPs. The quantity of b-NPs were equalized to the same weight used to MH-NPs group. * $P < 0.05$, significantly different from the control condition, at each time point.

2.3.3.2. Cell morphology

The morphology of grown fibroblastic cells in the presence of MH solution, b-NPs or MH-NPs was characterized at 48 h. Within control cultures, cytoskeletal evaluation following F-actin staining revealed a stretched and characteristic fibroblastic morphology, with evident organization in parallel stress fibers. Experimental conditions revealed a similar morphology and cytoskeletal organization with no significant differences regarding cell area or cell skewness level (Fig. 2.5).

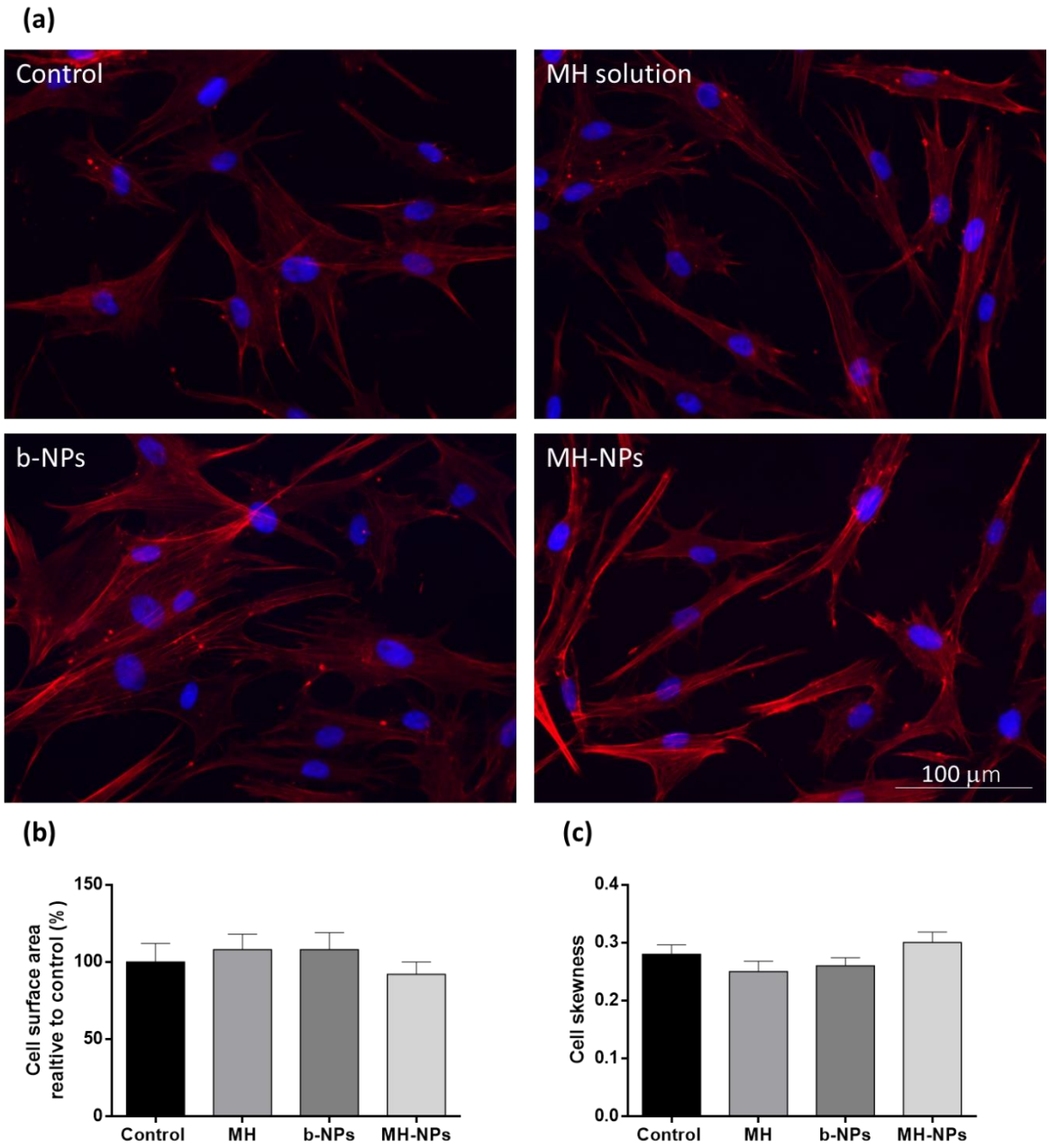

Figure 2.5. Representative immunofluorescent images of HGFs grown for 48 h in the absence (control) and presence of MH solution, b-NPs and MH-NPs, antibiotic dose-equivalent 2.0 µg/mL. Cells were stained for nucleus (DAPI) and actin cytoskeleton (red) (a). For each condition cell surface spreading (b) and cell skewness (width of the cell over the length of the cell) (c) were calculated.

2.3.3.3. Cellular uptake of nanoparticles

The cell-nanoparticles interaction and cellular uptake was evaluated by immunofluorescence, with FITC-labeled nanoparticles and TEM characterization. Following 3 h of incubation, b-NPs and MH-NPs were found to organize into small clusters that interacted with the cell membrane (Fig. 2.6 a - b), particularly within regions characterized by extensive filopodia extensions (Fig. 2.6 c).

TEM analysis further revealed that b-NPs and MH-NPs induced the formation of distinct membrane perturbations associated with the activation of two endocytic pathways: micropinocytosis and clathrin-mediated endocytosis. Upon contact with both particle clusters, cells activated membrane extensions, engulfing NPs and the surrounding extracellular milieu, in a characteristic process of micropinocytosis (Fig. 2.6 d - e). At the same time, small clathrin-coated pits could also be identified in association with NPs' contacting with the cell membrane (Fig. 2.6 f - g), as well as clathrin-coated vesicles, further sustaining the activation of clathrin-mediated endocytosis as an internalization pathway for both NPs (Fig. 2.6 h).

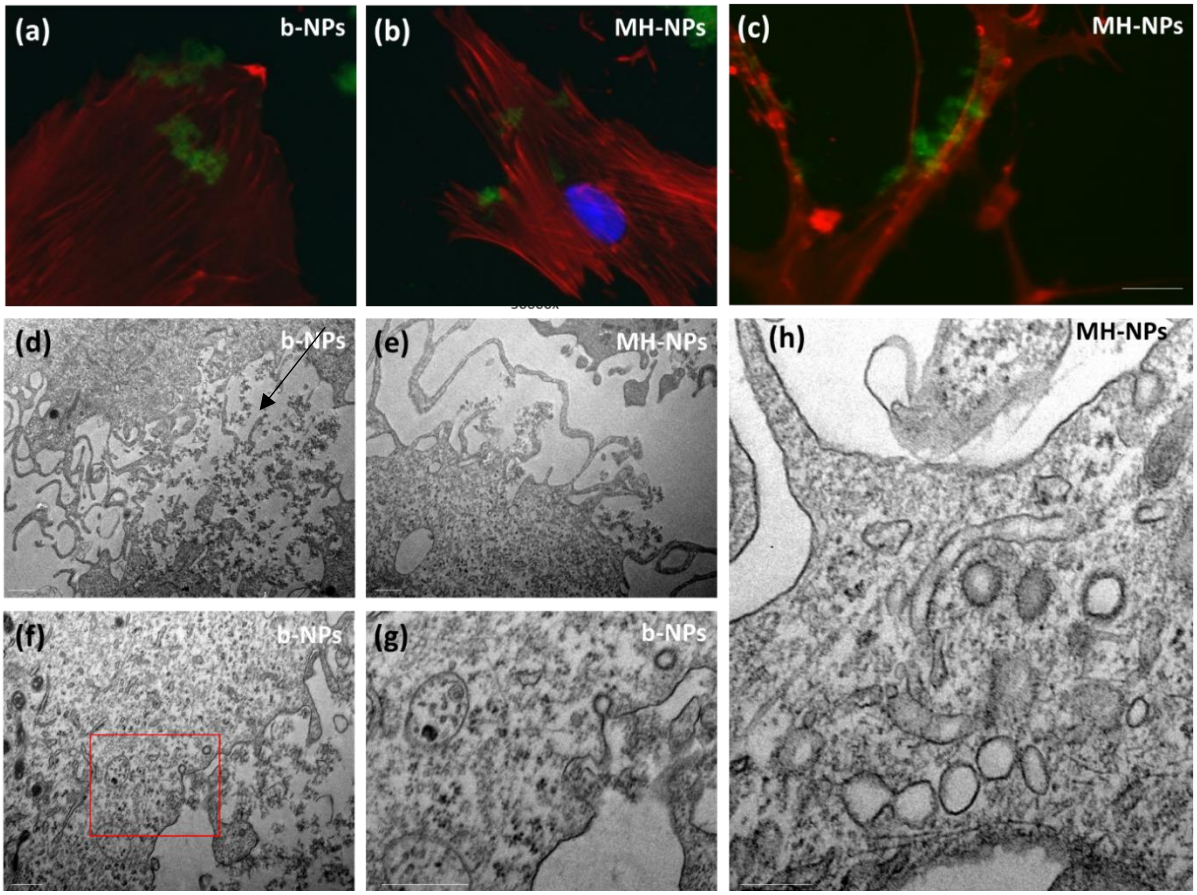

Figure 2.6. Internalization pathways of b-NPs and MH-NPs in HGFs, addressed by immunofluorescence (a-c) and TEM (d-h). Cell cultures were grown for 24 h and further incubated with b-NPs (a, d, f and g) or MH-NPs (b, c, e and h) for 3 h. In immunofluorescence images scale bar corresponds to 25 µm. in TEM images scale bar corresponds to 100 nm.

2.3.3.4. Inflammatory gene expression

With the current work, LPS treatment was found to significantly induce the expression of NF-kB and assayed cytokines and chemokines, i.e., IL-1, TNF-α and CXCL-8. LPS-stimulated cultures, grown in the presence of MH or b-NPs, were found to significantly reduce the expression of assayed markers. Additionally, in the presence of MH-NPs, a trend for a more

pronounced reduction was attained, suggesting a potential synergistic activity of MH and chitosan nanoparticles (Fig. 2.7).

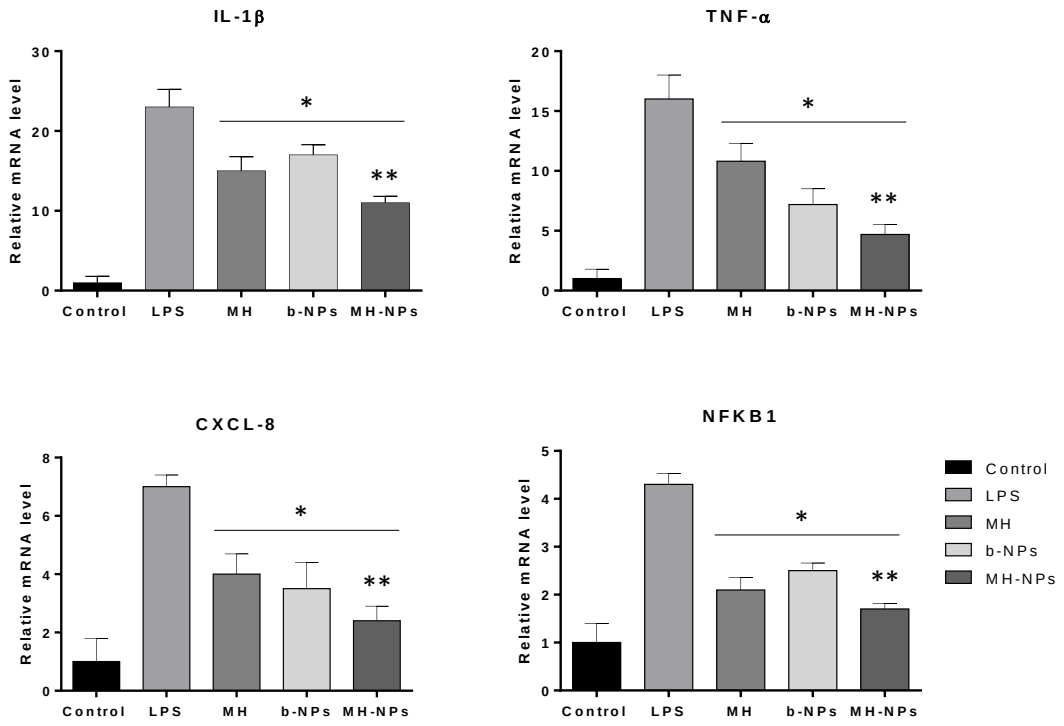

Figure 2.7. Relative expression of IL-1β, TNF-α, CXCL-8 and NFKB1 genes in HGFs cultures, stimulated with *P. gingivalis* LPS for 24 h, and subsequently cultured in the absence (control) and presence of MH, b-NPs and MH-NPs, antibiotic dose-equivalent 1µg/mL, for further 24 h. * * $P < 0.05$, significantly different from the control condition; ** * $P < 0.01$, significantly different from b-NPs and MH.

2.4. Discussion

In this study, chitosan nanoparticles loaded with minocycline were successfully produced using the ion gelation method. This technique is easy and inexpensive, involving neither the use of harsh chemicals nor elevated temperature [30]. The obtained nanoparticles counted on the negatively charged TPP that bounds to the chitosan positive chemical groups [24] and the usage of Tween80 in the formulation aimed the improvement of drug encapsulation efficiency (annex. 1) [25]. In fact, the production of natural polymer-derivative nanoparticle with MH is still a challenge without a perfect solution. MH is usually associated with poly-lactide-co-glycolic acid (PLGA) due to the more sustained release achieved, however PLGA NPs usually are produced with organic solvents as acetone and these nanoparticle can often present a toxicological profile, presenting accumulation in liver and bone marrow [31].

The NPs size was not changed significantly by the antibiotic incorporation, as well as the zeta potential (Fig. 2.1 f), probably positive by the presence of residual amino group which were unreacted with the TPP [25].

The release assay from MH-NPs showed an initial burst of 20% in the first 15 min and after, presented a more controlled antibiotic liberation until 24 h (Fig. 2.3). The possible reasons for the initial burst are the desorption of MH molecules located on the surface of the particles and/or some quantity of antibiotic lacking a strong interaction with the NPs as well as the MH water solubility, which can be related with a faster rate of the release [32,25]. In this study, MH-NPs reached an antibiotic concentration of 1.05 µg/mL in the first 30 min of the assay and, after 24 h, reached a cumulative concentration of 3.96 µg/mL, which is favorable for an initial antimicrobial activity and higher than the *P. gingivalis* minimal inhibitory concentration (MIC) for MH. Miyake et al. [33] worked with clinical isolates of *P. gingivalis* and obtained 0.031 µg/mL as MIC with MH while Zollinger et al. [34] obtained 0.25 µg/mL for *P. gingivalis* ATCC 33277. In addition, MH has been found to display a sustained reductive activity against other relevant subgingival pathogenic microorganisms, as *P. intermedius, E. eorrodens and F. nucleatum*, with a MIC at 90% less than 0.8 µg/mL [35].

Regarding the biological effects, outstanding results were observed, where the NPs presented significant improved results of the metabolic activity, with higher values at day 1 and day 6 when compared with the MH solution at the same concentration (Fig. 2.4). The positive effect of the b-NPs can be related with the presence of chitosan and apparently, there is a synergic effect when chitosan and MH are present regarding cytotoxic activity over fibroblastic cultures [36]. Studies observed that human gingival fibroblasts showed little, if any inhibitory effects on cell survival and mRNA osteogenic expression when exposed to MH until 5 µg/mL of concentration [6].

High levels of NPs uptake may interfere with the normal function of the endosomal/lysosomal compartments, leading to the disruption and remodeling of actin cytoskeleton and microtubule network, affecting cell area, spreading and cell ratio of with-over length [37,38]. In the present study, no significant alterations regarding cell morphology and actin cytoskeleton organization were verified, and no differences were found on cell area and cell skewness quantitative parameters (Fig. 2.5).

Aiming the use of NPs against intracellular infections, this study shows that MH-NPs were able to be uptaken by the HGFs (Fig. 2.6), which can play an important role for the treatment, once the main periodontal pathogens are capable of cellular internalization [9]. To the best of our knowledge, it is the first time that a study shows the uptake of chitosan NPs loaded with MH by HGFs *in vitro*.

Cellular internalization of chitosan NPs has been described to occur broadly through adsorptive endocytosis and clathrin-mediated endocytosis [39], allowing for a rapid overcoming of the cell membrane and, in drug-delivery strategies as verified in the present study, contributing to an increased intracellular drug concentration.

P. gingivalis is one of the major pathogens associated with periodontitis establishment and development with its LPS is being described to be a potent inflammatory inducer, modulating a phenotypic change in distinct cell populations, including HGFs [40]. Accordingly, HGFs culture incubation with *P. gingivalis* LPS for 24 h was found to increase significantly the expression of pro-inflammatory cytokines and chemokines, as presently verified.

MH has been found to reduce inflammatory activation associated with periodontal disease development [41], observed in this study with the MH solution, presenting anti-inflammatory activity in comparison with the control (Fig. 2.7). Proposed mechanisms include the ability to inhibit key inflammatory enzymes such as MMPs, TNF-α, NF-kB and IL-1β expression, further inhibiting the activation of inflammasome [13,42,43]. Also, previous works have sustained the anti-inflammatory properties of chitosan.

The use of chitosan oligosaccharide has been associated with the decrease of LPS-mediated release of inflammatory mediators [44], also observed in the present study, once the b-NPs presented some anti-inflammatory activity observed by the downregulation of inflammatory genes expression (Fig. 2.7). This process can be related with the inhibition of DNA-binding by the NF-kB transcription factor [45,46]. Moreover, a substantial downregulation in the inflammatory genes expression is observed in the MH-NPs group, presenting a higher downregulation when compared with the MH solution and the b-NPs, suggesting a synergic anti-inflammatory effect between the MH and the chitosan (Fig. 2.7).

In view of the results of this study, it is possible to conclude that chitosan nanoparticles could be considered an alternative form for local subgingival application of minocycline,

demonstrating anti-inflammatory and cellular proliferative effects that could complement the periodontal treatment and potentially reduce the tissue destruction.

Further studies should be conducted *in vitro* against the major periodontal pathogens, as well as *in vivo* studies to corroborate the previous results.

References

[1] Yao W, Xu P, Pang Z, Zhao J, Chai Z, Li X. Local delivery of minocycline-loaded PEG-PLA nanoparticles for the enhanced treatment of periodontitis in dogs. Int J Nanomedicine 2014;9:3963–70. doi:10.2147/IJN.S67521.

[2] Torshabi M, Nojehdehian H, Tabatabaei FS. In vitro behavior of poly-lactic-co-glycolic acid microspheres containing minocycline, metronidazole, and ciprofloxacin. J Investig Clin Dent 2017;8:1–8. doi:10.1111/jicd.12201.

[3] Lee BS, Lee CC, Wang YP, Chen HJ, Lai CH, Hsieh WL. Controlled-release of tetracycline and lovastatin by poly(D,L-lactide-co-glycolide acid)-chitosan nanoparticles enhances periodontal regeneration in dogs. Int J Nanomedicine 2016;11:285–97. doi:10.2147/IJN.S94270.

[4] Tilakaratne A, Soory M. Anti-inflammatory actions of adjunctive tetracyclines and other agents in periodontitis and associated comorbidities. Open Dent J 2014;8:109–24. doi:10.2174/1874210601408010109.

[5] Franco C, Patricia HR, Timo S, Claudia B, Marcela H. Matrix metalloproteinases as regulators of periodontal inflammation. Int J Mol Sci 2017;18:1–12. doi:10.3390/ijms18020440.

[6] Suzuki A, Yagisawa J, Kumakura S, Tsutsui T. Effects of minocycline and doxycycline on cell survival and gene expression in human gingival and periodontal ligament cells. J Periodontal Res 2006;41:124–31. doi:10.1111/j.1600-0765.2005.00843.x.

[7] Lu H, Liu Y, Guo J, Wu H, Wang J, Wu G. Biomaterials with antibacterial and osteoinductive properties to repair infected bone defects. Int J Mol Sci 2016;17:1–18. doi:10.3390/ijms17030334.

[8] Zhang W, Ju J, Rigney T, Tribble G. Porphyromonas gingivalis infection increases osteoclastic bone resorption and osteoblastic bone formation in a periodontitis mouse model. BMC Oral Health 2014;14:89. doi:10.1186/1472-6831-14-89.

[9] Zubery Y, Dunstan CR, Story BM, Kesavalu A, Ebersole JL, Holt SC. Bone resorption caused by three periodontal pathogens in vivo in mice is mediated in part by prostaglandin. Infect Immun 1998;66:4158–62.

[10] Finoti LS, Nepomuceno R, Pigossi SC, Secolin R, Scarel-caminaga RM. Association between interleukin-8 levels and chronic periodontal disease. Medicine (Baltimore) 2017;96:22.

[11] Bhattarai G, Poudel SB, Kook SH, Lee JC. Resveratrol prevents alveolar bone loss in an experimental rat model of periodontitis. Acta Biomater 2016;29:398–408. doi:10.1016/j.actbio.2015.10.031.

[12] Pan C, Liu J, Wang H, Song J, Tan L, Zhao H. Porphyromonas gingivalis can invade

periodontal ligament stem cells. BMC Microbiol 2017;17:1–10. doi:10.1186/s12866-017-0950-5.

[13] Garrido-Mesa N, Zarzuelo A, Gálvez J. Minocycline: Far beyond an antibiotic. Br J Pharmacol 2013;169:337–52. doi:10.1111/bph.12139.

[14] Yang Q, Nakkula RJ and Waters JD. Accumulation of Ciprofloxacin and Minocycline by Cultured Human Gingival Fibroblasts. J Dent Res 2002;81:836–40. doi:10.1037/a0018493.Understanding.

[15] Chiappe VB, Gomez M V, Rodriguez C, Fresolone M, Romanelli HJ. Subgingivally applied minocycline microgranules in subjects with chronic periodontitis: A randomized clinical and microbiological trial. Acta Odontol Latinoam 2015;28:122–31. doi:10.1590/S1852-48342015000200005.

[16] Ma S, Adayi A, Liu Z, Li M, Wu M, Xiao L. Asymmetric Collagen/chitosan Membrane Containing Minocycline-loaded Chitosan Nanoparticles for Guided Bone Regeneration. Sci Rep 2016;6:31822. doi:10.1038/srep31822.

[17] Silva T, Grenho L, Barros J, Silva J, Pinto R, Matos A. Minocycline-releasing PMMA system as a space maintainer for staged bone reconstructions – in vitro antibacterial, cytocompatibility and anti-inflammatory characterization. Biomed Mater 2017;12:35009. doi:10.1088/1748-605X/aa68b8.

[18] Almazin SM, Dziak R, Andreana S, Ciancio SG. The effect of doxycycline hyclate, chlorhexidine gluconate, and minocycline hydrochloride on osteoblastic proliferation and differentiation in vitro. J Periodontol 2009;80:999–1005. doi:10.1902/jop.2009.080574.

[19] Yoshinari N, Tohya T, Kawase H, Matsuoka M, Nakane M, Kawachi M. Effect of repeated local minocycline administration on periodontal healing following guided tissue regeneration. J Periodontol 2001;72:284–95. doi:10.1902/jop.2001.72.3.284.

[20] Uskoković V, Desai TA. Simultaneous bactericidal and osteogenic effect of nanoparticulate calcium phosphate powders loaded with clindamycin on osteoblasts infected with Staphylococcus aureus. Mater Sci Eng C 2014;37:210–22. doi:10.1016/j.msec.2014.01.008.

[21] Kashi TSJ, Eskandarion S, Esfandyari-Manesh M, Marashi SMA, Samadi N, Fatemi SM. 111 Solid/oil/water PLGA capsules protein. Int J Nanomedicine 2012;7:221–34. doi:10.2147/IJN.S27709.

[22] Croisier F, Jérôme C. Chitosan-based biomaterials for tissue engineering. Eur Polym J 2013;49:780–92. doi:10.1016/j.eurpolymj.2012.12.009.

[23] Azuma K, Osaki T, Minami S. Anticancer and Anti-Inflammatory Properties of Chitin and Chitosan Oligosaccharides. J Funct Biomater 2015;6:33–49. doi:10.3390/jfb6010033.

[24] Cadete A, Figueiredo L, Lopes R, Calado CCR, Almeida AJ, Gonalves LMD.

Development and characterization of a new plasmid delivery system based on chitosan-sodium deoxycholate nanoparticles. Eur J Pharm Sci 2012;45:451–8. doi:10.1016/j.ejps.2011.09.018.

[25] Nagpal K, Singh SK, Mishra DN. Formulation, optimization, in vivo pharmacokinetic, behavioral and biochemical estimations of minocycline loaded chitosan nanoparticles for enhanced brain uptake. Chem Pharm Bull (Tokyo) 2013;61:258–72. doi:10.1248/cpb.c12-00732..

[26] Ferreira IS, Bettencourt AF, Gonçalves LMD, Kasper S, Bétrisey B, Kikhney J. Activity of daptomycin- and vancomycin-loaded poly-epsilon-caprolactone microparticles against mature staphylococcal biofilms. Int J Nanomedicine 2015;10:4351–66. doi:10.2147/IJN.S84108.

[27] Silva MM, Calado R, Marto J, Bettencourt A, Almeida AJ, Gonçalves LMD. Chitosan nanoparticles as a mucoadhesive drug delivery system for ocular administration. Mar Drugs 2017;15:1–16. doi:10.3390/md15120370.

[28] Mosmann T. Rapid colorimetric assay for cellular growth and survival: Application to proliferation and cytotoxicity assays. J Immunol Methods 1983;65:55–63. doi:10.1016/0022-1759(83)90303-4.

[29] Duarte Junior AP, Tavares EJM, Alves TVG, de Moura MR, da Costa CEF, Silva Júnior JOC. Chitosan nanoparticles as a modified diclofenac drug release system. J Nanoparticle Res 2017;19. doi:10.1007/s11051-017-3968-6.

[30] Ahirrao SP, Gide PS, Shrivastav B, Sharma P. Ionotropic Gelation : A Promising Cross Linking Technique for Hydrogels . J Pharm Nanotechnol 2014;2:1–6.

[31] Bret UD, Lakshmi NS, Laurencin CT. Biomedical Applications of Biodegradable Polymers. J Polym Sci Part B Polym Phys 2011;3:832–64. doi:10.3390/polym3031377.Poly.

[32] Dou XC, Zhu XP, Zhou J, Cai H-Q, Tang J, Li QL. Minocycline-released hydroxyapatite-gelatin nanocomposite and its cytocompatibility in vitro. Biomed Mater 2011;6:025002. doi:10.1088/1748-6041/6/2/025002.

[33] Miyake Y, Tsuruda K, Okuda K, Widowati, Iwamoto Y, Suginaka H. In vitro activity of tetracyclines, macrolides, quinolones, clindamycin and metronidazole against periodontopathic bacteria. J Periodontal Res 1995;30:290–3. doi:10.1111/j.1600-0765.1995.tb02136.x.

[34] Zollinger L, Schnyder S, Nietzsche S, Sculean A, Eick S. In-vitro activity of taurolidine on single species and a multispecies population associated with periodontitis. Anaerobe 2015;32:18–23. doi:10.1016/j.anaerobe.2014.11.008.

[35] Vandekerckhove BNA, Quirynen M and Van-Steenberghe D. The use of locally-delivered minocycline in the treatment of chronic periodontitis . A review of the literature.

J Clin Periodontol 1998;25:964–8.

[36] Shi Z, Neoh KG, Kang ET, Wang W. Antibacterial and mechanical properties of bone cement impregnated with chitosan nanoparticles. Biomaterials 2006;27:2440–9. doi:10.1016/j.biomaterials.2005.11.036.

[37] Soenen SJH, Nuytten N, De Meyer SF, De Smedt SC, De Cuyper M. High intracellular iron oxide nanoparticle concentrations affect cellular cytoskeleton and focal adhesion kinase-mediated signaling. Small 2010;6:832–42. doi:10.1002/smll.200902084.

[38] Septiadi D, Crippa F, Moore TL, Rothen-Rutishauser B, Petri-Fink A. Nanoparticle-Cell Interaction: A Cell Mechanics Perspective. Adv Mater 2018;1704463:1–30. doi:10.1002/adma.201704463.

[39] Huang M, Ma Z, Khor E, Lim LY. Uptake of FITC-chitosan nanoparticles by A549 cells. Pharm Res 2002;19:1488–94. doi:10.1023/A:1020404615898.

[40] Bozkurt SB, Hakki SS, Hakki EE, Durak Y, Kantarci A. Porphyromonas gingivalis Lipopolysaccharide Induces a Pro-inflammatory Human Gingival Fibroblast Phenotype. Inflammation 2016:1–10. doi:10.1007/s10753-016-0463-7.

[41] Golub LM, Lee HM, Lehrer G, Nemiroff A, Mcnamara TF. Minocycline reduces gingival coiia-genoiytic activity during diabetes. J Periodontal Res 1983;18:516–126.

[42] Sun J, Shigemi H, Tanaka Y, Yamauchi T, Ueda T. Tetracyclines downregulate the production of LPS-induced cytokines and chemokines in THP-1 cells via ERK, p38, and nuclear factor-κB signaling pathways. Biochem Biophys Reports 2015;4:397–404. doi:10.1016/j.bbrep.2015.11.003.

[43] Kauppinen A, Salminen A, Kaarniranta K. Inflammation as a target of minocycline: special interest in the regulation of inflammasome signaling. Inflammasome 2013;3:2–14. doi:10.2478/infl-2013-0002.

[44] Qiao Y, Bai X, Du Y. International Immunopharmacology Chitosan oligosaccharides protect mice from LPS challenge by attenuation of inflammation and oxidative stress. Int Immunopharmacol 2011;11:121–7. doi:10.1016/j.intimp.2010.10.016.

[45] Li Yu, Liu Hongtao, Xu Qing-Song, Du Yu-Guang XJ. Chitosan oligosaccharides block LPS-induced O-GlcNAcylation of NF-κB and endothelial inflammatory response. Carbohydr Polym 2014;99:1–22. doi:10.1016/j.carbpol.2013.08.082.Chitosan.

[46] Azuma K, Osaki T, Kurozumi S, Kiyose M, Tsuka T. Anti-inflammatory effects of orally administered glucosamine oligomer in an experimental model of inflammatory bowel disease. Carbohydr Polym 2015;115:448–56. doi:10.1016/j.carbpol.2014.09.012.

Chapter 3. PDLLA scaffolds loaded with minocycline targeting bone regeneration and infection control

3.1. Introduction

Autologous bone graft has been commonly used for bone regeneration for large bone defects [1], however this type of graft presents associated drawbacks such as scarcity, the need of additional and painful surgery to harvest grafts, donor site morbidity and the difficulty of creating modifications that match the defect morphologies [2]. In the attempt to overcome these limitations, tissue engineering is being developed to be the future of critical size bone defect reconstructions by producing bone substitutes structurally similar to bones as three-dimensional scaffolds, with bioactive factors to mimic native bone development process [3,4]. As a temporary structure, scaffolds must present adequate mechanical properties, biodegradability and biocompatibility, degrading when new tissue and an extracellular matrix are formed [2]. Moreover, these structures should also present high porosity with interconnected pores facilitating cell migration, tissue ingrowth, neovascularization and the flow of nutrients and metabolic waste [3,5].

The scaffolding biomaterials applied to bone tissue engineering are principally made from natural bio-polymers, synthetic polymers or ceramic composites [6]. Natural bio-polymers, including collagen and chitosan present excellent biocompatibility and generally do not cause significant inflammatory responses when implanted into the body, however its usage may be limited owing to poor mechanical properties and a high degradation rate [7]. Ceramic composites, such as hydroxyapatite (HA) and calcium phosphates have excellent biocompatibility due to their chemical and structural similarity to the mineral phase of bones and bioactivity - an ability to bond directly to the surrounding bone tissue [7]. However, the slow degradation of these inorganic ceramics in the body and its unsatisfactory mechanical properties limits their utility for regenerative applications [6,7].

Synthetic polymers can overcome the limitations surrounding biopolymers and ceramics due to its controllable degradation rate, predictable mechanical properties, facility regarding the fabrication of different shapes and sterilization [7]. Among several options, polylactide (PLA) is one of the most interesting scaffolding polymers because it is easy to produce, shows good biocompatibility, its degradation products are non-toxic and it is approved by The Food and Drug Administration (FDA) for direct contacting with biological fluids [8,9]. There are three stereoisomers: poly(L-lactic acid) (PLLA), poly(D-lactic acid) (PDLA), and poly(D,L-lactic acid) (PDLLA). Among them, PDLLA presents improved osteoinductivity, mechanical properties and faster degradation [6,8]. However, all the stereoisomers present hydrophobicity and the low surface energy, affecting cell attachment and growth on the material [8].

To get over these disadvantages, researchers have tried to incorporate bioactive compounds as hydroxyapatite (HA) and bioactive glasses or functionalize the polymer surface. In fact, the addition of these compounds to polymer phases can improve the bioactivity of polymers, maintaining the mechanical advantages of the material [7].

45S5 Bioglass (BG) is a bioactive silicate glass known as an osteoinductive compound due to the enhancement of the secretion and gene expression of vascular endothelial growth factor (VEGF) [6]. Furthermore, the ionic dissolution products from BG can upregulate genes that control the osteoblast cycle, mitosis, and differentiation and can neutralize the acidic products from the degradation of polymers, avoiding a possible inflammatory response caused by these degradation products [3,5]. Larrañaga et al. [3,5] produced porous scaffolds with different polymers containing BG and positive results were obtained regarding the deposition of a mineral layer on the surface of the material and the osteogenic differentiation of stem cells.

About surface modification, several methods are described in the literature and one example is the alkali hydrolysis method, aiming the chemical change of the polymer surface by the cleavage of the ester bonds, producing hydrophilic polar carboxyl and hydroxyl groups [10]. For instance, Yang et al. [10] tested PLLA immersion in a low concentration of alkali solution and ethanol in a 1:1 (V/V) with different periods and concluded that treating 4 to 6 h is enough for improving the surface hydrophilicity, surface energy and surface roughness of PLLA without altering its bulk properties.

Going further, Guo et al. [11] tested a similar alkali hydrolysis method with an acidic wash right after the immersion, obtaining improved results regarding water contact angle and roughness of PLA comparing with the alkaline step only, which was favorable for the further surface coating process and Chen et al. [12] produced PLLA scaffolds and then coated the polymer with apatite/collagen for improved cells adhesion and proliferation.

One of the main concerns about bone grafts surgery is the risk of infections that can lead to a second intervention for the removal of contaminated bone graft and necrotic tissue, once bacteria related with osteomyelitis *as Staphylococcus aureus* is frequently present in human skin and oral surgeries are conceptually clean-contaminated [13,14]. At the moment, antibiotic prophylaxis is the standard approach for infection prevention using systemic antibiotic administration before and after the surgery [15]. Nevertheless, this mode of administration can lead to low local antibiotic concentration in the surgical wound and side effects such as altered host microbiome, bacterial resistance and allergic reactions [16,17]. Grafts containing antibiotics and capable of a controlled drug delivery could avoid those negative effects, however mixing the antibiotic powder with polymers before manufacturing the graft can inactivate and/or degrade the drug due to elevated temperatures and harsh chemicals as organic solvents [15]. Furthermore, post-processing steps such as porogen leaching or solvent evaporation can cause the premature release or deactivation of incorporated antibiotics [18].

Considering the previous information, we conjectured that a 3D porous PDLLA scaffold containing 45S5 bioglass, with the surface changed by alkali hydrolysis technique and loaded with collagen and minocycline hydrochloride (MH) – an antibiotic with broad spectrum, anti-inflammatory and osteoinductive effects [19], would be able to provide an enhanced bone regeneration with antimicrobial protection.

3.2. Materials and Methods

3.2.1. Materials

Poly-DL-lactic acid (Purasorb, Purac kindly donated by University of Basque Country), dichloromethane (molecular weight 84.93, Sigma Aldrich), sodium chloride (molecular weight 58.44, Honeywell, Fluka), bioactive synthetic graft (45S5 Bioglass, Novabone kindly donated by University of Basque Country), collagen hydrolysate type I fibrillar (kindly donated by Dra Mădălina Kaya from Department of Collagen Research, Romania [20]), ethanol anhydrous (molecular weight 46, Carlo Erba), citric acid monohydrate (molecular weight 214.14, Merck), minocycline hydrochloride (kindly donated by Atral Cipan, Portugal), sodium hydroxide (molecular weight 40, Akzo Nobel) and the silicon molds (kindly donated by University of Basque Country).

3.2.2. Preparation of solvent casting leaching scaffolds

The PDLLA porous scaffolds were prepared accordingly with [21] by solvent casting/particulate leaching using dichloromethane (DCM) as solvent and sodium chloride particles (355-500 mm) as porogen (Fig. 3.1). First, PDLLA was dissolved in DCM and then mixed and homogenized with the bioglass (BG) and then, salt particles were added in an approx. 1:9 (w/w) polymer to salt ratio. The mixture was transferred to a flexible square silicon mold (10x10x10mm) and the samples were placed in a vacuum chamber at 25°C overnight, in order to eliminate the DCM. After, scaffolds were placed in distilled water for 24 h under magnetic stirring to leach out the salt particles and then, samples were immersed in ethanol 70% (V/V) for 24 h aiming sterilization. Finally, samples returned to the vacuum chamber and were submitted to the same conditions to dry the scaffolds.

Figure. 3.1. Scaffolds sequence preparation: (A) is the PDLLA dissolution with DMC and the mixing of BG, followed by the porogen (salt) addition; (B) corresponds to the final mixture being transferred to a flexible square silicon mold; (C) shows the prepared samples in a vacuum chamber to eliminate the solvent.

3.2.3. Scaffolds surface treatment and functionalization

After the production scaffolds were submitted to alkali treatment, which consists in a 1 h immersion in a 1:1 NaOH 0.25M and ethanol 100% solution at room temperature under mixing plate (LD-40, Labinco) at 200 rpm [10]. After, samples were washed with citric acid 0.5%, and deionized water [11]. Subsequently, the samples were immersed in an adsorption solution containing 5 mg/mL of collagen (Col) (Col-PDLLA, Group 2) or 0.5 mg/mL of MH + 5 mg/mL of Col (MH-Col-PDLLA, Group 3) at room temperature and 200 rpm under mixing for 24 h and afterword dried in a dissector for at least 48 h. Samples without functionalization were used as negative control in some assays (PDLLA, Group 1). The procedure is illustrated by Fig. 3.2 and the groups by Table 3.1.

Table 3.1. Samples were divided in groups by the surface treatment and adsorption performed.

Group 1	Group 2	Group 3
PDLLA	Col-PDLLA	MH-Col-PDLLA
- BG within polymer - No treatment - No adsorption	- BG within polymer - Alkali treatment - Col adsorption	- BG within polymer - Alkali treatment - Col + MH adsorption

Abbreviations: BG – Bioglass 45S5; Col – Collagen solution 5 mg/mL; MH – minocycline hydrochloride solution 0.5 mg/mL.

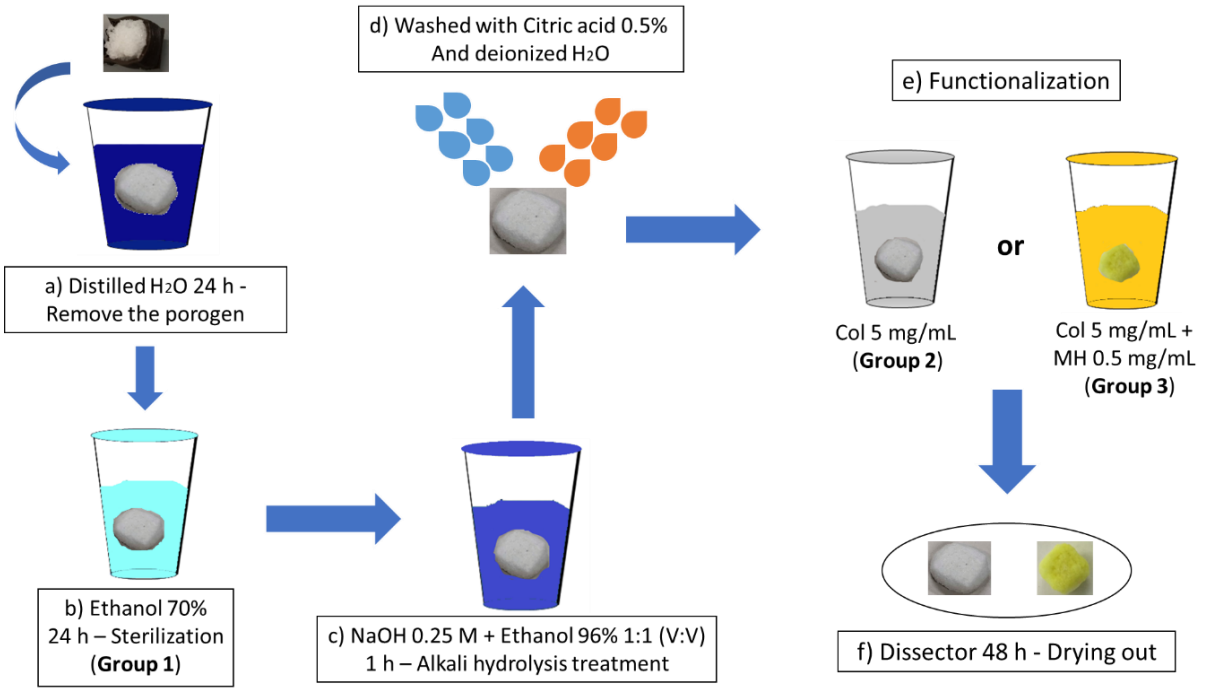

Figure 3.2. The sequence of procedures involving the removal of porogen, surface treatment and functionalization of the scaffolds.

3.2.4. Physico-chemical characterization of scaffolds

The morphological characterization of the Col-PDLLA (Group 2) and MH-Col-PDLLA (Group 3) surface was performed by scanning electron microscopy (SEM) using a JEOL-JSM7001F apparatus, as well as the elemental chemical composition by the respective X-ray energy dispersive spectrometer (EDS). To increase the conductivity of the samples a thin coating of conductive chromium (Polaron E-5100) was added. The crystalline structure was identified by X-ray diffraction (XRD) using a D8 Advance Bruker AXS θ-2θ diffractometer with a copper radiation source (Cu Kα, λ = 1.5406 Å) and a secondary monochromator operated at 40 kV and 40 mA over a 2θ range of 8° to 70°. Attenuated total reflectance (FT-IR/ATR) in transmittance mode was used to identify the functional groups present in the scaffolds, in the range of 600-4000 cm^{-1} using a Nicolet (Thermo Electron) spectrometer.

3.2.5. Minocycline release

Specimens of the groups described before were incubated in a 50 mL Falcon tube with 3 mL of two different solutions, Hepes 10 mM at pH 7.4 and a solution of NaCl 0.9%(m/V) with 0.05%(V/V) Tween20® at pH 5.0, in a shaking water-bath (Memmert) at 37 °C [22]. At predetermined time intervals throughout a 72 h period, aliquots of the supernatant were collected and analyzed in triplicate. The withdrawn aliquots were then replaced with equal volumes of fresh release solution and the medium was changed each 8 h. Minocycline content was determined by UV detection at 350 nm by a microplate reader (FLUOstar Omega, BMG Labtech).

3.2.6. Microbiological assays

Staphylococcus aureus (ATCC 25923) obtained from American Type Culture Collection (ATCC) was stored in 20% of glycerol in TSB and frozen at -80ºC. Aliquots from frozen stocks were used to culture microorganisms in Tryptic Soy Agar (TSA) for 24 h at 37ºC [23].

3.2.6.1. Antimicrobial activity of scaffolds

S. aureus inoculum was prepared following the guidelines of the Clinical and Laboratory Standards Institute (CLSI) [24]. Briefly, few colonies of *S. aureus* were spread into Mueller Hinton Broth (Biokar Diagnostics) and further diluted in order to achieve 0.5 McFarland units (1×10^8 CFU mL^{-1}) at 600 nm of wavelength, using the spectrophotometer (U-2000, Hitachi). The inoculum was swabbed on Mueller Hinton Agar (Biokar Diagnostics) plates and the scaffold samples were tested (Group 2 and 3), as well as the 6 mm filter disks containing 10µL of distilled water (negative control) or 10 µL of 3 mg/mL of MH aqueous solution (positive control). The petri dishes were further incubated (Ultima, Revco) at 37°C for 20 h. After the incubation period, the diameter of inhibition zone of the samples and the controls was measured three times with a vernier caliper. Assays were performed in three independent experiments.

3.2.6.2. Antimicrobial activity of release medium supernatants

The antimicrobial susceptibility of *S. aureus* to MH standard solution and to release medium supernatants was obtained by the Broth Microdilution Method described by CLSI [23,25]. All assayed samples were two-fold diluted in Müeller-Hinton broth (Biokar Diagnostics, France) and the final MH concentration ranged from 0.0078 to 2 µg/mL. *S. aureus* inoculum was prepared according to CLSI in Müeller-Hinton broth. Briefly, a 1×10^8 CFU/mL *S. aureus suspension* was obtained (as previously described in 3.2.6.1), further diluted to 1×10^6 CFU/mL and 100 µL of this last suspension were used to inoculate the microtiter plate wells reaching a final volume of 200 µL. Plates were incubated at 37°C for 16-20 h and afterwards visible growth of bacteria was inspected and absorbance at 595 nm was measured in a Microplate Multimode Detector (Anthos, Zenyth 3100). The lowest concentrations of MH that was able inhibit the visible growth of bacteria was considered the minimal inhibitory concentration (MIC).

All assays were performed with negative controls (not inoculated media) and positive controls (inoculated media). *Levofloxacin* was used as a quality control standard to guarantee that the test system performed as expected. Assays were carried out in three independent experiments.

3.2.6.3. Biofilm inhibition

PDLLA scaffolds were fixed at the bottom of a well in a 24-well-microtiter plate inside an airflow chamber. inoculum was prepared from direct colony suspension of *S. aureus* (24 h slants), adjusted to 3×10^8 CFU mL^{-1} and further diluted in BHI medium with glucose at 1% (W/V). In each well of the 24-well microtiter plate, containing PLA scaffolds, the final inoculum concentration was 3×10^6 CFU mL^{-1}.

Scaffolds without being inoculated were used as negative controls and Col-PDLLA (group 2) samples were used as positive controls [26]. After 24 h of incubation at 37ºC, samples were washed twice with PBS and fixed with different ethanol solutions, 75, 90 and 100% (v/v) for 40 min and the biofilm evaluation was performed by SEM analysis (JSM7001F-JEOL). To increase the conductivity of the specimens they were coated with a thin layer of conductive gold film, under vacuum in an argon atmosphere (Quorum Technologies, Polaron E5100).

3.2.7. Cytocompatibility Analysis

The cytocompatibility of the scaffolds was conducted *in vitro* by assessing the functionality of cultured human osteoblast cell line (MG-63, ATCC®CRL-1427™) in the presence of the samples and the antibiotic solution. The osteoblasts were expanded in RPMI 1640 culture medium (Life Technologies, UK), supplemented with 10% Fetal serum bovine (Life Technologies, UK), 100 units/mL of penicillin G (sodium salt) (Life Technologies, UK), 100 µg/mL of streptomycin sulfate (Life Technologies, UK), and 2 mM L-glutamine (Life Technologies, UK), at 37 °C and 5% CO_2 [22]. After reaching confluency, the cells were trypsinized and subcultured at 10 000 cells/cm^2 for further studies. Cells of the 6th passage were used. MG-63 cells were exposed to MH solution at concentrations between 0.098 and 200 µg/mL, as well as PDLLA (Group 1), Col-PDLLA (Group 2) and MH-Col-PDLLA (Group 3) samples.

3.2.7.1. Cell viability assays

In vitro cellular proliferation was investigated using alamarBlue® assay. The technique is based on the conversion of resazurin to the fluorescent by-product resorufin, by metabolically active and viable cells [27]. The half inhibitory concentration (IC50) was performed with 24 h-adhered cells exposed to MH solution with the previously range concentration at 37°C, 5% CO_2 until 48 h and cells without MH were used as negative control, while cells with 1 mg/mL sodium dodecyl sulfate (SDS) were used as positive control. Cell viability was assessed after 2 h of incubation with the resazurin solution and then resorufin fluorescence was determined (excitation: 530 nm, emission: 590 nm) by microplate reader (FLUOstar Omega, BMGLabtech, Germany).

To evaluate the scaffolds, cells were cultured with the 3 groups (PDLLA, Col-PDLLA or MH-Col-PDLLA) up to 28 days in a 24-well plate (non-treated surface, Costar, Corning

Incorporated) at 37 °C, 5% CO_2. The assay was performed once a week, where seeded scaffolds were changed to an empty well and put with new medium and incubated in a alamarBlue® solution at 37 °C for 2 h. The fluorescence was determined as described before. MG-63 cells cultured on the scaffolds were also qualitatively evaluated for cell viability using MTT assay, based on the conversion of a tetrazolium salt (MTT) into formazan crystals by viable cells [28]. After 28 days the seeded scaffolds were exposed to 50 µL of MTT solution (5 mg/mL) followed by 2 h incubation at 37 °C. Then the supernatant was removed and the pictures of the scaffolds with the formazan crystals were taken (Canon Powershot 35mm 6x zoom and microscope Meiji Techno TC 5400).

3.2.7.2. Alkaline phosphatase (ALP) activity

Proliferating osteoblasts show ALP activity which is greatly enhanced during *in vitro* bone formation and can be detected using 5-bromo-4-chloro-3-indoyl phosphate (BCIP) as a substrate solution, where the BCIP is hydrolyzed by alkaline phosphatase enzyme, producing an indigo dye and staining the cells with a blue-violet color [29].

MG-63 cells cultured with the scaffolds were qualitatively evaluated for ALP activity. After 28 days of scaffolds colonization, cells were washed 2 times with sodium chloride solution 0.9% and 500 µL of 5-bromo-4-chloro-3-indolyl-phosphate, 4-toluidine salt (BCIP-NBT, Sigma-Aldrich) solution was added and cells were incubated for 30 min at 37 ºC. After, photos of the stained scaffolds were taken (Canon Powershot 35mm 6x zoom and microscope Meiji Techno TC 5400).

3.2.8. Statistical Analysis

Statistical analysis was conducted with GraphPad Prism 6.01 software. All the data sets were identified by Shapiro-Wilk normality test as non-parametric data. The Mann-Whitney U test was performed for two group only data sets while Kruskal-Wallis followed by multiple comparisons using Dunn's tests was performed for multiple groups. Data is expressed as mean and standard deviation (SD). For all the assays, a P value < 0.05 was considered as statistically significant.

3.3. Results

3.3.1. Characterization of 3D PDLLA scaffolds

The Col-PDLLA (Group 2) and MH-Col-PDLLA (Group 3) were compared. All samples presented a sponge appearance and the color was different between them, where MH-Col-PDLLA presented a strong yellowish accent while Col-PDLLA presented the original white color of the polymer (Fig. 3.3, h). SEM images were displayed in Fig. 3.3 (a. to d.) and no differences were detected between groups. Both groups showed a variable porous size as well as interconnections among the bigger porous and the surface seems to be rough due to surface treatment (alkali hydrolysis). No salt or BG particles were observed.

XRD analysis showed the MH-Col-PDLLA group presents a distinct peak from the Col-PDLLA sample, suggesting the presence of the antibiotic in the polymer, however the crystallinity between groups is not significant different, illustrated by Fig. 3.3 (e.).

EDS analysis showed no important differences between the groups, none of components used in surface treatment were found in the samples, suggesting that the NaOH, ethanol and the citric acid were removed and unable to be incorporated on the surface of the polymer. EDS also showed that the BG particles were successfully incorporated to the scaffolds and the post-treatment steps, namely drying, sterilization and functionalization (adsorption of col or MH) were unable to remove or degrade the BG particles (Fig. 3.3, f).

A possible intermolecular interaction between the antibiotic and the polymer was qualitatively evaluated through FTIR-ATR analysis. The assay compared the intensity of the MH, MH-Col-PDLLA and Col-PDLLA and results showed new peaks in the analysis of MH-Col-PDLLA in comparison with the antibiotic and the Col-PDLLA, evidencing chemical interactions between the antibiotic and the polymer. The primary amine N–H deformation vibrations is detected at 1537 cm^{-1}; the small shoulder at 1649 cm^{-1}, corresponding to primary amide C═O bond stretching vibrations, between 2941 and 2881 cm^{-1} related to –CH– stretching vibrations The band at 3436 cm^{-1} was assigned to O-H stretching vibrations, illustrated by Fig. 3.3 (g).

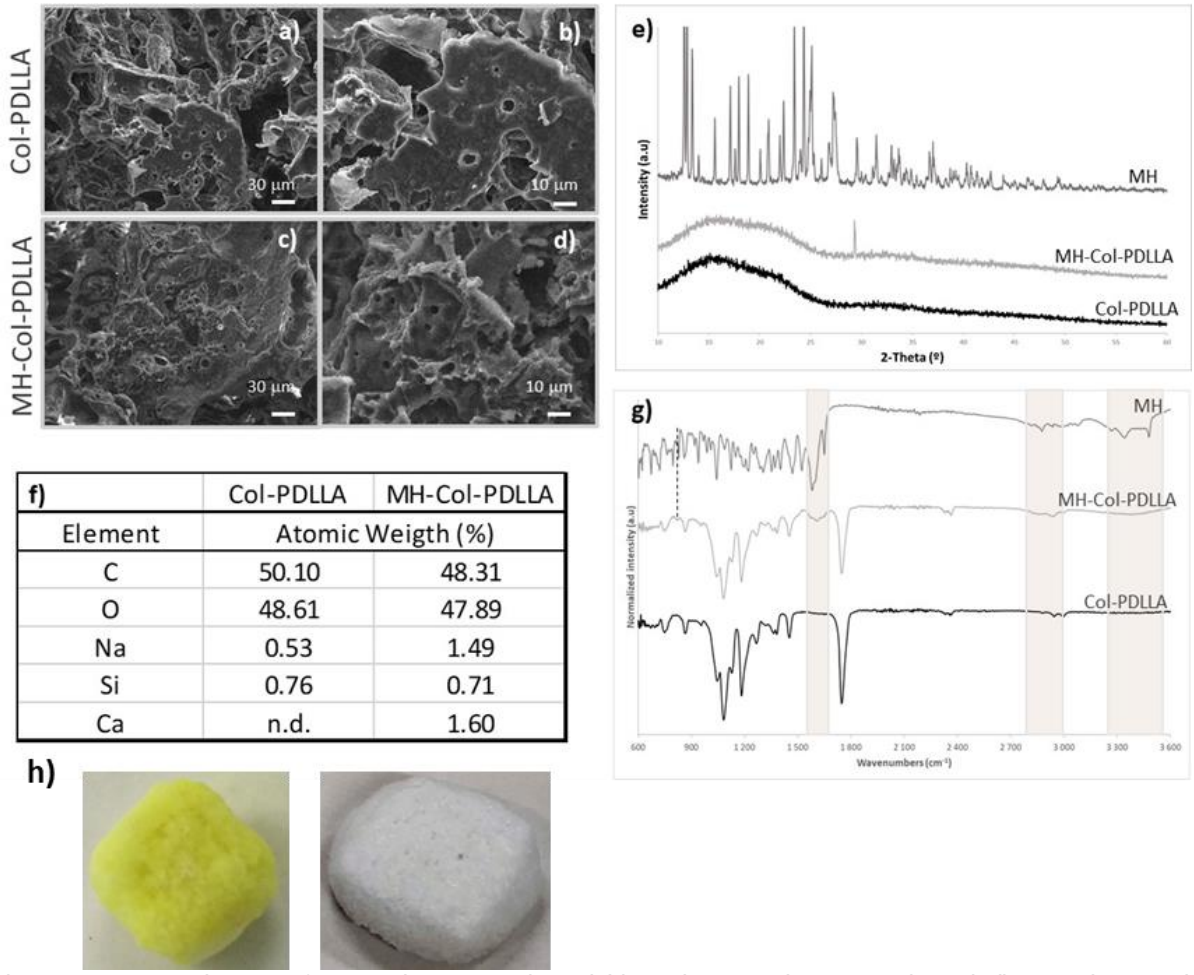

f)	Col-PDLLA	MH-Col-PDLLA
Element	Atomic Weigth (%)	
C	50.10	48.31
O	48.61	47.89
Na	0.53	1.49
Si	0.76	0.71
Ca	n.d.	1.60

Figure 3.3. SEM images from Col-PDLLA a) and b) and MH-Col-PDLLA c) and d) samples. Both presented a rough surface with porous in variable sizes and interconnectivity among them. No significant differences between groups were observed; e) XRD analysis showed no significant differences between MH-Col-PDLLA and Col-PDLLA samples regarding crystallinity degree, but also showed one peak different in the presence of the antibiotic, suggesting the presence of MH in the sample; f) EDS analysis showed the bioglass composition in the scaffolds and no alterations in the presence of the MH; g) FTIR-ATR results showed different patterns among the samples, using a wavelength range between 600 and 3600 cm^{-1}. Results suggest that the antibiotic modified the polymer surface, showing different peaks close to 1750 cm^{-1}, between 2800 to 3000 cm^{-1} and 3000 to 3600 cm^{-1}; h) the color difference after the MH adsorption on the polymer.

3.3.2. Minocycline release

MH was detected in the supernatant until 72 h of assay using water + NaCl + Tween20, at pH 5.0, with an initial burst release and reaching a cumulative concentration of 50.3 ± 19.2 µg/mL (Fig. 3.4). However, with the Hepes solution at pH 7.4, no detectable amount of MH was measured. The media were changed every 8 h in both assays. The results suggest that the antibiotic was bounded with the polymer, preventing the release of MH from the scaffold to the medium and this hypothesis is based on the FTIR-ATR and XRD analysis, where differences between the groups were detected in both assays (Fig. 3.3 e and g).

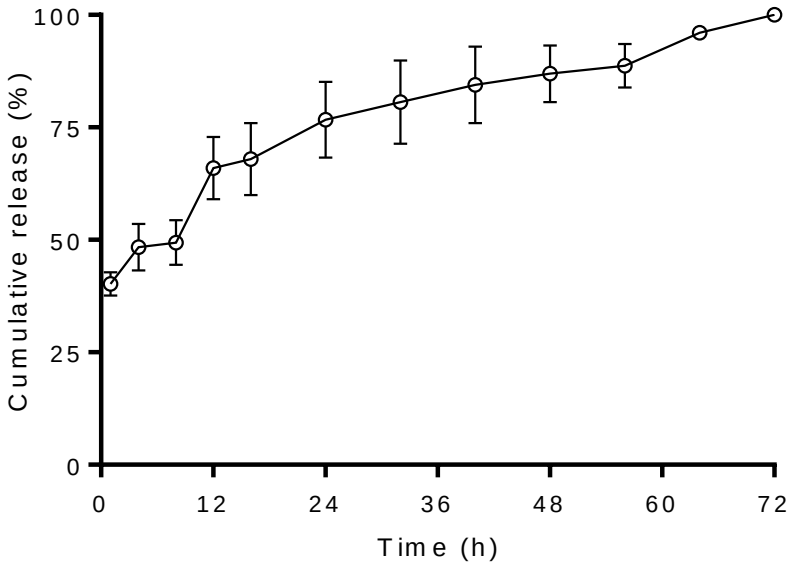

Figure 3.4. Cumulative release of the antibiotic from the MH-Col-PDLLA samples. Cumulative release is the relation of the partial with the total amount of MH released, where 100% corresponds to the concentration of the drug by 72 h. A controlled release was observed. Medium was changed every 8 h. Mean ± SD (n = 3).

3.3.3. Microbiological assays

3.3.3.1. Antimicrobial activity of scaffolds

After measuring the diameter of the inhibition zone produced by the samples and the antibiotic control (30 µg of MH), it was observed that MH-Col-PDLLA samples produced a diameter average of 27.69 ± 2.01 mm while the Col-PDLLA samples did not present any inhibition zone. The positive control exhibited a diameter average of 28.77 ± 0.70 mm, in accordance with the expected results for MH and *S. aureus* ATCC 25923 (25 to 30 mm) [24].

3.3.3.2. Antimicrobial activity of release medium supernatants

Results suggest that the MH antimicrobial activity was not affected by the production steps of adsorption, drying and storage, as well as the polymeric linkage. Both MH solution and MH-Col-PDLLA samples obtained the same minimal inhibitory concentration of 0.0625 µg/mL. Levofloxacin was used as an external control and the obtained MIC was 0.25 µg/mL, showing a high susceptibility of the used strain for minocycline and levofloxacin.

3.3.3.3. Biofilm inhibition

The biofilm formation inhibition was evaluated by SEM (Fig. 3.5), where it was observed that MH-Col-PDLLA samples presented a significant decrease in biofilm formation when comparing to the Col-PDLLA samples, which presented *S. aureus* biofilm covering the surface, with cells morphology looking similar to that of normal staphylococcal cells.

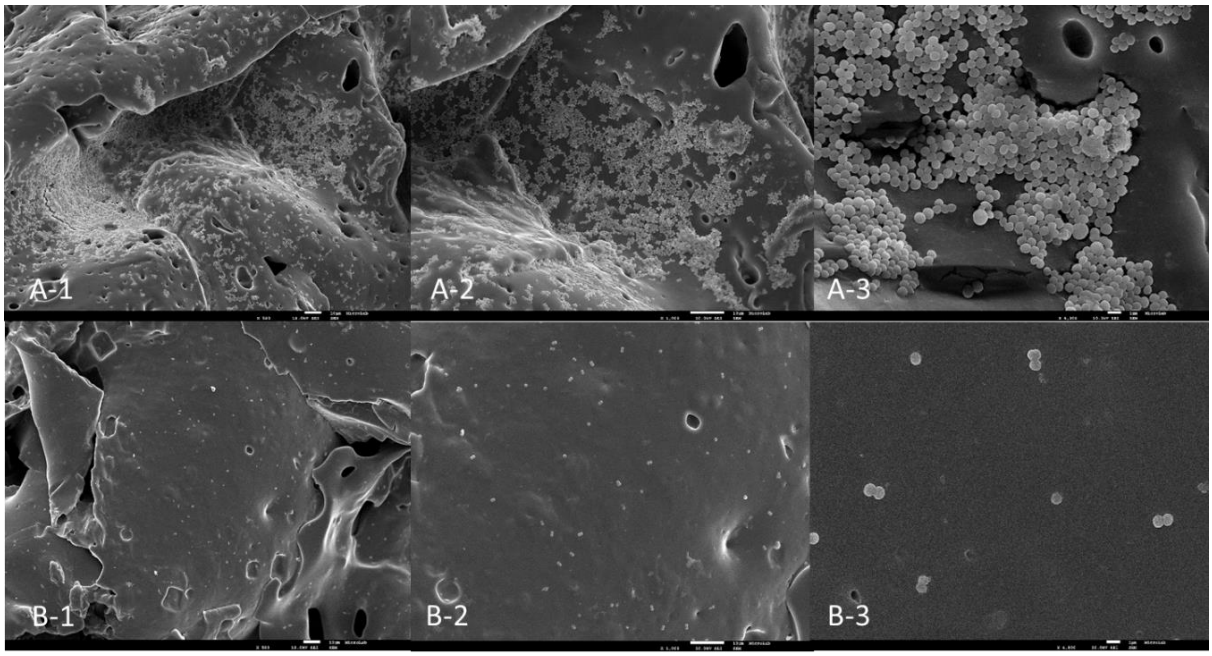

Figure 3.5. SEM images of the PDLLA surface samples, showing the presence of numerous *S. aureus* colonies on the surface of Col-PDLLA samples (A) and an important reduction of colonies on the surface of MH-Col-PDLLA samples (B). 1, 2 and 3 correspond to 500, 1000 and 4000x magnification, respectively.

3.3.4. Cytocompatibility Analysis

The IC50 data of MG-63 cells incubated with MH solution is illustrated by Fig. 3.6. The obtained values for 24 and 48 h of incubation are 67 µg/mL and 55 µg/mL respectively, using the alamarBlue technique.

After, as an exploratory assay, cells were incubated with small pieces of Col-PDLLA (Group 2) and MH-Col-PDLLA (Group 3) samples for 28 days and the alamarBlue was performed once a week during the incubation (Fig. 3.7). The MG-63 cells were found to proliferate actively over the surface of the assayed scaffolds during the 28 day culture period and the MH-Col-PDLLA scaffolds presented higher values from week 2 to 4, while the Col-PDLLA scaffolds presented higher values only in the first week.

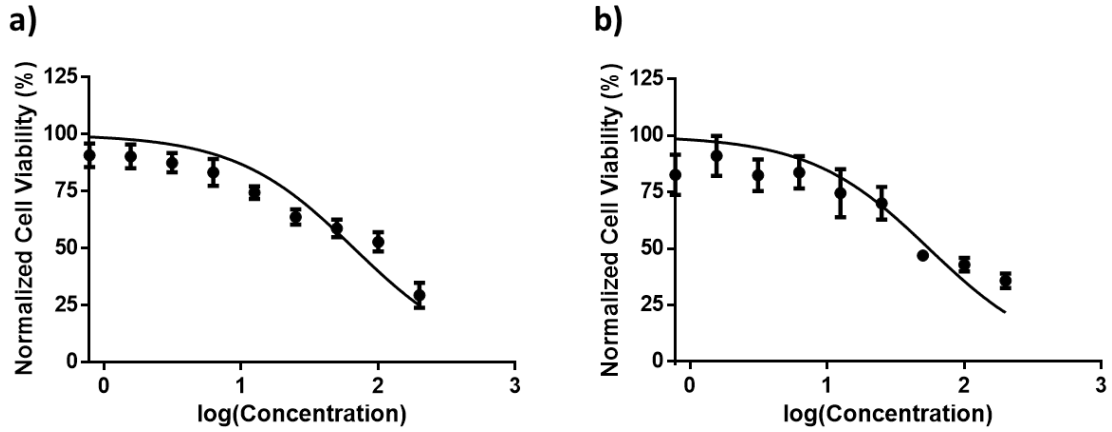

Figure 3.6. Effect of MH solution on IC50 of the MG-63 cell line; a) and b) corresponds to the IC50 using alamarBlue for 24 and 48h, respectively. Mean ± SD (n = 6).

With the preliminary results, the complete assay was performed using the same scaffold size as the microbial assays as well as PDLLA (Group 1) samples, where the cells were cultured with scaffolds during 28 days as previously described. AlamarBlue was performed once a week and after the 28 days and the MTT assay was performed only at 28 day measurement in order to show the formazan crystals inside and on the surface of the samples. However, these scaffolds were bigger and contained more MH than the samples previously tested, resulting in an increased released MH. Results found out that the MH-Col-PDLLA samples drastically decreased the cell viability (Fig. 3.8), confirmed with the MTT coloration (Fig. 3.9 and 3.10). Comparing the PDLLA and the Col-PDLLA scaffolds, Col-PDLLA presented higher fluorescent values in all measurements and a stronger staining by the formazan crystals (Fig. 3.9), showing a higher cell proliferation on this scaffold. In agreement with higher cell surface growth, the ALP activity assay using the BCIP/NBT solution, presented the same trend, where the samples containing MH showed a very poor staining due to the reduced number of cells, while the PDLLA and Col-PDLLA scaffolds presented the expected staining (Fig. 3.11).

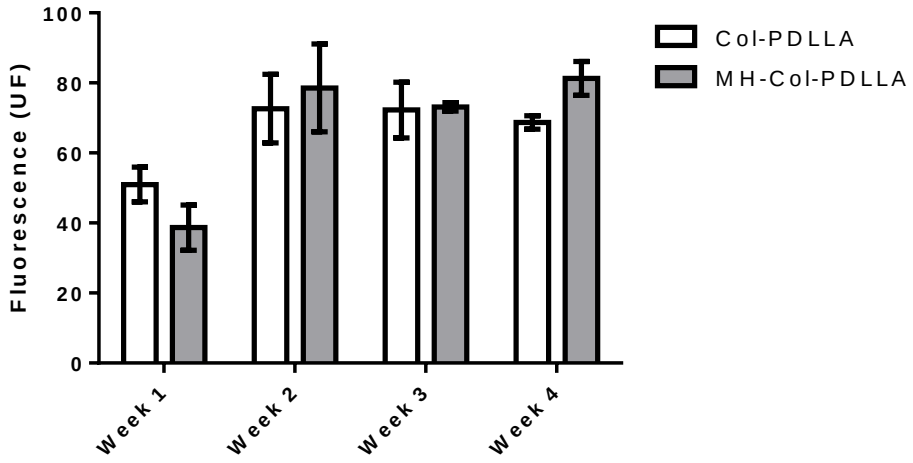

Figure 3.7. Preliminary alamarBlue assay showing the metabolic activity of the MG-63 cells when cultured with the smaller scaffolds for 28 days. Mean ± SD (n = 3). No significant differences were found between the groups.

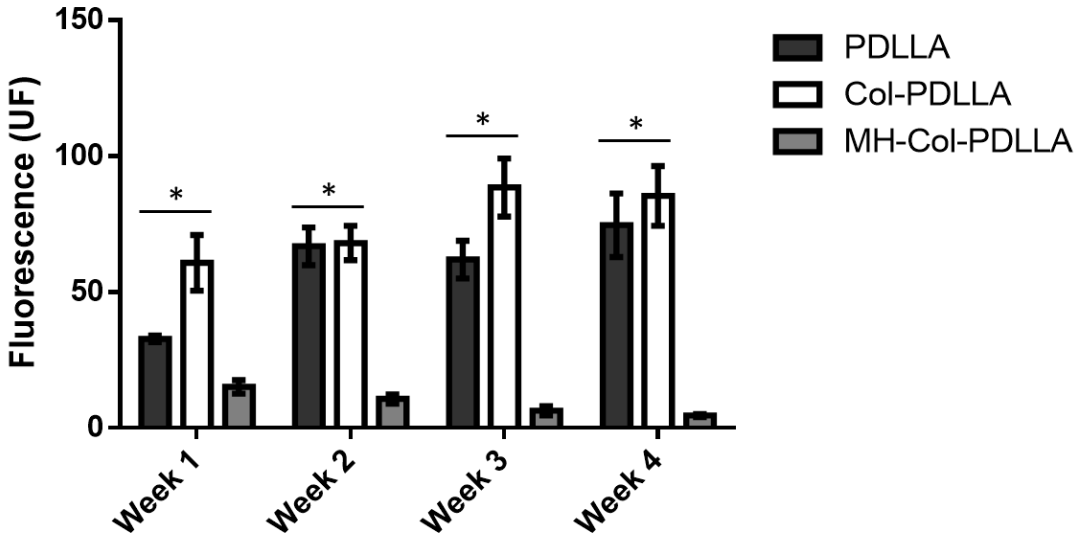

Figure 3.8. AlamarBlue assay showing the metabolic activity of the MG-63 cells when cultured with the larger size scaffolds, presenting an increase for Col-PDDLA group and an important reduction of the cell viability for the MH-Col-PDLLA samples. Mean ± SD (n = 6). *significant different ($P< 0.01$) from MH-Col-PDLLA. No significant differences were found comparing PDLLA and Col-PDLLA groups or PDLLA and MH-Col-PDLLA groups.

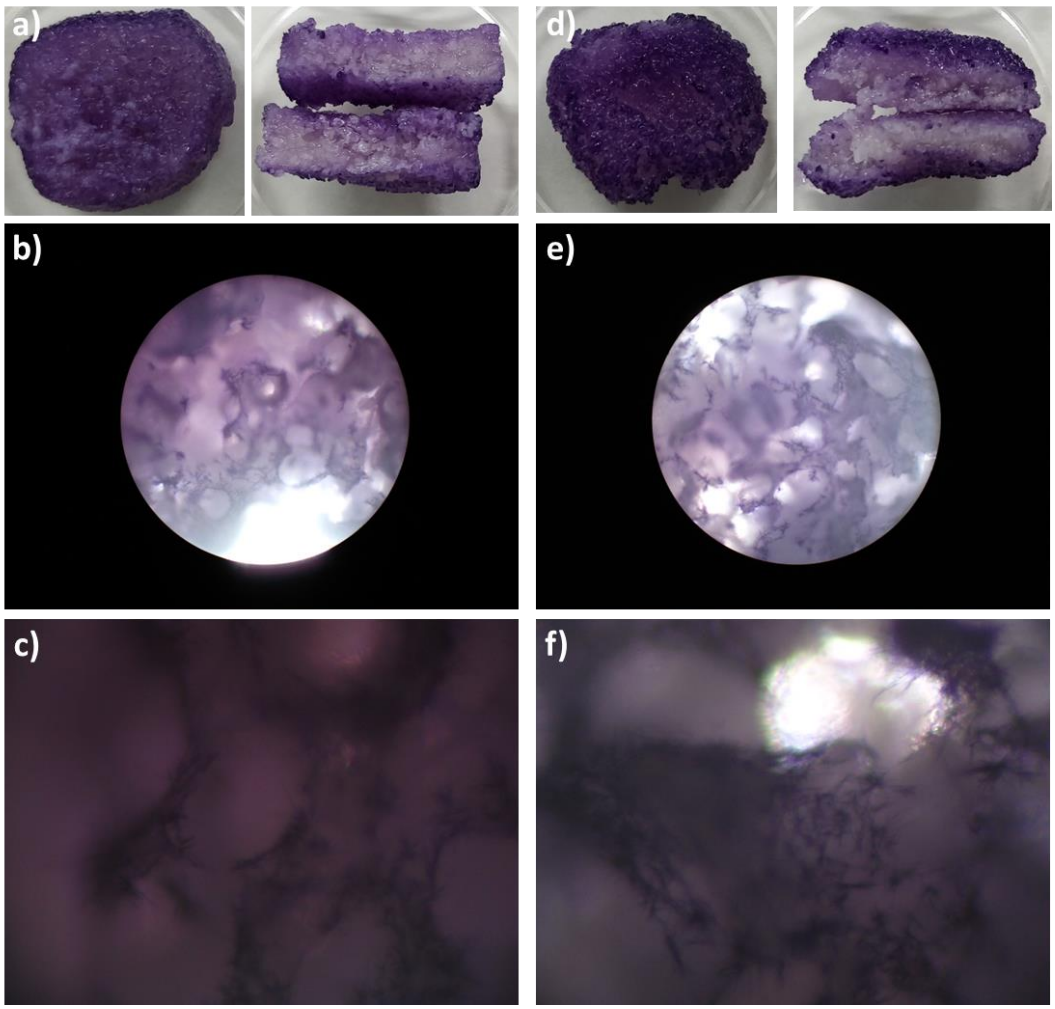

Figure 3.9. The qualitative MTT assay of the seeded scaffolds, showing the presence of the formazan crystals formed by the MTT reduction by the cells on the surface and inside the samples after 28 days of cell culture; a), b), c) corresponds to PDLLA samples, where b) is 100x magnification and c) 600x magnification; d), e), f) corresponds to the Col-PDLLA samples, with the same magnifications (n = 3).

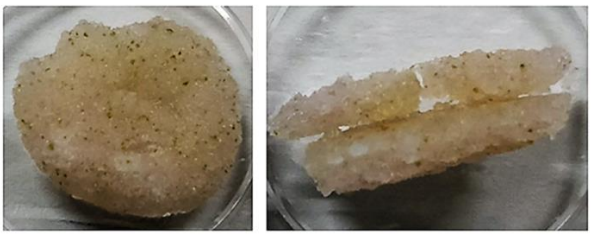

Figure 3.10. The qualitative MTT assay of the MH-Col-PDLLA scaffolds after 28 days of cell culture, showing the lack of the formazan crystals, confirming the resazurin assay, where the number of viable cells was drastically lower than the other samples (n = 3).

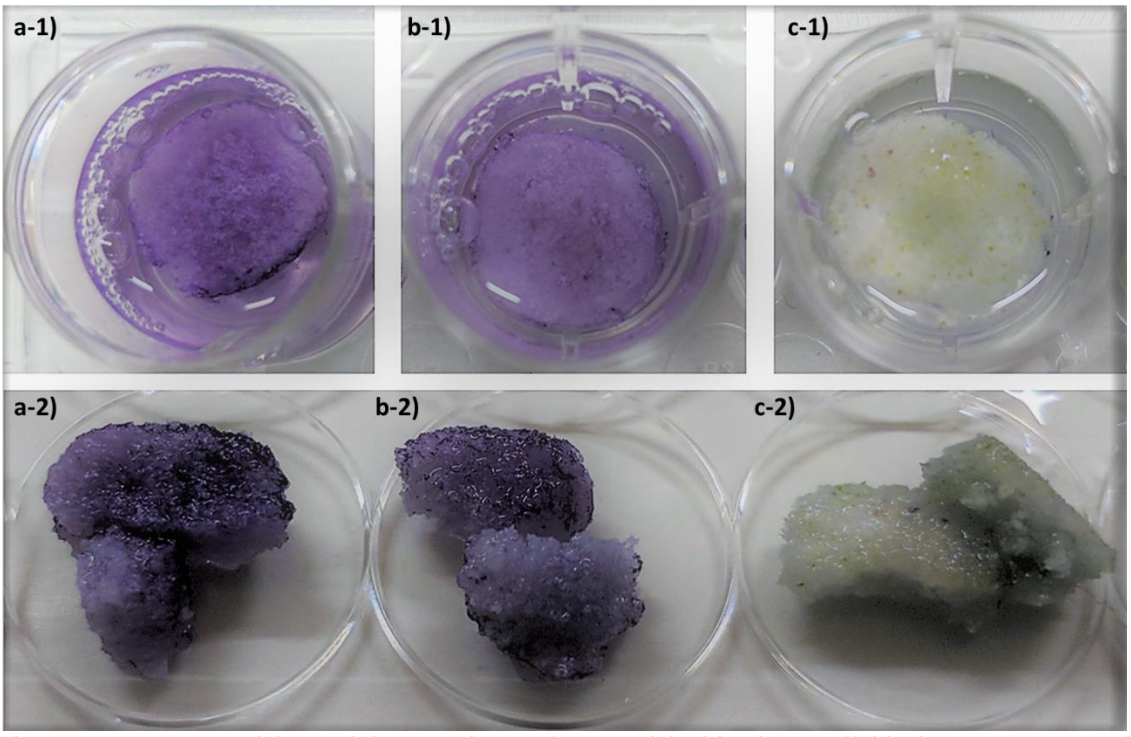

Figure 3.11. ALP activity staining on the surface and inside the scaffolds by BCIP-NBT substrate solution. The activity of the enzyme is related with osteoblasts proliferation and bone formation by the cells after 28 days of cell culture. The PDLLA samples (a-1) and 2) and Col-PDLLA (b-1) and 2) presented the blueish/purple coloration expected of MG-63 cells, which is not observed for the MH-Col-PDLLA (c-1) and 2) samples due to the reduced cell number (n = 3).

3.4. Discussion

In the present study, the approach to produce the 3D scaffolds containing BG was based on previous studies [3], where the solvent casting/salt leaching – a technique which presents an easy control of porosity and geometry [21] was used and modified regarding the amount of BG (10% instead of 15%) and the porogen size, maintaining the percentage of the porogen (90%). In comparison to other studies [3,21], a larger porogen particle (355 – 500 µm) was elected to produce bigger porous, facilitating the colonization by the osteoblasts [30]. SEM images (Fig. 3.3, a-d) displayed the porous polymer surface and the EDS analysis (Fig. 3.3, f) detected the BG elements (Na, Si and Ca) into the samples, even after the sterilization, alkali treatment and functionalization.

The 3D PDLLA scaffolds containing BG were functionalized with collagen and MH, after the alkali hydrolysis treatment (3.2.3). Alkaline hydrolysis was used to increase the wettability and roughness of the material [11], observed by SEM images (Fig. 3.3, f) and create carboxylic acids and hydroxyls groups by cleaving the ester bonds on the polymer surface, which can be conjugated with surface-modifying species containing amine or hydroxyl groups, as collagen and the MH [8,10]. The adsorption method to functionalize the samples was chosen to add the collagen and the antibiotic in order to avoid high temperatures and harsh chemicals of the fabrication processes [15]. The collagen was selected to improve the bioactivity of the scaffold surface [10]. XRD and FTIR/ATR analysis (Fig. 3.3 e and g) presented differences between groups, suggesting modifications in the polymer made by the MH and possible bonds between the PDLLA and the antibiotic. This fact was observed by the release profile of the MH-Col-PDLLA samples, where in Hepes at neutral pH, no release was observed and the samples maintained the yellowish accent after several days into the solution. The MH release was observed only in water at pH 5.0, suggesting that the acidic medium could unbridle the antibiotic from the polymer by changing the interactions between the polymer and the MH, namely, the cleavage of the bonds between then, producing a controlled release until 72 h (Fig. 3.4). In addition, pH can also influence the protein adsorption and interactions with polylactide surfaces [31]. This characteristic could be useful during an infection or inflammation, once the pH of the infected tissues is usually lower [32].

The degradation profile of PLA in general is a complex factor, which depends on the medium (pH, temperature and the presence of salt) and the sample itself (bulkiness and crystallinity degree) [33,34]. Some studies show that extreme basic or acidic pH can increase the degradation rate of PLA, changing even the cleavage behavior of the ester bonds, while pH close to 4 (the pKa of lactic acid), can decrease it [35]. On the other hand, some studies show that basic pH increase the degradation rate, while neutral and acid pH decrease it [33,34]. Overall, the detected release is originated from the interaction changes between the PDLLA

and MH at pH 5 and not from the polymer degradation, once the assays were conducted until 72 h, a short period of time to observe a significant PDLLA degradation.

Antimicrobial assays showed that the MH was able to present the same activity after the addition into the scaffolds. Results showed that the scaffolds containing MH presented antimicrobial and anti-biofilm formation activity against *S. aureus*, one of the most common bacteria seen in osteomyelitis [13,14] (Fig. 3.5). The supernatant collected during the release presented the same MIC of the positive control (MH solution), discarding any possibility of interference caused by other compounds or the functionalization procedure itself and showing that the scaffolds could be effective for a surgical antibiotic prophylaxis. The *S. aureus.* ATCC 25923 is a very sensitive strain to MH and in the present study showed lower concentrations in comparison to others studies that used the same strain [22,36]. However, our independent control (levofloxacin) presented the same MIC found in the literature [25,26], confirming the MH MIC results. Overall, the antimicrobial activity was not affected by the adsorption and the drying procedures and the scaffolds showed antimicrobial activity.

Regarding the cytotoxicity assays, MH presented toxic effects on the MG-63 cells in a concentration-dependent manner as already shown by other authors [36,39] (Fig. 3.6). When the scaffolds were colonized by the cells, this concentration-dependent toxicity was also observed. To avoid false positive results of cell viability assays, scaffolds were put in a new well of the plate with fresh medium immediately before the evaluation to eliminate any metabolic activity from cells unconnected to the samples. Small pieces of the MH-Col-PDLLA (Group 3) scaffolds presented a slightly higher cell viability in comparison to Group 2 (Col-PDLLA) for week 2 to 4 after an inhibition in week 1 (Fig. 3.7), while a bigger and bulky piece of the same scaffold completely inhibited the cell proliferation and activity (Fig. 3.8), corroborating to the literature that MH can increase cell proliferation and activity or inhibition in a concentration-dependent manner on different cell lines [36,39]. The scaffold samples were also submitted to MTT assays to observe if the formazan crystals would be formed into the scaffolds, confirming the samples colonization by the cells (Fig. 3.9 and 3.10). The images also confirmed the absence of crystals on the MH-Col-PDLLA samples (Fig. 3.10) corroborating the alamarBlue results. It is known that the cytotoxic mechanisms of tetracyclines against mammalian cells is related to the inhibition of macromolecule syntheses [40].

Between PDLLA (Group 1) and Col-PDLLA (Group 2), no significant differences were observed showing that the PDLLA in association with the BG could already offer a viable bone substitute, however the alamarBlue assay results were slightly higher for Col-PDLLA during all time points (Fig. 3.8) and the coloration of the formazan crystals seems to be stronger on this sample (Fig. 3.9), showing the benefits of a more hydrophilic surface and the presence of collagen [10]. To evaluate the osteoblasts activity, scaffolds were stained by BCIP-NBT metabolization by ALP enzyme (Fig. 3.11). Results were similar to MTT assay, where Group

1 (PDLLA) and Group 2 (Col-PDLLA) presented an intense purple coloration, showing the cell activity inside the scaffolds while with Group 3 (MH-Col-PDLLA) no coloration was observed, confirming the absence of viable and active cells inside them.

Conclusively, the present study evaluates the production of scaffolds using a cheap and easy technique. The scaffolds showed potential of being a bone substitute, offering antimicrobial activity (at acidic pH) and osteoinduction to an osteoconductive polymer. However, further studies must be conducted in order to provide a better understanding about the interactions between PDLLA and MH and to adjust the antibiotic concentration aiming a more predictable release before conducting *in vivo* studies.

References

[1] Wu H, Lei P, Liu G, Zhang YS, Yang J, Zhang L. Reconstruction of Large-scale Defects with a Novel Hybrid Scaffold Made from Poly(L-lactic acid) /Nanohydroxyapatite/Alendronate-loaded Chitosan Microsphere: In vitro and in vivo Studies. Sci Rep 2017;7:1–14. doi:10.1038/s41598-017-00506-z.

[2] Kim SE, Yun YP, Shim KS, Kim HJ, Park K, Song HR. 3D printed alendronate-releasing poly(caprolactone) porous scaffolds enhance osteogenic differentiation and bone formation in rat tibial defects. Biomed Mater 2016;11:55005. doi:10.1088/1748-6041/11/5/055005.

[3] Larrañaga A, Alonso-Varona A, Palomares T, Rubio-Azpeitia E, Aldazabal P, Martin FJ. Effect of bioactive glass particles on osteogenic differentiation of adipose-derived mesenchymal stem cells seeded on lactide and caprolactone based scaffolds. J Biomed Mater Res - Part A 2015;103:3815–24. doi:10.1002/jbm.a.35525.

[4] Zhang Q, Tan K, Zhang Y, Ye Z, Tan W, Lang M. In Situ Controlled Release of rhBMP - 2 in Gelatin-Coated 3D Porous Poly(ε -caprolactone) Sca ff olds for Homogeneous Bone Tissue Formation. Biomacromolecules 2014;15:84–94. doi:10.1021/bm401309u.

[5] Larrañaga A, Aldazabal P, Martin FJ, Sarasua JR. Hydrolytic degradation and bioactivity of lactide and caprolactone based sponge-like scaffolds loaded with bioactive glass particles. Polym Degrad Stab 2014;110:121–8. doi:10.1016/j.polymdegradstab.2014.08.021.

[6] Krebs MD, Sutter KA, Lin ASP, Guldberg RE, Alsberg E. Injectable poly(lactic-co-glycolic) acid scaffolds with in situ pore formation for tissue engineering. Acta Biomater 2009;5:2847–59. doi:10.1016/j.actbio.2009.04.035.

[7] Thavornyutikarn B, Chantarapanich N, Chen Q. Bone tissue engineering scaffolding : computer-aided scaffolding techniques. 2014. doi:10.1007/s40204-014-0026-7.

[8] Rasal RM, Janorkar A V., Hirt DE. Poly(lactic acid) modifications. Prog Polym Sci 2010;35:338–56. doi:10.1016/j.progpolymsci.2009.12.003.

[9] Yang J, Bei J, Wang S. Enhanced cell affinity of poly (D,L-lactide) by combining plasma treatment with collagen anchorage. Biomaterials 2002;23:2607–14. doi:10.1016/S0142-9612(01)00400-8.33

[10] Yang J, Wan Y, Tu C, Cai Q, Bei J, Wang S. Enhancing the cell affinity of macroporous poly(L-lactide) cell scaffold by a convenient surface modification method. Polym Int. 2003;52(12):1892–9.

[11] Guo C, Xiang M, Dong Y. Surface modification of poly (lactic acid) with an improved alkali-acid hydrolysis method. Mater Lett [Internet]. 2015;140:144–7.

[12] Chen Y, Mak AFT, Wang M, Li J, Wong MS. PLLA scaffolds with biomimetic apatite

coating and biomimetic apatite/collagen composite coating to enhance osteoblast-like cells attachment and activity. Surf Coatings Technol. 2006;201(3–4):575–80.

[13] Dorati R, De Trizio A, Genta I, Merelli A, Modena T, Conti B. Gentamicin-Loaded Thermosetting Hydrogel and Moldable Composite Scaffold: Formulation Study and Biologic Evaluation. J Pharm Sci. 2017. DOI:10.1016/j.xphs.2017.02.031. IN PRESS

[14] Gao J, Huang G, Liu G, Liu Y, Chen Q, Ren L. A biodegradable antibiotic-eluting PLGA nanofiber-loaded deproteinized bone for treatment of infected rabbit bone defects. J Biomater Appl. 2016;31(2):241–9.

[15] Visscher LE, Dang HP, Knackstedt MA, Hutmacher DW, Tran PA. 3D printed Polycaprolactone scaffolds with dual macro-microporosity for applications in local delivery of antibiotics. Mater Sci Eng C 2018;87:78–89. doi:10.1016/j.msec.2018.02.008.

[16] Lee BS, Lee CC, Wang YP, Chen HJ, Lai CH, Hsieh WL. Controlled-release of tetracycline and lovastatin by poly(D,L-lactide-co-glycolide acid)-chitosan nanoparticles enhances periodontal regeneration in dogs. Int J Nanomedicine 2016;11:285–97. doi:10.2147/IJN.S94270.

[17] Yoshinari N, Tohya T, Kawase H, Matsuoka M, Nakane M, Kawachi M. Effect of repeated local minocycline administration on periodontal healing following guided tissue regeneration. J Periodontol 2001;72:284–95. doi:10.1902/jop.2001.72.3.284.

[18] Hou Y, Hu J, Park H, Lee M. Chitosan based nanoparticles as a sustained protein release carrier for tissue engineering applications. J Biomed Mater Res A Growth 2012:1–7. doi:doi:10.1002/jbm.a.34031.

[19] Martin V, Bettencourt A. Bone regeneration : Biomaterials as local delivery systems with improved osteoinductive properties. Mater Sci Eng C 2017;82:363–71. doi:10.1016/j.msec.2017.04.038.

[20] Voicu G, Geanaliu RE, Ghiţulică CD, Ficai A, Grumezescu AM, Bleotu C. Synthesis, characterization and bioevaluation of irinotecan-collagen hybrid materials for biomedical applications as drug delivery systems in tumoral treatments. Cent Eur J Chem Synth 2013;11:2134–43. doi:10.2478/s11532-013-0341-1.

[21] Khang G, Kim MS, Lee HB. A Manual for Biomaterials/Scaffold fabrication technology. Vol. 4. World Scientific Publishing Co. Pte. Ltd.; 2007. 1-255 p.

[22] Matos AC, Gonçalves LM, Rijo P, Vaz MA, Almeida AJ, Bettencourt AF. A novel modified acrylic bone cement matrix. A step forward on antibiotic delivery against multiresistant bacteria responsible for prosthetic joint infections. Mater Sci Eng C 2014;38:218–26. doi:10.1016/j.msec.2014.02.002

[23] Clinical and Laboratory Standards Institute. Methods for Dilution Antimicrobial Susceptibility Tests for Bacteria That Grow Aerobically ; Approved Standard. Ninth

Edition. vol. 32. 2012. doi:10.4103/0976-237X.91790.

[24] Clinical and Laboratory Standards Institute, CLSI. CLSI-M100-S27 Performance standards for antimicrobial susceptibility testing. 2017.

[25] Matos AC, Marques CF, Pinto R V, Ribeiro IAC, Gonçalves LM, Vaz MA, Ferreira JMS, Almeida AJ, Bettencourt AF. Novel doped calcium phosphate-PMMA bone cement composites as levofloxacin delivery systems. Int J Pharm 2015;490:200–8. doi:10.1016/j.ijpharm.2015.05.038.

[26] Matos AC, Ribeiro IAC, Guedes RC, Pinto R, Vaz MA, Gonçalves LM, Vaz MA, Ferreira JMS, Almeida AJ, Bettencourt AF. Key-properties outlook of a levofloxacin-loaded acrylic bone cement with improved antibiotic delivery. Int J Pharm 2015;485:317–28. doi:10.1016/j.ijpharm.2015.03.035.

[27] Silva MM, Calado R, Marto J, Bettencourt A, Almeida AJ, Gonçalves LMD. Chitosan nanoparticles as a mucoadhesive drug delivery system for ocular administration. Mar Drugs 2017;15:1–16. doi:10.3390/md15120370.

[28] Mosmann T. Rapid colorimetric assay for cellular growth and survival: Application to proliferation and cytotoxicity assays. J Immunol Methods 1983;65:55–63. doi:10.1016/0022-1759(83)90303-4.

[29] Kundu S. Biomed Recent Advances in Immunoassays. 2014. doi:10.13140/2.1.3444.5449.

[30] Watanabe S, Takabatake K, Tsujigiwa H, Watanabe T, Tokuyama E, Ito S. Efficacy of honeycomb TCP-induced microenvironment on bone tissue regeneration in craniofacial area. Int J Med Sci 2016;13:466–76. doi:10.7150/ijms.15560.

[31] Khakalo A, Filpponen I, Rojas OJ. Protein Adsorption Tailors the Surface Energies and Compatibility between Polylactide and Cellulose Nano fibrils. Biomacromolecules 2017;18:1426–33. doi:10.1021/acs.biomac.7b00173.

[32] Honda H and Mcdonald JR. Current Recommendations in the Management of Osteomyelitis of the Hand and Wrist. J Hand Surg Am 2009;34:1135–6. doi:10.1016/j.immuni.2010.12.017.Two-stage.

[33] Cardoso, JJF; Queirós, YGC; Machado, KJA; Costa, JM; Lucas E. Synthesis, characterization, and in vitro degradation of poly (lactic acid) under petroleum production conditions. Brazilian J Pet Gas 2013;7:57–69. doi:10.5419/bjpg2013-0005.

[34] Xu L, Crawford K, Gorman CB. Effects of Temperature and pH on the Degradation of Poly (lactic acid) Brushes. Macromolecules 2011;44:4777–82.

[35] Kim K, Elsawy MA, Kim K, Park J, Deep A. Hydrolytic degradation of polylactic acid (PLA) and its composites. Renew Sustain Energy Rev 2017;79:1346–52. doi:10.1016/j.rser.2017.05.143.

[36] Silva T, Grenho L, Barros J, Silva J, Pinto R, Matos A, Bettencourt A, Gomes PS.

Minocycline-releasing PMMA system as a space maintainer for staged bone reconstructions – in vitro antibacterial, cytocompatibility and anti-inflammatory characterization. Biomed Mater 2017;12:35009. doi:10.1088/1748-605X/aa68b8.

[37] Dou XC, Zhu XP, Zhou J, Cai HQ, Tang J, Li QL. Minocycline-released hydroxyapatite-gelatin nanocomposite and its cytocompatibility in vitro. Biomed Mater 2011;6:025002. doi:10.1088/1748-6041/6/2/025002.

[38] Gomes PS, Fernandes MH. Effect of therapeutic levels of doxycycline and minocycline in the proliferation and differentiation of human bone marrow osteoblastic cells. Arch Oral Biol 2007;52:251–9. doi:10.1016/j.archoralbio.2006.10.005.

[39] Park JB. Effects of Doxycycline, Minocycline, and Tetracycline on Cell Proliferation, Differentiation, and Protein Expression in Osteoprecursor Cells. J Craniofac Surg 2011;22:1839–42. doi:10.1097/SCS.0b013e31822e8216.

[40] Suzuki A, Yagisawa J, Kumakura S, Tsutsui T. Effects of minocycline and doxycycline on cell survival and gene expression in human gingival and periodontal ligament cells. J Periodontal Res 2006;41:124–31. doi:10.1111/j.1600-0765.2005.00843.x.

Chapter 4. 3D-Printed polylactide scaffolds nanofunctionalized with hydroxyapatite nanoparticles and minocycline aiming bone regeneration and antibiotic prophylaxis

4.1. Introduction

Bone defects are one of the leading worries regarding life quality of millions of people around the world and currently are among the most important topics of research in the orthopedic and maxillofacial areas [1]. Bone grafts are the main approach for the repair of wider bone defects caused by trauma, infection, tumor resection and bone remodelation [2]. In addition, bone substitute sales are expected to rise with a compound annual growth rate of 3.8% and the key drivers for this accentuate growth are pandemic aging and obesity, meaning that the number of patients undergoing orthopedic and/or dental procedures will increase and, consequently, the need for optimal bone grafts will greatly increase [1-3].

Until today, the gold standard to treat large bone defects is the autologous bone grafting, which is, unfortunately, associated with donor site morbidity, the need of one or more additional chirurgical interventions and the quantity is limited [2,4,5]. Researchers have been focused on producing bone substitutes structurally similar to bones such as three-dimensional (3D) scaffolds with high porosity and interconnected pores to promote cell growth, migration, differentiation, and vascularization, as well as the diffusion of nutrients [6]. Scaffolds can be made with ceramics and polymers and can reduce the time of the surgery, morbidity and provide an unlimited source [5,7,8]. However, those grafts can provide mainly osteoconduction, limiting its usage in bone reconstruction [2,9].

One promising material to build scaffolds is polylactide (PLA) - a biopolymer approved for direct contact with biological fluid by the Food and Drug Administration (FDA), displaying mechanical stability and non-toxic hydrolysis products [4,10]. However, PLA is relatively hydrophobic, which can lead to substandard tissue formation by low cell adhesion and osteogenic differentiation [10-12]. In addition, hydrophobic surfaces can facilitate bacterial adhesion and biofilm formation [13]. Several studies have been conducted to overcome these drawbacks, for instance the alkali hydrolysis treatment, which consists in chemical modifications on the polymer surface [14] or coating the surface with bioactive compounds as collagen - an extracellular matrix molecule widely employed as biomaterials for being well-tolerated and degraded in non-toxic and non-immunogenic peptides [4].

Another usual approach for surface improvement is the incorporation of bioactive compounds as bioactive glasses and hydroxyapatite (HA) particles into the polymer, enhancing the bioactivity and avoiding the ceramic based scaffolds disadvantages, the slow degradation rate and unsatisfactory mechanical properties [15]. HA is a ceramic commonly found in human teeth and bones that can improve the cell activity and viability of the graft, buffer the acidic

degradation products from the polymer and improve the protein adsorption ability of the scaffolds [10,16].

Recently, PLA has been used to produce 3D printed structures for biomedical applications, including porous scaffolds for bone tissue engineering [11]. In fact, 3D printing is one of the main promising technologies [17], offering new strategies for a rapid and accurate regenerative medicine, capable of producing customized scaffolds with a desired architecture, shape, porosity and pore size [18-21]. This technique can produce structures based on medical imaging [22] such as micro-computed tomography and magnetic resonance imaging (MRI), where the 3D images of the bones can be re-constructed and prototyped [23]. Moreover, the combination of a printed scaffold with controlled drug-delivery properties is yet insufficient explored [24]. Printed scaffolds have been impregnated with growth factors as bone morphogenetic proteins and vascular endothelial growth factor, however the short half-life, dosage risks and high cost of growth factors limit their clinical application [25].

Minocycline hydrochloride (MH) is a semi-synthetic tetracycline with a broad antibacterial spectrum, inhibiting bacterial protein synthesis [26]. Additionally, displays also non-antimicrobial activities as anti-inflammatory due to matrix metalloproteinases inhibition, antioxidant and anti-apoptotic effects [27]. Also, tetracyclines are known for osteoinductive properties, namely the increase of osteoblasts activation, upregulation of osteogenic protein synthesis as collagen type 1 and inhibition of osteoclast-mediated bone resorption, resulting in the increase of mineralized bone matrix [28].

In addition, grafts and implants can contribute to the formation of bacterial biofilm, leading to bone infections and coating the surface with extra-cellular matrix compounds that can facilitate the bacterial adhesion on the material, enhancing even more the biofilm formation [29]. As a result, a local delivery MH system could help to prevent biofilm associated infections [30] and the non-antimicrobial activity would be explored, making it a good choice to be loaded in the scaffolds [28].

Our hypothesis is that a PLA 3D printed scaffold with an enhanced hydrophilic surface can be an optimal osteoconductive material. Besides, MH will be added in order to provide anti-microbial activity and increase the osteoinduction of the material [26]. Furthermore, the scaffold will be nanofunctionalized with HA nanoparticles to enhance the bioactivity of the material, improving the cellular response and mimicking the natural bone tissue [31].

4.2. Materials and Methods

4.2.1. Fabrication and characterization of 3D PLA scaffolds functionalized with hydroxyapatite nanoparticles and minocycline

4.2.1.1. Materials

The Polylactic acid (PLA) was purchased from Real PLA (Real), collagen hydrolysate type I fibrillar (kindly donated by Dra Mădălina Kaya from Department of Collagen Research, Romania [32]), ethanol anhydrous (Carlo Erba), citric acid monohydrate (Merck), minocycline hydrochloride (kindly donated by Atral Cipan, Portugal), sodium hydroxide (Akzo Nobel) and nanosized hydroxyapatite nanoparticles (HA) were synthesized by a hydrothermal method reported elsewhere [33].

4.2.1.2. Fabrication of 3D printed PLA scaffolds

All 3D printed PLA scaffolds were produced using a printer BQ Prusa i3 Hephestos. Three-dimensional structures were built by layer-by-layer deposition. In the case of PLA scaffolds, a white filament with a 1.75 mm diameter, a motor speed of 20 mm s^{-1} (travel speed of 120 mm s^{-1}) and a 250 µm diameter nozzle were used. The printing temperature was 195 ± 1 ºC and bed temperature was room temperature. A Raft was created under the sample with 1 mm extra margin and 0.15 mm initial layer Z overlap. 3D printed PLA scaffolds were built from CATIA V5 drawing software by extruding the material layer by layer (Fig. 4.1).

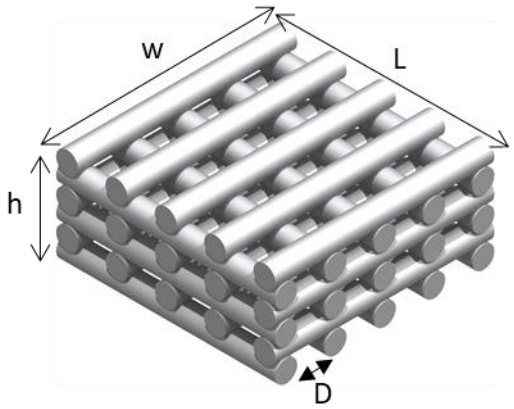

Figure 4.1. 3-D view of the theoretical 3-D structures of PLA scaffolds. D= 0.1 mm; w= scaffold width; L= scaffold length; h= scaffold height.

4.2.1.3. Scaffolds surface treatment and functionalization

After the fabrication, the scaffolds were sterilized by immersion into ethanol 70% (V/V) solution for 24 h (Fig. 4.2). Subsequently to this procedure, the scaffolds were divided into 6 groups according to the surface treatment or functionalization (i.e. adsorption of collagen, MH or HA nanoparticles), detailed in Table 4.1 and Fig. 4.2. Surface treatment consisted in submitting the scaffolds to alkali hydrolysis by immersion into a 1:1 NaOH 0.25 M and ethanol 96% (V/V) at room temperature and 200 rpm in a mixing plate (LD-40, Labinco) for 4 h and washing with

citric acid 0.5% and deionized water [14,34]. Scaffolds without the surface treatment (Group 1) were used as control in determined assays. The adsorption procedure was conducted at room temperature and 200 rpm in a mixing plate, for 24 h. All the scaffolds were dried in a dissector for at least 48 h.

Table 4.1. Groups separated accordingly with the surface treatment and functionalization. Col solution (5 mg/mL), MH solution (0.5 mg/mL) and 10 mg of HA were used.

Group 1	Group 2	Group 3	Group 4	Group 5	Group 6
PLA	MH-PLA	Alkali-PLA	Col-PLA	MH-Col-PLA	HA-MH-Col-PLA
- No treatment - No adsorption	- No treatment - MH adsorption	- Alkali treatment - No adsorption	- Alkali treatment - Col adsorption	- Alkali treatment - MH + Col adsorption	- Alkali treatment - HA + MH + Col adsorption

Abbreviations: PLA – polylactide; Alkali – Alkali hydrolysis treatment, MH – minocycline hydrochloride, HA – hydroxyapatite nanoparticles, Col – collagen.

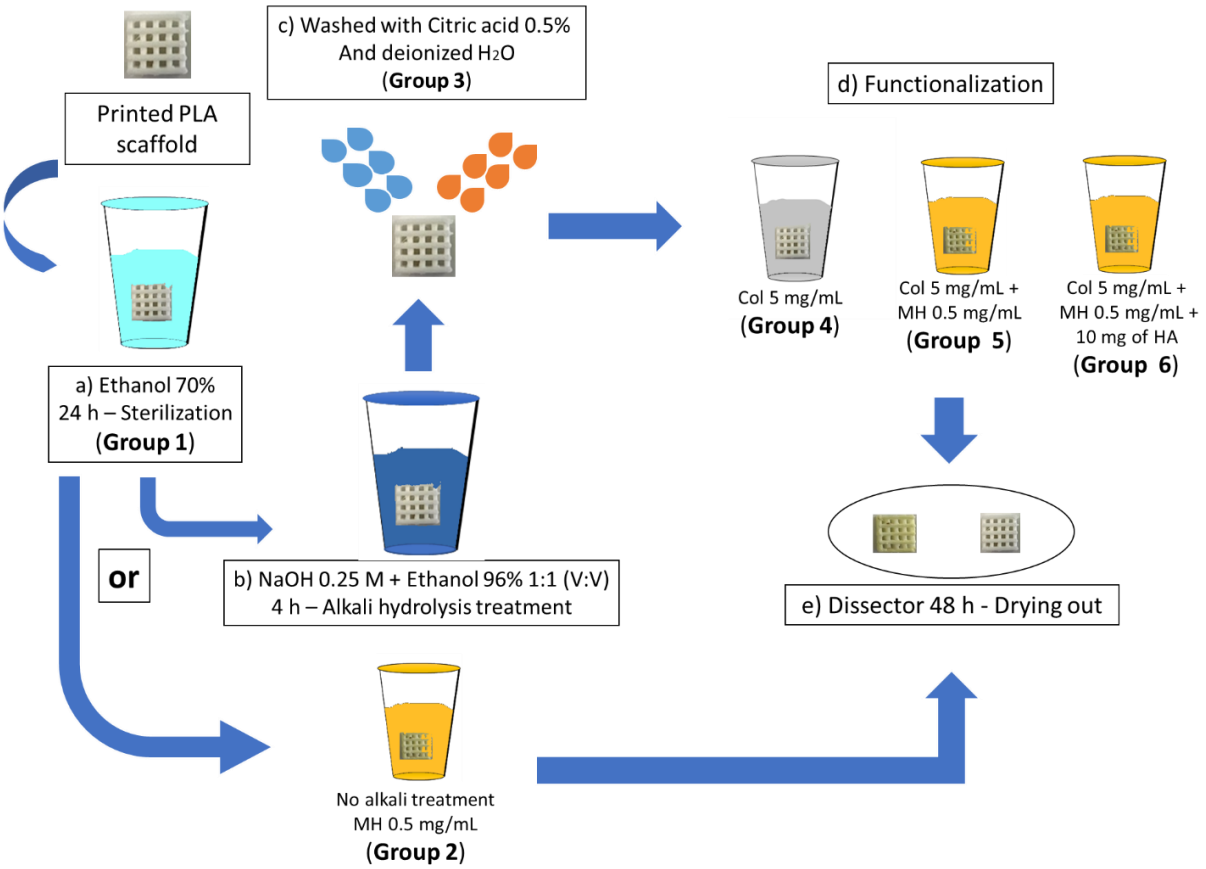

Figure 4.2. Illustration of the sequence of procedures involving the surface treatment and functionalization of the scaffolds.

4.2.2. Scaffold's surface characterization

The morphological characterization of the Groups 1, 3, 5 and 6 was conducted by scanning electron microscopy (SEM) using a JEOL JSM-7001F equipment, and the elemental chemical composition by the respective X-ray energy dispersive spectrometer (EDS). To increase the conductivity of the samples a thin coating of conductive chromium (Polaron E-5100) was added. The crystalline structure was identified by X-ray diffraction (XRD) using a D8 Advance Bruker AXS θ-2θ diffractometer with a copper radiation source (Cu Kα, λ = 1.5406 Å) and a secondary monochromator operated at 40 kV and 40 mA over a 2θ range of 8° to 70°. Attenuated total reflectance (FT-IR/ATR) in transmittance mode was used to identify the functional groups present in the PLA functionalized surfaces, in the range of 600-4000 cm^{-1} using a Nicolet (Thermo Electron) spectrometer.

3D micro architectural morphology and porosity of each PLA scaffold were also characterised by X-Ray microtomography (micro-CT), using a Phoenix V|TOME|X, GE. µCT. For that, 3D PLA scaffolds were scanned at voltage of 80 kV with current intensity of 80 mA. The scanning angular increment was 0.15 degrees, and the special resolution 6.7 µm. Acquired image data were qualitatively and quantitatively interpreted using 3D tomographic reconstruction and analysis software (Volume Graphics 3.04 software, Volume Graphics).

The hydrophilicity of the scaffolds was determined by the sessile drop method using distilled water. Water drops of 4–6 µL were generated with a micrometric syringe and deposited on the 3D PLA surface. Contact angle evolution was monitored during 10 s following drop deposition using a video camera coupled to a microscope (Wild M3Z) and to a frame grabber (Data Translation DT3155). Reported results correspond to the mean of at least five experiments. All measurements were performed at room temperature using samples of Groups 1, 4, 5 and 6.

4.2.3. Minocycline release

Specimens of the Groups 2, 4, 5 and 6 were incubated in a 50 mL Falcon tube with 3 mL of 1) Hepes 10 mM at pH 7.4 or 2) NaCl 0.9%(m/V) with 0.05%(V/V) Tween20® at pH 5.0, in a shaking water-bath (Memmert) at 37 °C [35]. At predetermined intervals, during 24h period, aliquots of the supernatant were collected and analyzed in triplicate. The withdrawn aliquots were then replaced with equal volumes of fresh release solution and the medium was changed each 8 h. The sink conditions were guaranteed during the whole study. Minocycline content was determined by UV detection at 350 nm with a microplate reader (FLUOstar Omega, BMG Labtech).

4.2.4. Microbiological assays

Staphylococcus aureus (ATCC 25923) obtained from American Type Culture Collection (ATCC) was stored in 20% of glycerol in TSB and frozen at -80ºC. Aliquots from frozen stocks were used to culture microorganisms in Tryptic Soy Agar (TSA) for 24 h at 37ºC.

4.2.4.1. Antimicrobial activity of scaffolds

S. aureus inoculum was prepared following the guidelines of the Clinical and Laboratory Standards Institute (CLSI) [36]. Briefly, few colonies of *S. aureus* were spread into Mueller Hinton Broth (Biokar Diagnostics) and further diluted in order to achieve 0.5 McFarland units (1×10^8 CFU mL^{-1}) at 600 nm of wavelength, using the spectrophotometer (U-2000, Hitachi). The inoculum was swabbed on Mueller Hinton Agar (Biokar Diagnostics) plates and the scaffold samples were tested (Group 4 and 6), as well as the 6 mm filter disks containing 10µL of distilled water (negative control) or 10 µL of 3 mg/mL of MH aqueous solution (positive control). The petri dishes were further incubated (Ultima, Revco) at 37°C for 20 h. After the incubation period, the diameter of inhibition zone of the samples and the controls was measured three times with a vernier caliper. Assays were performed in three independent experiments.

4.2.4.2. Antimicrobial activity of release medium supernatants

The antimicrobial susceptibility of *S. aureus* to MH standard solution and to release medium supernatants was obtained by the Broth Microdilution Method described by CLSI [36]. All assayed samples were two-fold diluted in Müeller-Hinton broth (Biokar Diagnostics) and the final MH concentration ranged from 0.0078 to 2 µg/mL. *S. aureus* inoculum was prepared according to CLSI [36] in Müeller-Hinton broth. Briefly, a 1×10^8 CFU/mL *S. aureus suspension* was obtained (as previously described in 4.2.4.1), further diluted to 1×10^6 CFU/mL and 100 µL of this last suspension were used to inoculate the microtiter plate wells reaching a final volume of 200 µL. Plates were incubated at 37°C for 16-20 h and afterwards visible growth of bacteria was inspected and absorbance at 595 nm was measured in a Microplate Multimode Detector (Anthos, Zenyth 3100). The lowest concentrations of MH that was able inhibit the visible growth of bacteria was considered the minimal inhibitory concentration (MIC).

All assays were performed with negative controls (not inoculated media) and positive controls (inoculated media). *Levofloxacin* was used as a quality control standard to guarantee that the test system performed as expected. Assays were carried out in three independent experiments.

4.2.4.3. Biofilm inhibition

PLA scaffolds were fixed at the bottom of a well in a 24-well-microtiter plate inside an airflow chamber. Inoculum was prepared from direct colony suspension of *S. aureus* (24 h slants), adjusted to 3×10^8 CFU mL^{-1} and further diluted in BHI medium with glucose at 1% (W/V). In each well of the 24-well microtiter plate, containing PLA scaffolds, the final inoculum concentration was 3×10^6 CFU mL^{-1}.

Scaffolds without being inoculated were used as negative controls and Col-PLA (Group 4) samples were used as positive controls. After 24 h of incubation at 37ºC, samples were washed twice with PBS and fixed with different ethanol solutions, 75, 90 and 100% (v/v) for 40 min and the biofilm evaluation was performed by SEM analysis (JEOL JSM-7001F). To increase the conductivity of the specimens they were coated with a thin layer of conductive gold film, under vacuum in an argon atmosphere (Quorum Technologies, Polaron E5100).

4.2.5. Cytocompatibility assays

Human bone marrow-derived mesenchymal stem cell cultures were established from freshly harvested bone marrow samples, obtained from orthopedic surgery procedures, as previously described [37]. Attained cells were characterized by flow cytometry, and found to be positive for CD105, CD73 and CD90, and negative for CD45, CD34 and CD31 markers [37]. Cells from the 4^{th} passage were used in the present experiment. Briefly, cultures were maintained in minimum essential Eagle's medium with alpha modification (α-MEM; Sigma), containing 10% fetal bovine serum, 50 µg/mL ascorbic acid, 100 U/mL penicillin and 100 µg/mL streptomycin (all from Thermo Fisher). Cells were grown at 37ºC in a humid atmosphere with 5% CO_2, with the culture medium being changed twice a week. Each scaffold was seeded with 10^5 cells and cultures were maintained as described. At determined time points, cultures established over the scaffolds surface were processed and the culture's metabolic activity/viability was determined by the resazurin assay, while cell adhesion/morphology were characterized by scanning electron microscopy (SEM) and fluorescence microscopy following cytoskeletal staining and nucleus counterstaining. Finally, PCR analysis was conducted using total RNA isolated from the cell cultures.

4.2.5.1. Resazurin assay

The metabolic activity of the cultured cells was measured with the alamarBlue® assay (Invitrogen, Carlsbad, CA), based on the conversion of resazurin to the fluorescent by product resorufin, by metabolically active and viable cells [38]. Briefly, seeded scaffolds were removed from culture and rinsed with PBS and incubated in a 1× alamarBlue® solution at 37°C for 3 h. Resorufin fluorescence was then determined (excitation: 540 nm, emission: 590 nm).

4.2.5.2. Scanning and Fluorescent microscopy assay

SEM analysis was conducted following the fixation of the cultures with glutaraldehyde (1.5% in cacodylate buffer, pH 7.3; 10 min). Fixed samples were following dehydrated in graded ethanol series, critical point dried and sputtered with an Au-Pd thin film, prior to the observation in a FEI Quanta 400FEG ESEM.

Fluorescent microscopy observation was conducted following cells fixation with formaldehyde (3.7% in PBS, 15 min) and permeabilization with 0.1% Triton. To reduce unspecific staining, cultures were incubated with bovine serum albumin (10 mg/mL in PBS, 1 h). Subsequently, cells were incubated with Alexa-Fluor 488-phalloidin conjugated antibody (1:50, 30 min) for F-actin staining, and DAPI (1 µg/mL, 10 min) for nucleus counterstain. Images of fluorescent-labelled cells were obtained with a Selena S digital imaging system (Logos Biosystems).

4.2.5.3. Osteoblastic differentiation quantitative PCR assay

Total RNA was isolated from cell cultures grown for 15 days within the scaffolds by Trizol reagent (Invitrogen, Carlsbad, USA), in accordance with the standard manufacturers protocol. RNA concentration and quality were assessed with NanoDrop (NanoDrop Technologies). The conversion to cDNA was conducted with a reverse transcription system (QuantiTect RT Kit, Qiagen). Quantitative PCR was performed using an iCycler iQ Real-time PCR system (Bio-Rad), with the QuantiTect SYBR green PCR Kit (Qiagen). The relative quantification of each target gene, was normalized to beta-actin levels, and calculated via the $2^{-\Delta\Delta Ct}$ method. Primer sequences were designed on Primer 5.0 software, according to the sequences available in GenBank database and are presented on Table 4.2.

Table 4.2. Primer sequences used to amplify the targeted genes. β-actin was used to normalize the relative quantification of the osteogenic genes.

	Foward	Reverse
Runx2	ACCCAGAAGGCACAGACAGAAG	AGGAATGCGCCCTAAATCACT
OCN	AGGGCAGCGAGGTAGTGA	CCTGAAAGCCGATGTGGT
OPN	GAAGCCCAGCGGTGCA	CACTACCTCGCTGCCCTCC
β-actin	GTTGCTATCCAGGCTGTG	TGATCTTGATCTTCATTGTG

Abbreviations: Runx2 - runt related transcription factor 2; OCN – Osteocalcin; OPN – Osteopontin.

4.2.6. Statistical Analysis

Statistical analysis was conducted with GraphPad Prism 6.01 software. Data normality was determined by the Shapiro-Wilk test. For normal data sets, one-way ANOVA was performed, followed by multiple comparisons using Tukey's test. For non-parametric data sets, Kruskal-Wallis test was performed, followed by multiple comparisons using Dunn's tests. *P* values less than 0.05 were considered significant.

4.3. Results

4.3.1. Characterization of 3D PLA Scaffolds

Samples containing MH (Group 2, 5 and 6) presented a strong yellowish accent while Groups 1, 2 and 4 presented the original white color of the polymer (Fig. 4.3 a). Different tests were conducted to assess the effect of PLA surface treatment and functionalization. Comparing the PLA sample (Group 1, Fig. 4.3 b and c) with Alkali-PLA (Group 3, Fig. 4.3 d and e) it is possible to observe an increase of surface roughness after the alkali treatment. Samples submitted to functionalization (Groups 5 and 6) presented a layer on the surface, most likely made of collagen (Fig. 4.3. f to i). HA nanoparticles clusters were formed and some particles were found dispersed on the scaffold surface (Fig. 4.4. a), confirming the possibility of having particles on the surface with the adsorption method.

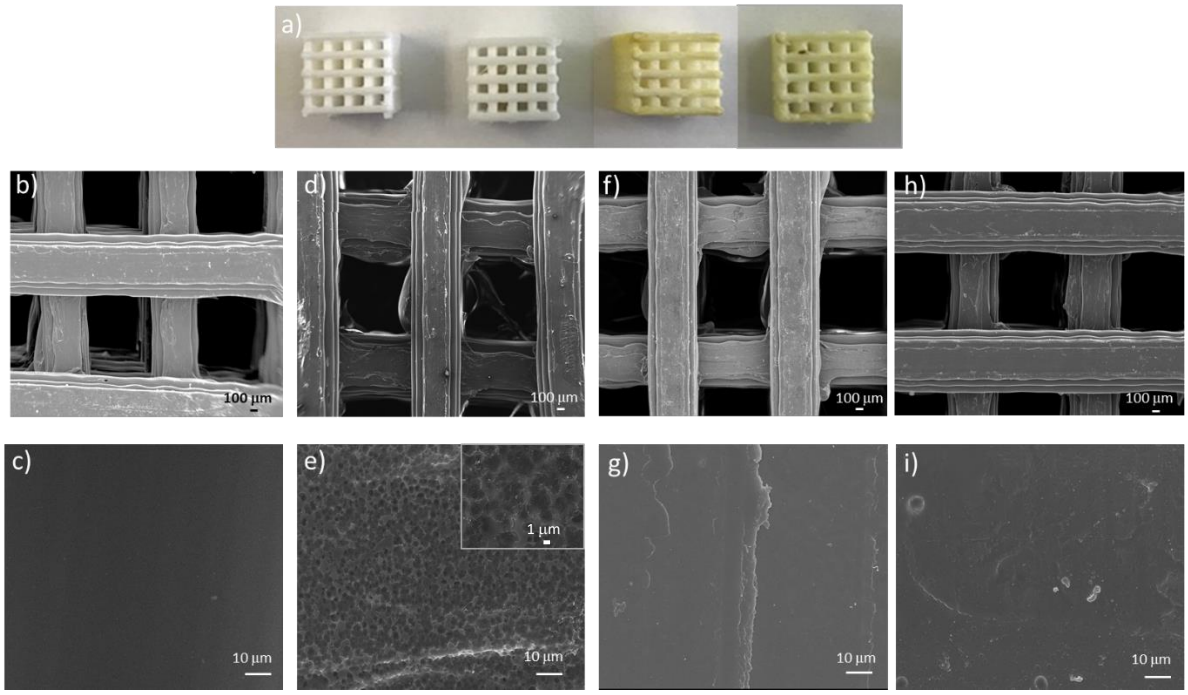

Figure 4.3. a) The color differences among the groups, where it is possible to identify the samples containing MH (yellowish); b) to i) correspond to SEM images, where b) and c) corresponds to Group 1 (PLA), d), e) to Group 3 (Alkali-PLA), f) and g) to group 5 (MH-Col-PLA) and h) and i) to Group 6 (HA-MH-Col-PLA). The differences caused by the alkali treatment, where observed comparing c) with an unlined surface to e) with a porous and rough surface, while g) and i) show the coated surface with collagen.

EDS analysis showed important differences of the Group 6 (HA-MH-Col-PLA) from the others, presenting calcium and phosphorus ions, absent in the other samples (Fig. 4.4). No differences among the other groups were found with the EDS analysis. No alkali hydrolysis components were found in the samples, suggesting that the NaOH, ethanol and the citric acid were removed and unable to be incorporated on the surface of the polymer. SEM images (Fig. 4.4, a) and EDS analysis (Fig. 4.4, b) to d) prove that the HA nanoparticles were incorporated in the scaffolds with the adsorption method.

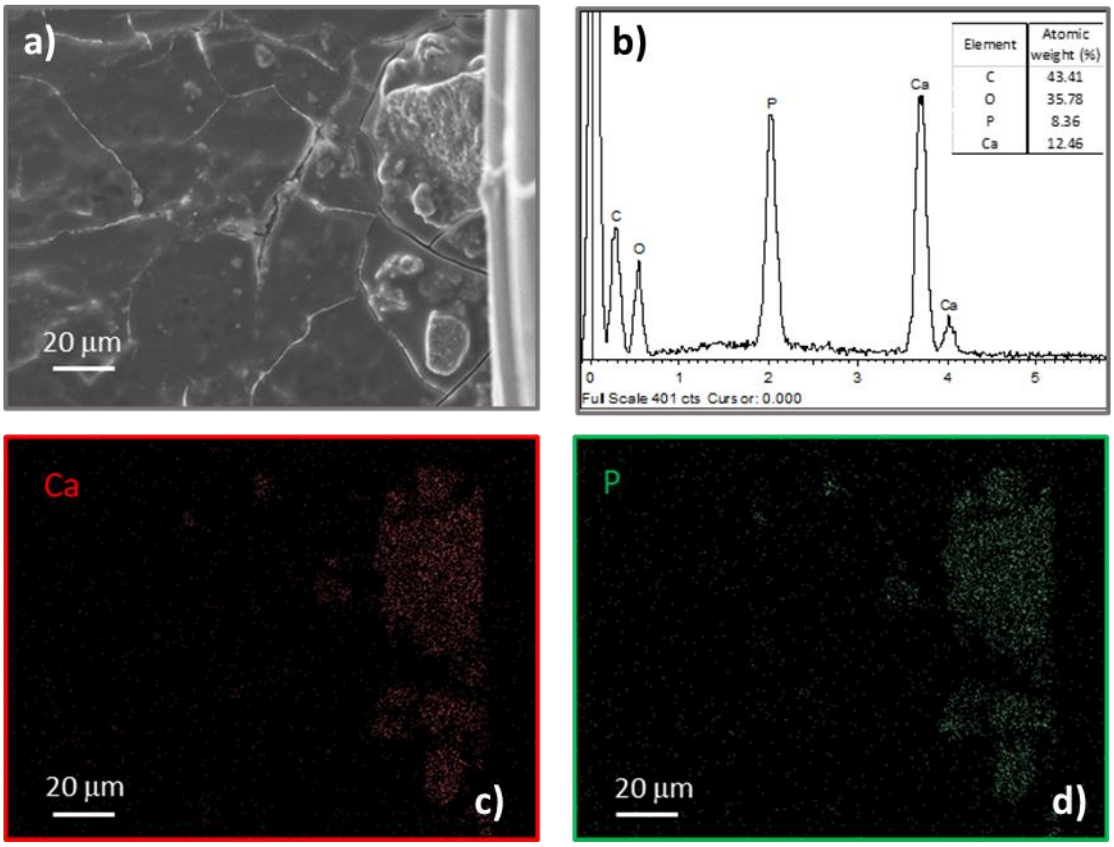

Figure 4.4. Hydroxyapatite presence and distribution into the Group 6 (HA-MH-Col-PLA) samples. a) corresponds to SEM images of a HA nanoparticle on polymer's surface, b) corresponds to EDS analysis of Group 6, c) and d) corresponds to the distribution of calcium and phosphate ions into the Group 6.

The XRD patterns of the samples are shown in Fig. 4.5 (a). It is observed that PLA (group 1) exhibited a broad hump showing pour crystalline nature. This broad hump increase slightly with the surface treatment that was indicative of increase in the crystallinity of the PLA. This results reflects the fact that hydrolytic chain cleavage, due to alkali treatment, proceeds preferentially in the amorphous regions, leading therefore to an increase of the PLA crystallinity. No differences between Group 3 and 6 were observed, suggesting that the functionalization compounds (MH, collagen or HA) did not altered the crystallinity of the samples.

FT-IR/ATR assay compared the intensity of the MH, Group 1 (PLA), Group 3 (Alkali-PLA) and Group 6 (HA-MH-Col-PLA). Results showed a completely different pattern between Group 1 to Group 3 and 6, due to the alkali treatment. Between Group 3 and 6, no remarked differences are clearly detected, providing direct evidence of the amount of HA and MH were not enough to be detected by this technique (Fig. 4.5 b).

The wettability properties of Group 4 (Col-PLA), 5 (MH-Col-PLA) and 6 (HA-MH-Col-PLA) were assessed through contact angle measurements (Fig. 4.5, c). Results showed that contact angle of group 4, 5 and 6 decreased significantly (from 55 ± 2º to 15 ± 3º after 10 seconds) in comparison to Group 1 (PLA) due to the alkali treatment and the Col coating. No differences

were observed among the functionalized groups, suggesting that the antibiotic and/or HA nanoparticles did not interfered with the wettability of the surface. (Fig. 4.5, c)

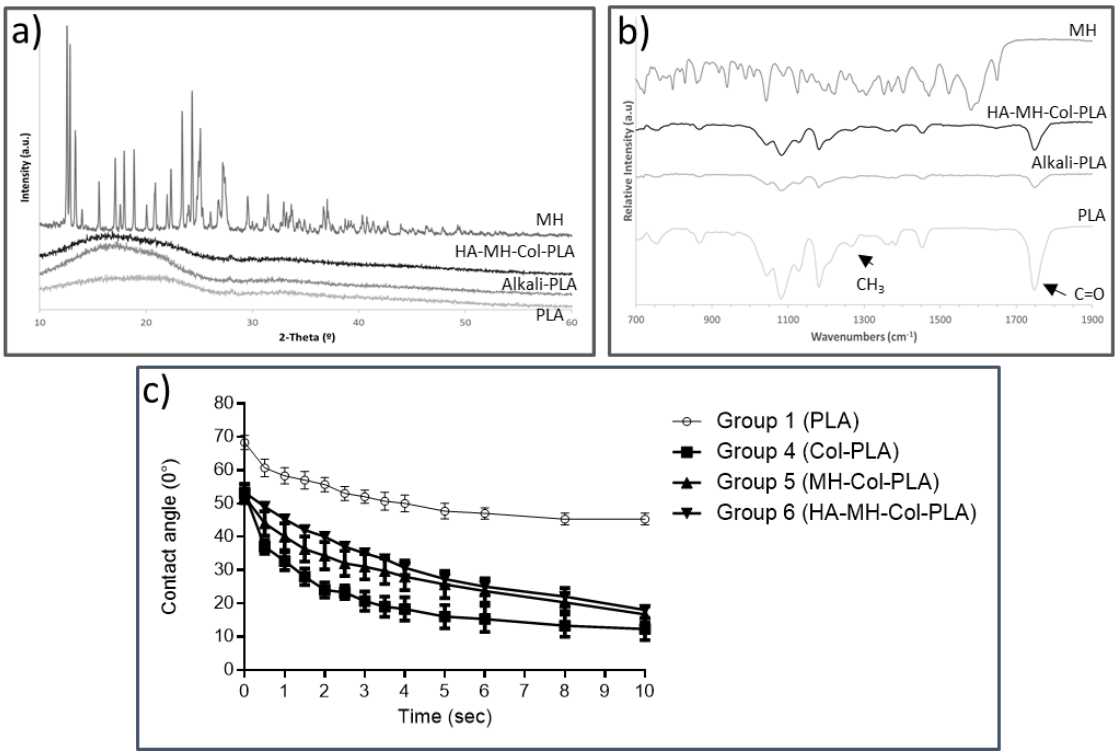

Figure 4.5. a) XRD analysis. The major difference is observed between the Group 1 (PLA) and the other groups, showing differences on the surface crystallinity. No differences among Group 3 and 6 were found. The peaks of the antibiotic (MH) were not observed in the samples. b) FT-IR results show different patterns among the samples, using a wavelength range of 1900 to 700 cm^{-1}. Results suggest that the functionalization can modify the polymer surface, showing different peaks close to 1750 cm^{-1} and between 1000 and 1500 cm^{-1}. (c) The surface water contact angle results. Group 1 (PLA) presented a higher contact angle in comparison with the other samples.

Micro-CT images revealed that the scaffolds had an interconnected 3D structure with well-defined geometry (Fig. 4.6). After functionalization with MH-Col (Group 5) and HA-MH-Col (Group 6), the outer structure of each scaffold did not change from setting values. Additionally, due to nanometric size of HA nanoparticles it was not possible to detect those NPs on micro-CT image (Fig. 4.6, c). Apart from the designed macropore structure, micropores between filaments were also detected (Fig. 4.6). Besides, it was observed that the volumetric ratio of micropores decrease with the functionalization (Fig. 4.6 b and c).

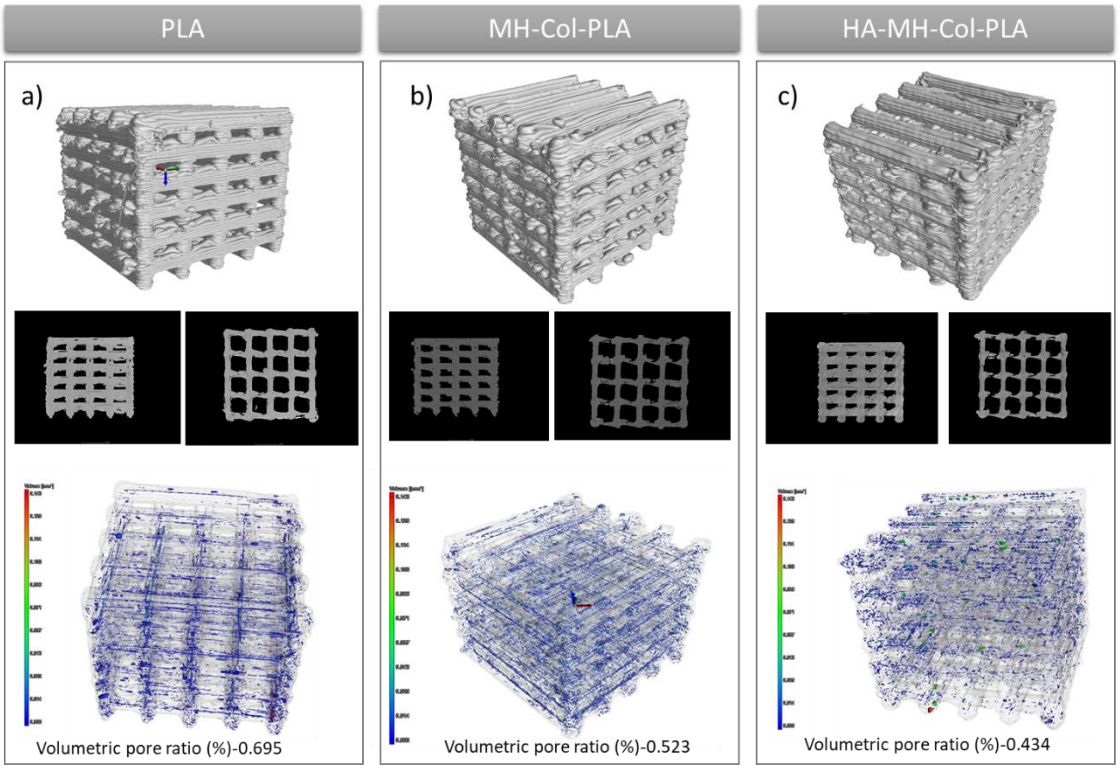

Figure 4.6. Micro-CT images with the porosity distribution of a) PLA (Group 1), b) MH-Col-PLA (Group 5) and c) HA-MH-Col-PLA (Group 6).

4.3.2. Minocycline release

The influence of the alkali treatment was evaluated, where the scaffolds functionalized with only MH (Group 2) were compared with Group 6 (HA-MH-Col-PLA) and results suggest that the alkali treatment and collagen coat can increase the amount of adsorbed MH and release it in a more progressive manner at neutral pH (Fig. 4.7). The total amount of MH and the release progression presented important differences between these groups, showed in Fig. 4.7 (a and b). MH was detected until 24 h of the assay.

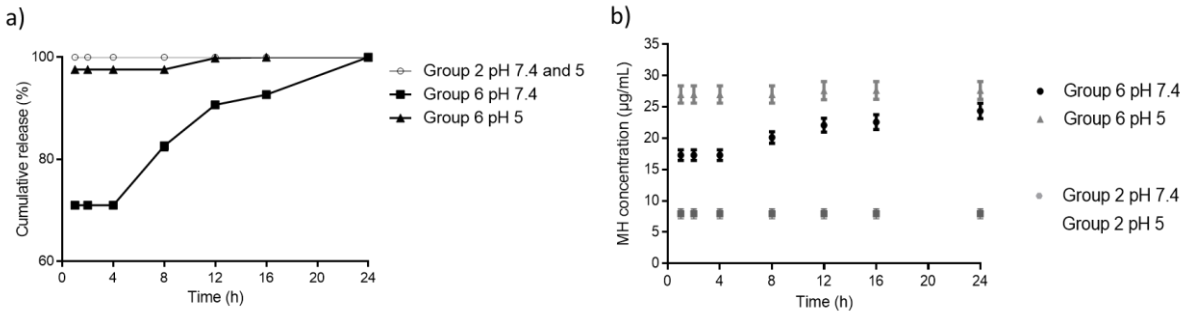

Figure 4.7. Comparison between Group 2 (MH-PLA) and Group 6 (HA-MH-Col-PLA) samples. The influence of the pH regarding the release is also demonstrated. Cumulative release is the relation of the partial with the total amount of MH released, where 100% corresponds to the concentration of the release by 24 h. a) corresponds to cumulative release of MH (in percentage) and b) to the cumulative concentration (µg/mL) of the released antibiotic during 24 h. Mean ± SD (*n* = 3).

Furthermore, the release profiles of Groups 5 and 6 were also compared and no differences were detected at any pH. At pH 7.4, samples of Group 5 released 72 ± 0.1 % of the antibiotic, reaching a concentration of 16 ± 1.8 µg/mL by the first hour and 100 % was released by 24 h, reaching 23 ± 2.5 µg/mL. Group 6 released 70 ± 1.5 %, reaching 18 ± 2.5 µg/mL by the first hour and reached 26 ± 1.8 µg/mL of cumulative release after 24 h. Results suggest that the presence of HA did not influence in the adsorption or in the release of the antibiotic. The MH discharge was more progressive at higher pH and presented a higher initial burst at lower pH.

4.3.3. Microbiological assays

4.3.3.1. Antimicrobial activity of scaffolds

After measuring the diameter of the inhibition zone produced by the samples and the antibiotic control (30 µg of MH), it was observed that MH samples of Group 6 produced a diameter average of 30.86 ± 0.39 mm while the samples without antibiotic (Group 4) did not present any inhibition zone. The positive control exhibited a diameter average of 29.57 ± 0.88 mm, in accordance with the expected results for MH and *S. aureus* ATCC 25923 (25 to 30 mm) [39].

4.3.3.2. Antimicrobial activity of release medium supernatants

Results suggest that the MH antimicrobial activity was not affected by the production steps of adsorption, drying and storage, as well as the polymeric linkage. Both MH solution and HA-MH-Col-PLA supernatants revealed a minimal inhibitory concentration of 0.0625 µg/mL. Levofloxacin was used as an external control and the obtained MIC was 0.25 µg/mL, showing a high susceptibility of the used strain for minocycline and levofloxacin.

4.3.3.3. Biofilm inhibition

The biofilm formation inhibition was evaluated by SEM (Fig. 4.8), where it was observed that Group 6 (HA-MH-Col-PLA) samples presented a significant decrease in biofilm formation when comparing to Group 4 (Col-PLA), which presented *S. aureus* biofilm covering the surface, with cells morphology looking similar to that of normal staphylococcal cells.

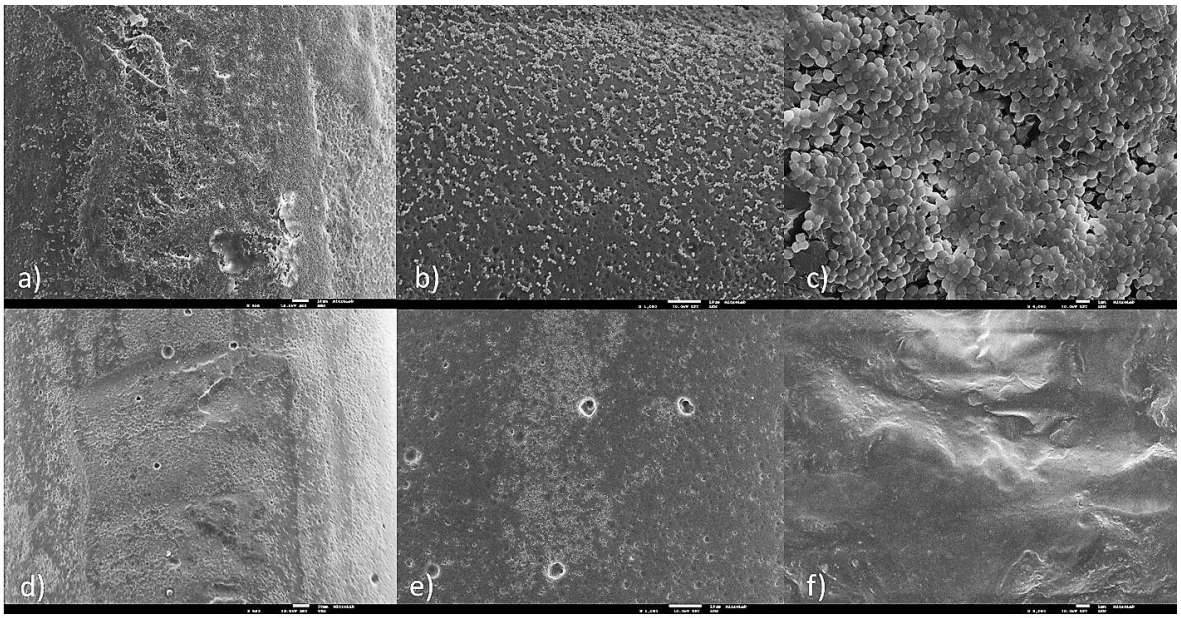

Figure 4.8. SEM images of the PLA scaffolds after the incubation with *S. aureus*, showing that Group 4 (a to c) presented numerous *S. aureus* colonies on its surface, while Group 6 (d to f) presented the absence of the colonies on its surface. Images a) to c) and d) to f) correspond to 500, 1000 and 4000x magnification, respectively.

4.3.4. Cytocompatibility assays

4.3.4.1. Viability/Metabolic activity

The hMSCs cultures were found to proliferate actively over the surface of the assayed scaffolds during the 15 day culture period (Fig. 4.9). Comparatively, increased resazurin reduction values were attained at day 5 for the HA-MH-Col-PLA composition (Group 6), a trend further maintained during the remaining culture period. Further, cultures grown over MH-Col-PLA scaffolds (Group 5) presented significant higher reduction values than control, from day 10 onwards (Fig. 4.9).

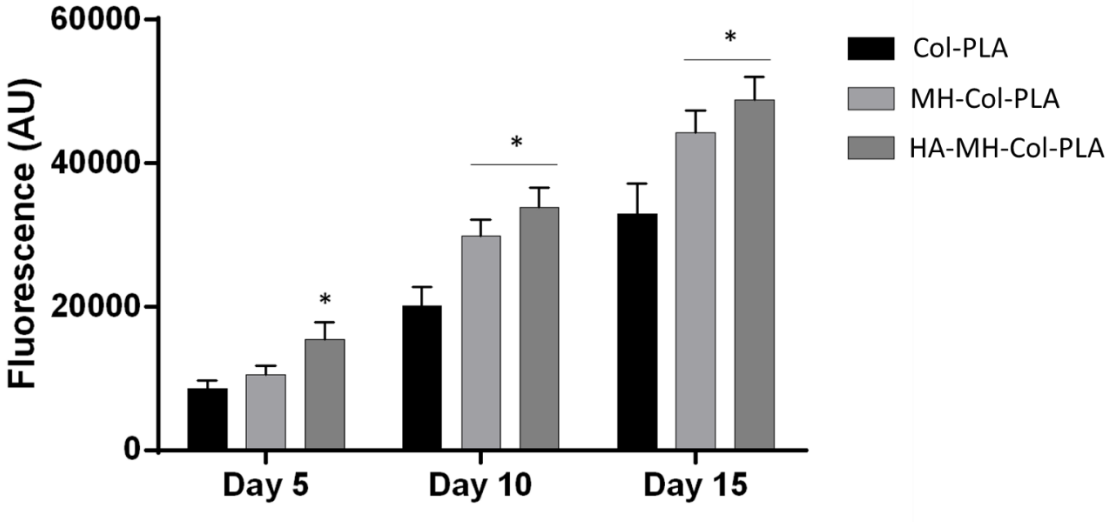

Figure 4.9. Resazurin viability assay of hMSCs cultures established for 15 days on control (Group 4, Col-PLA), Group 5 (MH-Col-PLA) and Group 6 (HA-MH-Col-PLA). * marks Tukey's post-hoc test being significantly different from Col-PLA, at each time point, with $P < 0.05$.

4.3.4.2. Cell morphology and distribution

hMSCs were found to adhere and proliferate actively over the surface of seeded scaffolds. SEM analysis allowed for a detailed morphological analysis of adhered cells, as well as the characterization of the cell-material interaction (Fig. 4.10). On Group 4 (Col-PLA), cells presented a flat morphology with a high degree of cytoplasmic spreading and a trend for a global round morphology, with evident lamellipodia cytoplasmic digitations. On MH-Col-PLA scaffolds (Group 5), cells presented a more skewed and elongated morphology, with evidence of filopodial protrusions extending and establishing direct contact with the scaffold surface and with neighboring cells. Cells grown on Group 6 (HA-MH-Col-PLA) also presented an elongated morphology and a higher evidence of direct cell-to-cell contact, as well as cell-to-scaffold interactions trough interdigitating filopodial extensions.

Both SEM (Fig. 4.10) and immunofluorescent imaging (Fig. 4.11) revealed that, over Col-PLA scaffolds (Group 4), cells organized into structured aggregates, while a more spread organization with a scatter distribution could be identified over MH-Col-PLA (Group 5) and HA-MH-Col-PLA scaffolds (Group 6). In the later, cultures presented areas of high cellular density with abundant intercellular contacts established through filopodial projections (Fig. 4.10 and 4.11).

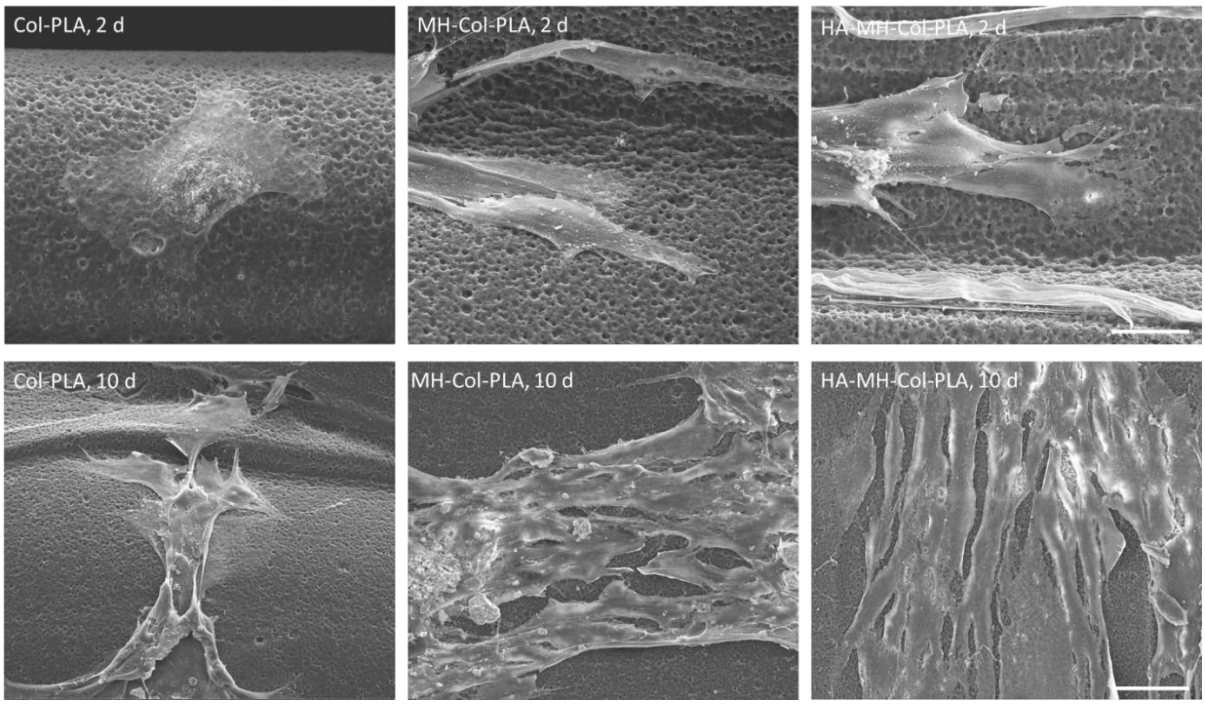

Figure 4.10. Representative SEM images of hMSCs cultures established for 2 days (top row) and 10 days (bottom row), on the surface of control (Group 4, col-PLA), Group 5 (MH-Col-PLA) and Group 6

(HA-MH-Col-PLA) scaffolds. Scale bar corresponds to 20 µm on the top row and 50 µm on the bottom row.

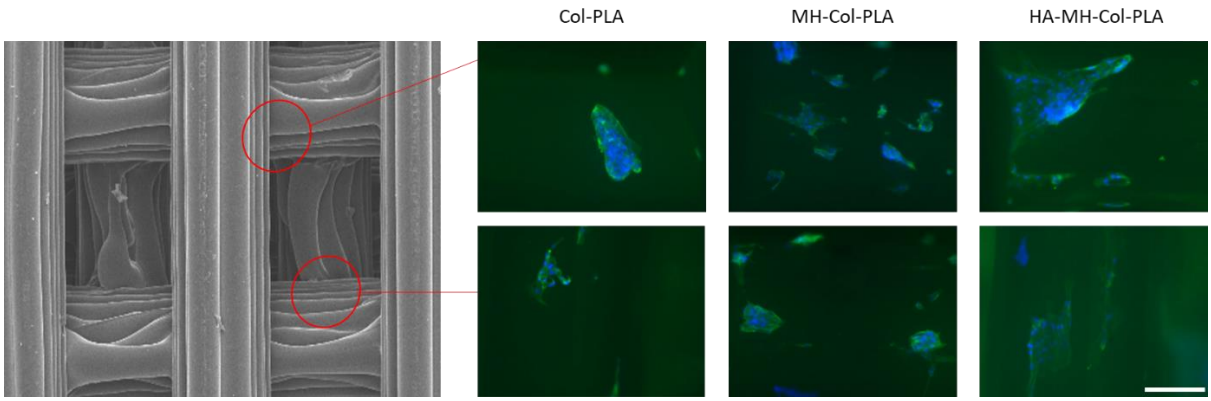

Figure 4.11. Representative immunofluorescent images of hMSCs cultures established for 10 days on the surface of Group 4 (Col-PLA), Group 5 (MH-Col-PLA) and Group 6 (HA-MH-Col-PLA) scaffolds. Cells were stained for nucleus (DAPI - blue) and actin cytoskeleton (F-actin – green). Scale bar corresponds to 200 µm.

4.3.4.3. Osteogenic differentiation

The hMSCs cultured with the scaffolds showed significant differences regarding the upregulation of the osteogenic genes (Fig. 4.12). Comparatively, increased mRNA levels of the three amplified genes were found at cells cultured with scaffolds containing MH (Group 5) and the association of MH with HA (Group 6) in comparison with control (Group 4). Further, Group 6 (HA-MH-Col-PLA) showed a higher upregulation in comparison with Group 5 (HM-Col-PLA), significant for the gene OCN (Fig. 4.12).

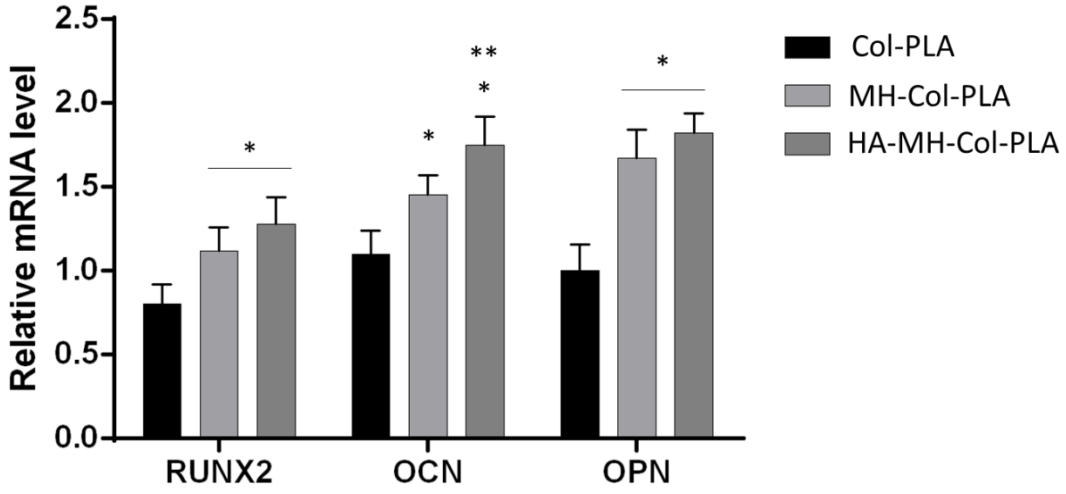

Figure 4.12. Relative expression of RUNX2, OCN and OPN osteogenic genes in hMSCs after 15 days cultured with the scaffolds, Group 4 (Col-PLA) as control, Group 5 (MH-Col-PLA) and Group 6 (HA-MH-Col-PLA) showing the differences of the upregulation for MH and HA+MH.
* - significantly different from Col-PLA ** - significantly different from MH-Col-PLA with $P < 0.01$.

4.4. Discussion

The aim of this study was to produce functionalized 3D scaffolds for bone regeneration using inexpensive production methods to be a viable alternative for the autograft bone.

Regarding conventional fabrication techniques as solvent casting, it is difficult to control the internal pore size, geometry and distribution [40], as well as the struggle of removing completely the porogen of thicker pieces [41]. In contrast, the fused deposition modeling technique using a filament can overcome these limitations for 3D porous structures fabrication with a significant improve in the samples reproducibility, production speed and volume [17]. Consequently, this method is adequate for designing artificial bone substitutes with complex inner and outer geometries that can produce structures based on medical images as topographies or MRI for an improved fit in patient's bone defects [22,23].

In the present study, 3D printed PLA scaffolds with pore sizes of 1000 µm were prepared and functionalized with collagen, HA and MH, after an alkali hydrolysis treatment. Alkaline surface hydrolysis is a simple and permanent way to create reactive functional groups as carboxylic acids and hydroxyls on PLA, which can readily be conjugated with surface-modifying species containing amine or hydroxyl groups [12]. The alkali treatment increased the polymer crystallinity (Fig. 4.5 a), surface porosity (Fig. 4.3, e) and dramatically increased the wettability of the surface (Fig. 4.5 c). The FT-IR/ATR analysis (Fig. 4.5 b) also showed a very different infrared spectrum after the alkali treatment, suggesting that the surface was chemically changed. Since collagen and minocycline present amine groups, it was expected that scaffolds submitted to alkali hydrolysis would display a higher affinity to the adsorption phase, consequently presenting greater antibiotic concentrations and a more controlled release, that was observed in the present study, where alkali treated samples presented a higher cumulative concentration, up to 4x and a slower release rate (Fig. 4.7).

Typically, PLA has been coated with biomimetic apatite and extra cellular matrix proteins like fibronectin and collagen [13], presenting improvements regarding cellular response, as the recent study of Ritz et al. [4], where printed polymeric scaffolds were coated with collagen and Roh et al. [19], that produced treated polymeric scaffolds with HA particles into the samples. In the present study, we chose associate collagen to HA and MH by the adsorption method. Adsorption will avoid the necessity of the compounds went through the fabrication process that often involves elevated temperatures and harsh chemicals, which can degrade and inactivate those [30]. A collagen cover and the HA nanoparticles were observed in Fig. 4.3 (g and i) and Fig. 4.4 respectively, showing the success of the adsorption technique in adding the compounds on the scaffold surface. Also, the XRD, EDS and surface water contact angle showed that the presence of MH and HA did not altered any other physico-chemical property (Fig. 4.4 and 4.5).

Antimicrobial assays were performed in order to prove that the MH was still able to present the same activity after the addition into the scaffolds. Results showed that the scaffolds containing MH presented antimicrobial and biofilm formation inhibition activity *against S. aureus*, one of the most common bacteria seen in osteomyelitis (Fig. 4.8). MIC assays using the released supernatant of the samples showed that *S. aureus* ATCC 25923 is a very sensitive strain to MH, presenting lower concentrations in comparison to other studies [27,35] and the scaffolds loaded with MH presented the same results as the positive control (MH solution), discarding any possibility of interference caused by other compounds or the functionalization procedure itself. Additionally, our independent control (levofloxacin) presented the same MIC reported in other studies [42,43], validating our MH results. In general, results show that the antimicrobial activity was not hampered by the adsorption and the drying procedures and the scaffolds could play a consistent role in preventing infections.

The viability assays (resazurin reduction, Fig. 4.9) using hMSCs cultures presented significant higher values for Group 6 since the first fluorescence reading in comparison with control (Group 4, Col-PLA). Comparing Group 5 to 6, the second presented improved cell viability during all the assay, being significant at day 5, showing a remarkable cellular response in the presence of HA.

Being the hMSCs a precursor osteoblastic cell line, we were able to evaluate the osteoblastic differentiation by quantitative PCR amplifying the gene that mediates osteogenic differentiation (RUNX2) and other osteoblast specific genes as OCN and OPN [37]. Samples containing MH presented an upregulation of these genes in comparison with control (Group 4, Col-PLA), with Group 6 presenting the strongest upregulation, showing the effect of the HA nanoparticles bioactivity on the scaffold (Fig. 4.12).

In the literature, studies show that MH can induce proliferation of different cell lines as osteoblasts [27], bone marrow osteoblastic/stem cells [44,45] and murine osteoprecursor cells [46], however in a dependent concentration manner, where higher concentrations of MH can inhibit cell proliferation and differentiation, also illustrated by the studies, and the inhibition of macromolecule synthesis may be one of the cytotoxic mechanisms of tetracyclines against mammalian cells and difference in the cytotoxic effects among cell lines might be attributed to the difference in the permeability and/or retentivity of MH into the cells [47]. In the present study, the controlled release of the MH in proper concentrations was able to deliver antibacterial activity and, at the same time, improved cellular response *in vitro*. Remarkably, the presence of HA nanoparticles with MH enhanced even further the cellular response of the scaffold, presenting increase cell viability and osteogenic differentiation, which result in a faster bone regeneration. Further studies should be conducted *in vivo* in order to corroborate these results.

References

[1] Kargozar S, Hashemian SJ, Soleimani M, Milan PB, Askari M, Khalaj V. Acceleration of bone regeneration in bioactive glass/gelatin composite scaffolds seeded with bone marrow-derived mesenchymal stem cells over-expressing bone morphogenetic protein-7. Mater Sci Eng C 2017;75:688–98. doi:10.1016/j.msec.2017.02.097.

[2] Martin V, Bettencourt A. Bone regeneration: Biomaterials as local delivery systems with improved osteoinductive properties. Mater Sci Eng C 2017. doi:http://doi.org/10.1016/j.msec.2017.04.038.

[3] Global Data. Bone Grafts and Substitutes - Global Analysis and Market Forecasts. Res Mark 2014:232.

[4] Ritz U, Gerke R, Götz H, Stein S, Rommens PM. A new bone substitute developed from 3D-prints of polylactide (PLA) loaded with collagen i: An in vitro study. Int J Mol Sci 2017;18. doi:10.3390/ijms18122569.

[5] Kim SE, Yun YP, Shim KS, Kim HJ, Park K, Song HR. 3D printed alendronate-releasing poly(caprolactone) porous scaffolds enhance osteogenic differentiation and bone formation in rat tibial defects. Biomed Mater 2016;11:55005. doi:10.1088/1748-6041/11/5/055005.

[6] Larrañaga A, Aldazabal P, Martin FJ, Sarasua JR. Hydrolytic degradation and bioactivity of lactide and caprolactone based sponge-like scaffolds loaded with bioactive glass particles. Polym Degrad Stab 2014;110:121–8. doi:10.1016/j.polymdegradstab.2014.08.021.

[7] Tarafder S, Bose S. Polycaprolactone-coated 3D printed tricalcium phosphate scaffolds for bone tissue engineering: in vitro alendronate release behavior and local delivery effect on in. ACS Appl Mater Interfaces 2014;6:9955-9965. dx.doi.org/10.1021/am501048n

[8] Zabeu JLA, Mercadante MT. Substitutos ósseos comparados ao enxerto ósseo autólogo em cirurgia ortopédica: revisão sistemática da literatura. Rev Bras Ortop 2008;43:59–68. doi:10.1590/S0102-36162008000200002.

[9] Kumar P, Vinitha B, Fathima G. Bone grafts in dentistry. J Pharm Bioallied Sci 2013;5:S125-7. doi:10.4103/0975-7406.113312.

[10] Do A, Khorsand B, Geary SM, Salem AK. 3D Printing of Scaffolds for Tissue Regeneration Applications. Adv Heal Mater 2015;4:1742–62. doi:10.1002/adhm.201500168.3D.

[11] Bae E, Park K, Shim J, Chung H, Choi J, Lee J. Efficacy of rhBMP-2 Loaded PCL/B-TCP/bdECM Scaffold Fabricated by 3D Printing Technology on Bone Regeneration 2018;2018. doi:10.1155/2018/2876135.

[12] Rasal RM, Janorkar A V., Hirt DE. Poly(lactic acid) modifications. Prog Polym Sci 2010;35:338–56. doi:10.1016/j.progpolymsci.2009.12.003.

[13] Krasowska A, Sigler K. How microorganisms use hydrophobicity and what does this mean for human needs? Front Cell Infect Microbiol 2014;4:1–7. doi:10.3389/fcimb.2014.00112.

[14] Yang J, Wan Y, Tu C, Cai Q, Bei J, Wang S. Enhancing the cell affinity of macroporous poly(L-lactide) cell scaffold by a convenient surface modification method. Polym Int 2003;52:1892–9. doi:10.1002/pi.1272.

[15] Krebs MD, Sutter KA, Lin ASP, Guldberg RE, Alsberg E. Injectable poly(lactic-co-glycolic) acid scaffolds with in situ pore formation for tissue engineering. Acta Biomater 2009;5:2847–59. doi:10.1016/j.actbio.2009.04.035.

[16] Wu H, Lei P, Liu G, Zhang YS, Yang J, Zhang L. Reconstruction of Large-scale Defects with a Novel Hybrid Scaffold Made from Poly(L-lactic acid)/Nanohydroxyapatite/Alendronate-loaded Chitosan Microsphere: In vitro and in vivo Studies. Sci Rep 2017;7:1–14. doi:10.1038/s41598-017-00506-z.

[17] Stansbury JW, Idacavage MJ. 3D printing with polymers: Challenges among expanding options and opportunities. Dent Mater 2016;32:54–64. doi:10.1016/j.dental.2015.09.018.

[18] Zhang W, Feng C, Yang G, Li G, Ding X, Wang S. 3D-printed scaffolds with synergistic effect of hollow-pipe structure and bioactive ions for vascularized bone regeneration. Biomaterials 2017;135:85–95. doi:10.1016/j.biomaterials.2017.05.005.

[19] Roh HS, Lee CM, Hwang YH, Kook MS, Yang SW, Lee D. Addition of MgO nanoparticles and plasma surface treatment of three-dimensional printed polycaprolactone/hydroxyapatite scaffolds for improving bone regeneration. Mater Sci Eng C 2017;74:525–35. doi:10.1016/j.msec.2016.12.054.

[20] Wang M, Favi P, Cheng X, Golshan NH, Ziemer KS, Keidar M. Cold atmospheric plasma (CAP) surface nanomodified 3D printed polylactic acid (PLA) scaffolds for bone regeneration. Acta Biomater 2016;46:256–65. doi:10.1016/j.actbio.2016.09.030.

[21] Lim SH, Chia SMY, Kang L, Yap KYL. Three-Dimensional Printing of Carbamazepine Sustained-Release Scaffold. J Pharm Sci 2016;105:2155–63. doi:10.1016/j.xphs.2016.04.031.

[22] Lai Y, Cao H, Wang X, Chen S, Zhang M, Wang N. Porous composite scaffold incorporating osteogenic phytomolecule icariin for promoting skeletal regeneration in challenging osteonecrotic bone in rabbits. Biomaterials 2018;153:1–13. doi:10.1016/j.biomaterials.2017.10.025.

[23] Stephanie Ishack, Aranzazu Mediero, Tuere Wilder, John L. Ricci and BN, Cronstein. Bone Regeneration in Critical Bone Defects Using Three- Dimensionally Printed β-

Tricalcium Phosphate/Hydroxyapatite Scaffolds Is Enhanced by Coating Scaffolds with Either Dipyridamole or BMP-2. J Biomed Mater Res B Appl Biomater 2017;105:366–75. doi:doi:10.1002/jbm.b.33561.

[24] Baumann B, Jungst T, Stichler S, Feineis S, Wiltschka O, Kuhlmann M. Control of Nanoparticle Release Kinetics from 3D Printed Hydrogel Scaffolds. Angew Chemie - Int Ed 2017;56:4623–8. doi:10.1002/anie.201700153.

[25] Li J, Xu Q, Teng B, Yu C, Li J, Song L. Investigation of angiogenesis in bioactive 3-dimensional poly(D,L-lactide-co-glycolide)/nano-hydroxyapatite scaffolds by in vivo multiphoton microscopy in murine calvarial critical bone defect. Acta Biomater 2016;42:389–99. doi:10.1016/j.actbio.2016.06.024.

[26] Garrido-Mesa N, Zarzuelo A, Gálvez J. Minocycline: Far beyond an antibiotic. Br J Pharmacol 2013;169:337–52. doi:10.1111/bph.12139.

[27] Silva T, Grenho L, Barros J, Silva J, Pinto R, Matos A, Bettencourt A, Gomes PS. Minocycline-releasing PMMA system as a space maintainer for staged bone reconstructions – in vitro antibacterial, cytocompatibility and anti-inflammatory characterization. Biomed Mater 2017;12:35009. doi:10.1088/1748-605X/aa68b8.

[28] Tilakaratne A, Soory M. Anti-inflammatory actions of adjunctive tetracyclines and other agents in periodontitis and associated comorbidities. Open Dent J 2014;8:109–24. doi:10.2174/1874210601408010109.

[29] Claes J, Liesenborghs L, Lox M, Verhamme P, Vanassche T, Peetermans M. In Vitro and In Vivo Model to Study Bacterial Adhesion to the Vessel Wall Under Flow Conditions. J Vis Exp 2015;100:1–10. doi:10.3791/52862.

[30] Visscher LE, Dang HP, Knackstedt MA, Hutmacher DW, Tran PA. 3D printed Polycaprolactone scaffolds with dual macro-microporosity for applications in local delivery of antibiotics. Mater Sci Eng C 2018;87:78–89. doi:10.1016/j.msec.2018.02.008.

[31] Duan B, Cheung WL, Wang M. Optimized fabrication of Ca–P/PHBV nanocomposite scaffolds via selective laser sintering for bone tissue engineering. Biofabrication 2011;3:015001. doi:10.1088/1758-5082/3/1/015001.

[32] Voicu G, Geanaliu RE, Ghiţulică CD, Ficai A, Grumezescu AM, Bleotu C. Synthesis, characterization and bioevaluation of irinotecan-collagen hybrid materials for biomedical applications as drug delivery systems in tumoral treatments. Cent Eur J Chem Synth 2013;11:2134–43. doi:10.2478/s11532-013-0341-1.

[33] Santos C, Gomes PS, Duarte JA, Franke RP, Almeida MM, Costa MEV. Relevance of the sterilization-induced effects on the properties of different hydroxyapatite nanoparticles and assessment of the osteoblastic cell response. J R Soc Interface 2012;9:3397–410. doi:10.1098/rsif.2012.0487.

[34] Guo C, Xiang M, Dong Y. Surface modification of poly (lactic acid) with an improved alkali-acid hydrolysis method. Mater Lett 2015;140:144–7. doi:10.1016/j.matlet.2014.10.099.

[35] Matos AC, Gonçalves LM, Rijo P, Vaz MA, Almeida AJ, Bettencourt AF. A novel modified acrylic bone cement matrix. A step forward on antibiotic delivery against multiresistant bacteria responsible for prosthetic joint infections. Mater Sci Eng C 2014;38:218–26. doi:10.1016/j.msec.2014.02.002.

[36] Clinical and Laboratory Standards Institute. Methods for Dilution Antimicrobial Susceptibility Tests for Bacteria That Grow Aerobically ; Approved Standard — Ninth Edition. vol. 32. 2012. doi:10.4103/0976-237X.91790.

[37] Carvalho A, Cangueiro L, Oliveira V, Vilar R, Fernandes MH, Monteiro FJ. Femtosecond laser microstructured Alumina toughened Zirconia: A new strategy to improve osteogenic differentiation of hMSCs. Applied Surface Science. 2018 Mar 30;435:1237-45.

[38] Silva MM, Calado R, Marto J, Bettencourt A, Almeida AJ, Gonçalves LMD. Chitosan nanoparticles as a mucoadhesive drug delivery system for ocular administration. Mar Drugs 2017;15:1–16. doi:10.3390/md15120370.

[39] Clinical and Laboratory Standards Institute, CLSI. CLSI-M100-S27 Performance standards for antimicrobial susceptibility testing. 2017.

[40] Kwon BJ, Seon G, Lee M, Koo MA, Kim M, Kim D. Locally delivered ethyl-2,5-dihydroxybenzoate using 3D printed bone implant for promotion of bone regeneration in a osteoporotic animal model. Eur Cells Mater 2018;35:1–12. doi:10.22203/eCM.v035a01.

[41] Khang G, Kim MS, Lee HB. A Manual For Biomaterials/Scaffold Fabrication Technology. vol. 4. World Scientific Publishing Co. Pte. Ltd.; 2007.

[42] Matos AC, Marques CF, Pinto R V., Ribeiro IAC, Gonçalves LM, Vaz MA, Ferreira JMS, Almeida AJ, Bettencourt AF. Novel doped calcium phosphate-PMMA bone cement composites as levofloxacin delivery systems. Int J Pharm 2015;490:200–8. doi:10.1016/j.ijpharm.2015.05.038.

[43] Matos AC, Ribeiro IAC, Guedes RC, Pinto R, Vaz MA, Gonçalves LM, Vaz MA, Ferreira JMS, Almeida AJ, Bettencourt AF. Key-properties outlook of a levofloxacin-loaded acrylic bone cement with improved antibiotic delivery. Int J Pharm 2015;485:317–28. doi:10.1016/j.ijpharm.2015.03.035.

[44] Dou XC, Zhu XP, Zhou J, Cai HQ, Tang J, Li QL. Minocycline-released hydroxyapatite-gelatin nanocomposite and its cytocompatibility in vitro. Biomed Mater 2011;6:025002. doi:10.1088/1748-6041/6/2/025002.

[45] Gomes PS, Fernandes MH. Effect of therapeutic levels of doxycycline and minocycline

in the proliferation and differentiation of human bone marrow osteoblastic cells. Arch Oral Biol 2007;52:251–9. doi:10.1016/j.archoralbio.2006.10.005.

[46] Park JB. Effects of Doxycycline, Minocycline, and Tetracycline on Cell Proliferation, Differentiation, and Protein Expression in Osteoprecursor Cells. J Craniofac Surg 2011;22:1839–42. doi:10.1097/SCS.0b013e31822e8216.

[47] Suzuki A, Yagisawa J, Kumakura S, Tsutsui T. Effects of minocycline and doxycycline on cell survival and gene expression in human gingival and periodontal ligament cells. J Periodontal Res 2006;41:124–31. doi:10.1111/j.1600-0765.2005.00843.x.

Chapter 5. Conclusions and future perspectives

The general aim of the thesis was the development of three different polymeric platforms carrying minocycline aiming two clinical conditions: Periodontal disease with the chitosan nanoparticles and bone regeneration using two different polylactide scaffolds. Minocycline was chosen due to the combination of anti-inflammatory and antimicrobial effects, equally important for both clinical conditions. Regarding periodontal disease, the inflammation induced by bacteria substratum as LPS, is the responsible for the tissue destruction and tooth lost, making the reduction of this inflammation essential for the disease control. The antimicrobial activity is important as therapeutic adjuvant for root plaining treatment, once the disease is caused by the presence of anaerobic bacteria as *P. gingivalis* and *A. actinomycetemcomitans* into gingival crest fluids.

Regarding bone regeneration, the anti-inflammatory properties of minocycline are also important, once the surgical procedure and tissue manipulation will inevitably cause a local inflammation and it can delay and/or reduce the regeneration if it is not controlled. Also, inflammation is related with edemas, hyperemia and pain, bringing discomfort to patients during the post-chirurgical period. The antimicrobial activity is important to avoid infections in the surgical wound, once the area is more vulnerable after the manipulation and infections can lead to delays, poor regeneration or even tissue necrosis and graft loss.

The thesis project started by producing and characterizing chitosan nanoparticles with different reagent proportions, at different pH values, and the best formulation (chitosan and tri-polyphosphate 3:1 at pH 5.5, containing surfactant) was used for the further assays, reaching nanoparticulate size and stable zeta potential (372 ± 55 nm; ZP of +23 ± 1 mV). The characterization carried out showing its rounded morphology, low crystallinity degree and the absent of chemical interactions between the antibiotic and the carrier, presenting a release up to 24 hours. *In vitro* cellular assays were carried out using human gingival fibroblasts (HGFs) and the nanoparticles loaded with minocycline presented higher cell viability with a pronounced downregulation of inflammatory genes due to a possible synergetic effect between minocycline and the chitosan. The assays also showed that nanoparticles were successfully internalized by the cells, increasing the intracellular drug concentration, which could play an important role, once the main pathogens can invade the host cells and be protected against host defenses and antibiotics. However, due to the lack of time and the complexity of the manipulation of anaerobic bacteria, the antimicrobial assays were not performed with the nanoparticles. Concerning the solvent casting/particulate leaching scaffolds, they were added of bioglass and its surface was functionalized, aiming an improved cellular response and colonization. The antibiotic incorporation into the scaffolds was accomplished through adsorption, maintaining its characteristics and properties, without being exposed to high temperatures or organic

solvents, which commonly occurs with other methods. The characterization showed interconnected porous, the presence of bioglass elements and interactions between the polymer and the minocycline. These interactions could explain the lack of *in vitro* antibiotic release at neutral pH, however, at acidic pH a constant release up to 72 hours was reached. The antimicrobial assays showed that the minocycline activity was maintained, inhibiting biofilm formation, bacterial growth and presenting the same MIC as the control against *S. aureus*. The cellular assays were performed with human osteoblasts cells and showed the importance of dose-dependent toxicity. Using small pieces of the scaffolds we observed first an inhibition of cellular proliferation in the presence of minocycline and later on, an enhancement, however, with a larger and bulky pieces, cell viability was dramatically dropped. The third platform corresponded to the scaffolds produced by 3D printing, functionalized with minocycline and hydroxyapatite nanoparticles (HA), aimed the improvement of the polymeric surface biocompatibility towards cells. The characterization showed that the HA nanoparticles were present on the scaffold surface, meaning that the adsorption was effective in attaching the particles to the scaffolds and the surface become significant more hydrophilic than the polymer without functionalization. The antibiotic release reached 24 h and from the microbial assays, it was possible to observe as in the previous scaffolds, the inhibition of *S. aureus* growth and biofilm formation, presenting the same MIC as the positive control. The samples functionalized with antibiotic and HA showed a clearly improvement regarding cellular osteogenic differentiation and viability. Both pathological conditions targeted in this project affect millions of people around the globe and the population aging is contributing for the increase of the incidence, making the need for improvements regarding these biomaterials, urgent. For future works, these materials should be tested *in vivo* to corroborate these results, once *in vitro* studies are unable to mimic the whole scenario, for instance the scaffold release profile involved with a stable clot or the antimicrobial activity of the nanoparticles against a complex and variable bacterial eco-system, with a fast gingival fluid turnover. Also, there is always space for improvements about the materials as controlled release profiles, stability in biological fluids and so on. The 3D printing techniques can offer several new options yet unexplored such as hybrid scaffolds with different layers, the possibility of using a prepared viscous solution containing nanoparticles to print the materials or even to cover up each layer of the scaffold with some bio-compound.

Overall, it can be concluded that the addition of minocycline into scaffolds containing bio-ceramics and nanoparticles can be accomplished with simple production methods and present improved cellular response and reduction of inflammation, maintaining the antimicrobial activity. Further studies need to be assessed to better understand the interaction of these materials with the biological environment and ensure a safe biomedical application.

References

[1] Davies JE, Hosseini MH. Histodynamics of Endosseous Wound Healing. EM Squared Incorporated Bone Engineering, 1st ed 2000, pp. 1–14, ISBN:096869800x.

[2] Junqueira LC CJ. Histologia básica. Guanabara Koogan, 12th ed., Chapter, 8, 2008, pp. 132–135.

[3] Mazzonetto R, Netto HD, Nascimento FF. Enxertos Ósseos Em Implantodontia, 1a ed. Editora Napoleão, 2012 ISBN: 978-85-60842-32.

[4] Zabeu JLA, Mercadante MT. Substitutos ósseos comparados ao enxerto ósseo autólogo em cirurgia ortopédica: revisão sistemática da literatura. Rev Bras Ortop 2008;43:59–68. doi:10.1590/S0102-36162008000200002.

[5] Franco C, Patricia HR, Timo S, Claudia B, Marcela H. Matrix metalloproteinases as regulators of periodontal inflammation. Int J Mol Sci 2017;18:1–12. doi:10.3390/ijms18020440.

[6] Yao W, Xu P, Pang Z, Zhao J, Chai Z, Li X. Local delivery of minocycline-loaded PEG-PLA nanoparticles for the enhanced treatment of periodontitis in dogs. Int J Nanomedicine 2014;9:3963–70. doi:10.2147/IJN.S67521.

[7] Global Data. Bone Grafts and Substitutes - Global Analysis and Market Forecasts. Res Mark 2014:232.

[8] Kumar P, Vinitha B, Fathima G. Bone grafts in dentistry. J Pharm Bioallied Sci 2013;5:S125-7. doi:10.4103/0975-7406.113312.

[9] Altaie A, Owston H, Jones E. Use of platelet lysate for bone regeneration - are we ready for clinical translation? World J Stem Cells 2016;8:47–55. doi:10.4252/wjsc.v8.i2.47.

[10] Muschler GF, Age and gender-related changes in the cellularity of human bone marrow and the prevalence of osteoblastic progenitors, J. Orthop. 2001;19:1:117–125.

[11] Boraiah S, Paul O, Hawkes D, Wickham M, Lorich DG, Complications of recombinant human BMP-2 for treating complex tibial plateau fractures: a preliminary report, Clin. Orthop. 2009;467:3257–3262.

[12] Arora NS, Ramanayake T, Ren YF, Romanos GE, Platelet-rich plasma: a literature review, Implant. Dent. 2009;18:43:03–310.

[13] Martin V, Bettencourt A. Bone regeneration: Biomaterials as local delivery systems with improved osteoinductive properties. Mater Sci Eng C 2017.

doi:http://doi.org/10.1016/j.msec.2017.04.038.

[14] Thavornyutikarn B, Chantarapanich N, Chen Q. Bone tissue engineering scaffolding : computer-aided scaffolding techniques. 2014. doi:10.1007/s40204-014-0026-7.

[15] Khang G, Kim MS, Lee HB. A Manual For Biomaterials/Scaffold Fabrication Technology. vol. 4. World Scientific Publishing Co. Pte. Ltd.; 2007. ISBN:3 978-981-270-595-2

[16] Roh HS, Lee CM, Hwang YH, Kook MS, Yang SW, Lee D. Addition of MgO nanoparticles and plasma surface treatment of three-dimensional printed polycaprolactone/hydroxyapatite scaffolds for improving bone regeneration. Mater Sci Eng C 2017;74:525–35. doi:10.1016/j.msec.2016.12.054.

[17] Stansbury JW, Idacavage MJ. 3D printing with polymers: Challenges among expanding options and opportunities. Dent Mater 2016;32:54–64. doi:10.1016/j.dental.2015.09.018.

[18] Ferreira-Santos I, Bettencourt A, Almeida AJ. Nanoparticulate Platforms for Targeting Bone Infections: Meeting a Major Therapeutic Challenge. Nanomedicine 2015;10:3131–45. doi:10.2217/nnm.15.134.

[19] Kashi TSJ, Eskandarion S, Esfandyari-Manesh M, Marashi SMA, Samadi N, Fatemi SM. 111 Solid/oil/water PLGA capsules protein. Int J Nanomedicine 2012;7:221–34. doi:10.2147/IJN.S27709.

[20] Anusuya GS, Kandasamy M, Raja SAJ, Sabarinathan S, Ravishankar P, Kandhasamy B. Bone morphogenetic proteins : Signaling periodontal bone regeneration and repair 2016;8:10–5. doi:10.4103/0975-7406.191964.

[21] Kushwaha P, Khedgikar V, Gautam J, Dixit P, Chillara R, Verma A. A novel therapeutic approach with Caviunin-based isoflavonoid that en routes bone marrow cells to bone formation via BMP2/Wnt-β-catenin signaling. Cell Death Dis 2014;5:e1422. doi:10.1038/cddis.2014.350.

[22] Crasto GJ, Kartner N, Reznik N, Spatafora M V, Chen H, Williams R. Controlled bone formation using ultrasound-triggered release of BMP-2 from liposomes. J Control Release 2016. doi:10.1016/j.jconrel.2016.09.032.

[23] Shields LBE, Raque GH, Glassman SD, Campbell M, Vitaz T, Harpring J, Shields CB. Adverse effects associated with high-dose recombinant human bone morphogenetic protein-2 use in anterior cervical spine fusion. Spine 2006;31:542–547.

[24] Boerckel JD, Kolambkar YM, Dupont KM, Uhrig BA, Phelps EA, Stevens HY, Garcia AJ, Guldberg RE. Effects of protein dose and delivery system on BMP-mediated bone regeneration, Biomaterials 2011;32:5241–5251

[25] Lee EU, Lim HC, Hong JY, Lee JS, Jung UW, Choi SH. Bone regenerative efficacy of biphasic calcium phosphate collagen composite as a carrier of rhBMP-2. Clin Oral Implants Res 2015:1–9. doi:10.1111/clr.12568.

[26] Watanabe S, Takabatake K, Tsujigiwa H, Watanabe T, Tokuyama E, Ito S. Efficacy of honeycomb TCP-induced microenvironment on bone tissue regeneration in craniofacial area. Int J Med Sci 2016;13:466–76. doi:10.7150/ijms.15560.

[27] Kim JS, Cha JK, Lee JS, Choi SH, Cho KS. Increased osteoinductivity and mineralization by minimal concentration of bone morphogenetic protein-2 loaded onto biphasic calcium phosphate in a rabbit sinus. J Periodontal Implant Sci 2016;46:350. doi:10.5051/jpis.2016.46.5.350.

[28] Olthof MGL, Kempen DHR, Herrick JL, Yaszemski MJ, Dhert WJA, Lu L. Effect of different sustained bone morphogenetic protein-2 release kinetics on bone formation in poly(propylene fumarate) scaffolds. J Biomed 2017:1–11. doi:10.1002/jbm.b.33866.

[29] Bhattacharjee P, Naskar D, Maiti TK, Bhattacharya D, Kundu SC. Non-mulberry silk fibroin grafted poly (Ie-caprolactone)/nano hydroxyapatite nanofibrous scaffold for dual growth factor delivery to promote bone regeneration. J Colloid Interface Sci 2016;472:16–33. doi:10.1016/j.jcis.2016.03.020.

[30] Mantripragada VP, Jayasuriya AC. Bone regeneration using injectable BMP-7 loaded chitosan microparticles in rat femoral defect. Mater Sci Eng C 2016;63:596–608. doi:10.1016/j.msec.2016.02.080.

[31] Liu Y, Deng LZ, Sun HP, Xu JY, Li YM, Xie X. Sustained dual release of placental growth factor-2 and bone morphogenic protein-2 from heparin-based nanocomplexes for direct osteogenesis. Int J Nanomedicine 2016;11:1147–58. doi:10.2147/IJN.S100156.

[32] Khojasteh A, Fahimipour F, Eslaminejad MB, Jafarian M, Jahangir S, Bastami F. Development of PLGA-coated β-TCP scaffolds containing VEGF for bone tissue engineering. Mater Sci Eng C 2016;69:780–8. doi:10.1016/j.msec.2016.07.011.

[33] Jilka RL, Oapos-Brien CA, Bartell SM, Weinstein RS, Manolagas SC. Continuous elevation of PTH increases the number of osteoblasts via both osteoclast-dependent and -independent mechanisms. J Bone Miner Res 2010;25:2427–37. doi:10.1002/jbmr.145.

[34] Dempster DW, Cosman F, Kurland ES, Zhou H, Nieves J, Woelfert L, Shane E, Plavetić K, Müller R, Bilezikian J, Lindsay R. Effects of daily treatment with parathyroid hormone on bone micro-architecture and turnover in patients with osteoporosis: a paired biopsy study, J. Bone Miner. 2001;16:1846–1853.

[35] Liedert A, Wagner L, Seefried L, Ebert R, Jakob F, Ignatius A. Estrogen receptor and Wnt signaling interact to regulate early gene expression in response to mechanical strain in osteoblastic cells, Biochem. Biophys. 2010;394:755–759.

[36] Beral V. Million Women Study Collaborators, Breast cancer and hormone-replacement therapy in the million women study. Lancet 2003;362:419–427.

[37] Bhattarai G, Poudel SB, Kook SH, Lee JC. Resveratrol prevents alveolar bone loss in an experimental rat model of periodontitis. Acta Biomater 2016;29:398–408. doi:10.1016/j.actbio.2015.10.031.

[38] Baur JA, Sinclair DA. Therapeutic potential of resveratrol: the in vivo evidence, Nat. Rev. Drug Discov. 2006;5:493–506.

[39] Dang M, Koh AJ, Jin X, McCauley LK, Ma PX. Local pulsatile PTH delivery regenerates bone defect via enhanced bone remodeling in a cell-free scaffold. Biomaterials 2016;114:1–9. doi:10.1016/j.biomaterials.2016.10.049.

[40] Li Y, Dnmark S, Edlund U, Finne-Wistrand A, He X, Norgrd M. Resveratrol-conjugated poly-Caprolactone facilitates in vitro mineralization and in vivo bone regeneration. Acta Biomater 2011;7:751–8. doi:10.1016/j.actbio.2010.09.008.

[41] Wang W, Sun L, Zhang P, Song J, Liu W. An anti-inflammatory cell-free collagen/resveratrol scaffold for repairing osteochondral defects in rabbits. Acta Biomater 2014;10:4983–95. doi:10.1016/j.actbio.2014.08.022.

[42] Kamath MS, Ahmed SSSJ, Dhanasekaran M, Winkins Santosh S. Polycaprolactone scaffold engineered for sustained release of resveratrol: Therapeutic enhancement in bone tissue engineering. Int J Nanomedicine 2013;9:183–95. doi:10.2147/IJN.S49460.

[43] Rodan GA, Martin TJ. Therapeutic approaches to bone diseases, Science 2000;289:1508–1514.

[44] Tenenbaum HC, Shelemay A, Girard B, Zohar R, Fritz PC. Bisphosphonates and periodontics: potential applications for regulation of bone mass in the periodontium and other therapeutic/diagnostic uses, J. Periodontol. 2002;73:813–822.

[45] Giuliani N, Pedrazzoni M, Negri G, Passeri G, Impicciatore M, Girasole G. Bisphosphonates stimulate formation of osteoblast precursors and mineralized nodules in murine and human bone marrow cultures in vitro and promote early osteoblastogenesis in young and aged mice in vivo, Bone 1998;22:455–461.

[46] Kang AR, Oh YR, Kim HY, Park MJ, Joo BS, Choi WJ. Up-regulation of inhibitors of DNA binding/differentiation gene during alendronate-induced osteoblast differentiation. Arch Gynecol Obstet 2012;285:1331–8. doi:10.1007/s00404-011-2141-1.

[47] Toker H, Ozdemir H, Ozer H, Eren K. A comparative evaluation of the systemic and local alendronate treatment in synthetic bone graft: A histologic and histomorphometric study in a rat calvarial defect model. Oral Surg Oral Med Oral Pathol Oral Radiol 2012;114:S146–52. doi:10.1016/j.oooo.2011.09.027.

[48] Drake MT, Clarke BL, Khosla S. Bisphosphonates: mechanism of action and role in clinical practice. Mayo Clin Proc 2008;83:1032–45. doi:10.4065/83.9.1032.

[49] Park KW, Yun YP, Kim SE, Song HR. The effect of alendronate loaded biphasic calcium phosphate scaffolds on bone regeneration in a rat tibial defect model. Int J Mol Sci 2015;16:26738–53. doi:10.3390/ijms161125982.

[50] Hur W, Park M, Lee JY, Kim MH, Lee SH, Park CG. Bioabsorbable bone plates enabled with local, sustained delivery of alendronate for bone regeneration. J Control Release 2016;222:97–106. doi:10.1016/j.jconrel.2015.12.007.

[51] Liu YS, Ou ME, Liu H, Gu M, Lv LW, Fan C, Chen T, Zhao XH, Jin CY, Zhang X, Ding Y, Zhou YS. The effect of simvastatin on chemotactic capability of SDF-1alpha and the promotion of bone regeneration, Biomaterials 2014;35:4489–4498.

[52] Zhang Y, Bradley AD, Wang D, Reinhardt RA. Statins, bone metabolism and treatment of bone catabolic diseases, Pharmacol. 2014;88:53–61.

[53] Yue X, Niu M, Zhang T, Wang C, Wang Z, Wu W, Zhang Q, Lai C, Zhou L. In vivo evaluation of a simvastatin-loaded nanostructured lipid carrier for bone tissue regeneration. Nanotechnology 2016;27:115708. doi:10.1088/0957-4484/27/11/115708.

[54] Maximov P, Lee T, Jordan VC. The discovery and development of selective estrogen receptor modulators (SERMs) for clinical practice, Curr. Clin. Pharmacol. 2013;8:135–155.

[55] Zhang ML, Cheng J, Xiao YC, Yin RF, Feng X. Raloxifene microsphere-embedded collagen/chitosan/β-tricalcium phosphate scaffold for effective bone tissue engineering. Int J Pharm 2017;518:80–5. doi:10.1016/j.ijpharm.2016.12.031.

[56] Zubery Y, Dunstan CR, Story BM, Kesavalu A, Ebersole JL, Holt SC. Bone resorption caused by three periodontal pathogens in vivo in mice is mediated in part by prostaglandin. Infect Immun 1998;66:4158–62.

[57] Zhang W, Ju J, Rigney T, Tribble G. Porphyromonas gingivalis infection increases osteoclastic bone resorption and osteoblastic bone formation in a periodontitis mouse model. BMC Oral Health 2014;14:89. doi:10.1186/1472-6831-14-89.

[58] Alenezi A, Naito Y, Terukina T, Prananingrum W, Jinno Y, Tagami T. Controlled release of clarithromycin from PLGA microspheres enhances bone regeneration in rabbit calvaria defects. J Biomed Mater Res Part B Appl Biomater 2017:1–8. doi:10.1002/jbm.b.33844.

[59] Sadowski T, Steinmeyer J. Effects of tetracyclines on the production of matrix metalloproteinases and plasminogen activators as well as of their natural inhibitors, tissue inhibitor of metalloproteinases-1 and plasminogen activator inhibitor-1, Inflamm. 2001;50:175–182.

[60] Tilakaratne A, Soory M. Anti-inflammatory actions of adjunctive tetracyclines and other agents in periodontitis and associated comorbidities. Open Dent J 2014;8:109–24. doi:10.2174/1874210601408010109.

[61] Garrido-Mesa N, Zarzuelo A, Gálvez J. Minocycline: Far beyond an antibiotic. Br J Pharmacol 2013;169:337–52. doi:10.1111/bph.12139.

[62] Gomes N, Paula A, Nunes N, Góes P, Dutra P. Doxycycline induces bone repair and changes in Wnt signalling. Int J Oral Sci 2017;9:158–66. doi:10.1038/ijos.2017.28.

[63] Golub L, Lee HM, Ryan M. Tetracyclines inhibit connective-tissue break-down by multiple non-antimicrobial mechanisms, Adv. Dent. Res. 1998;12:12–26.

[64] Silva T, Grenho L, Barros J, Silva J, Pinto R, Matos A. Minocycline-releasing PMMA system as a space maintainer for staged bone reconstructions – in vitro antibacterial, cytocompatibility and anti-inflammatory characterization. Biomed Mater 2017;12:35009. doi:10.1088/1748-605X/aa68b8.

[65] Fischer J, Ganellin CR. Analogue-Based Drug Discovery, JWS, 2006 489 ISBN9783527607495.

[66] Yoshinari N, Tohya T, Kawase H, Matsuoka M, Nakane M, Kawachi M. Effect of repeated local minocycline administration on periodontal healing following guided tissue regeneration. J Periodontol 2001;72:284–95. doi:10.1902/jop.2001.72.3.284.

[67] Gomes PS, Fernandes MH. Effect of therapeutic levels of doxycycline and minocycline in the proliferation and differentiation of human bone marrow osteoblastic cells. Arch Oral Biol 2007;52:251–9. doi:10.1016/j.archoralbio.2006.10.005.

[68] Dou XC, Zhu XP, Zhou J, Cai HQ, Tang J, Li QL. Minocycline-released hydroxyapatite-gelatin nanocomposite and its cytocompatibility in vitro. Biomed Mater 2011;6:025002. doi:10.1088/1748-6041/6/2/025002.

[69] Ma S, Adayi A, Liu Z, Li M, Wu M, Xiao L. Asymmetric Collagen/chitosan Membrane Containing Minocycline-loaded Chitosan Nanoparticles for Guided Bone Regeneration. Sci Rep 2016;6:31822. doi:10.1038/srep31822.

[70] Matos AC, Gonçalves LM, Rijo P, Vaz MA, Almeida AJ, Bettencourt AF. A novel modified acrylic bone cement matrix. A step forward on antibiotic delivery against multiresistant bacteria responsible for prosthetic joint infections. Mater Sci Eng C 2014;38:218–26. doi:10.1016/j.msec.2014.02.002.

[71] Marycz K, Pazik R, Zawisza K, Wiglusz K, Maredziak M, Sobierajska P. Multifunctional nanocrystalline calcium phosphates loaded with Tetracycline antibiotic combined with human adipose derived mesenchymal stromal stem cells (hASCs). Mater Sci Eng C 2016;69:17–26. doi:10.1016/j.msec.2016.06.051.

[72] Lee BS, Lee CC, Wang YP, Chen HJ, Lai CH, Hsieh WL. Controlled-release of tetracycline and lovastatin by poly(D,L-lactide-co-glycolide acid)-chitosan nanoparticles enhances periodontal regeneration in dogs. Int J Nanomedicine 2016;11:285–97. doi:10.2147/IJN.S94270.

[73] Rao SK, Setty S, Acharya AB, Thakur SL. Efficacy of locally-delivered doxycycline microspheres in chronic localized periodontitis and on Porphyromonas gingivalis. J Investig Clin Dent 2012;3:128–34. doi:10.1111/j.2041-1626.2011.00110.x.

[74] Chiappe VB, Gomez MV, Rodriguez C, Fresolone M, Romanelli HJ. Subgingivally applied minocycline microgranules in subjects with chronic periodontitis: A randomized clinical and microbiological trial. Acta Odontol Latinoam 2015;28:122–31. doi:10.1590/S1852-48342015000200005.

[75] Dorati R, De Trizio A, Genta I, Merelli A, Modena T, Conti B. Gentamicin-Loaded Thermosetting Hydrogel and Moldable Composite Scaffold: Formulation Study and Biologic Evaluation. J Pharm Sci 2017. doi:10.1016/j.xphs.2017.02.031.

[76] Gao J, Huang G, Liu G, Liu Y, Chen Q, Ren L. A biodegradable antibiotic-eluting PLGA nanofiber-loaded deproteinized bone for treatment of infected rabbit bone defects. J

Biomater Appl 2016;31:241–9. doi:10.1177/0885328216654424.

[77] Lim SH, Chia SMY, Kang L, Yap KYL. Three-Dimensional Printing of Carbamazepine Sustained-Release Scaffold. J Pharm Sci 2016;105:2155–63. doi:10.1016/j.xphs.2016.04.031.

[78] Ishack S, Mediero A, Wilder T, Ricci JL, Cronstein BN. Bone Regeneration in Critical Bone Defects Using Three-Dimensionally Printed β-Tricalcium Phosphate/Hydroxyapatite Scaffolds Is Enhanced by Coating Scaffolds with Either Dipyridamole or BMP-2. J Biomed Mater Res B Appl Biomater 2017;105:366–75. Doi:10.1002/jbm.b.33561.

[79] Zhu W, Xu C, Ma BP, Zheng ZB, Li YL, Ma Q. Three-dimensional printed scaffolds with gelatin and platelets enhance in vitro preosteoblast growth behavior and the sustained-release effect of growth factors. Chin Med J (Engl) 2016;129:2576–81. doi:10.4103/0366-6999.192770.

[80] Suzuki A, Yagisawa J, Kumakura S, Tsutsui T. Effects of minocycline and doxycycline on cell survival and gene expression in human gingival and periodontal ligament cells. J Periodontal Res 2006;41:124–31. doi:10.1111/j.1600-0765.2005.00843.x.

[81] Rasal RM, Janorkar A V, Hirt DE. Poly(lactic acid) modifications. Prog Polym Sci 2010;35:338–56. doi:10.1016/j.progpolymsci.2009.12.003.

[82] Wu H, Lei P, Liu G, Zhang YS, Yang J, Zhang L. Reconstruction of Large-scale Defects with a Novel Hybrid Scaffold Made from Poly(L-lactic acid)/Nanohydroxyapatite/Alendronate-loaded Chitosan Microsphere: In vitro and in vivo Studies. Sci Rep 2017;7:1–14. doi:10.1038/s41598-017-00506-z.

Annex 1

Preparation of Chitosan nanoparticles: formulation optimization

In order to choose the best procedure for chitosan (Chi) nanoparticles (NPs) preparation different tests were conducted to:

1) *Develop a suitable nanoparticle formulation for scale up according to the following criteria:*

a) Drug entrapment efficiency

b) Size distribution

c) Zeta potential

2) Evaluate the effect of NPs freeze drying on size distribution and zeta potential values.

The methodology and obtained results of the previously mentioned tests will be next presented.

1) *Development of nanoparticles formulation for scale up*

For NPs preparation different solutions of Chi, tripolyphosphate (TPP) and minocycline hydrochloride (MH) were prepared as next detailed.

Chi solutions

Two approaches were used in the attempt of obtaining the best nanoparticle formulation for scale up. First, the Chi solution was set without surfactant, where a Chi stock solution of 10mg/mL was prepared by dissolving the chitosan polymer in ultra-pure water with 1% (*V/V*) of acetic acid, leaving it under magnetic stirring for 4 h. After, the Chi stock solution was diluted with ultra-pure water to 1 mg/mL. Then, three Chi solutions groups, with different pH were obtained by adjusting the pH to 3.9, 4.7 and 5.5 with a 0.5 N sodium hydroxide solution.

Second, the solution was set with a surfactant, where a Tween80 (2% *w*/*V*) solution was prepared in ultra-pure water. Then, 900 mL of this solution was added to 100 mL of Chi solution (10 mg/mL) under magnetic stirring, producing a 1mg/mL Chi solution with Tween80 and the pH was adjusted to 5.5 with 0.5 N sodium hydroxide solution, creating the fourth Chi solution group.

TPP solution

A 10 mg/mL tripolyphosphate pentasodium (TPP) solution was prepared by dissolving TPP in ultra-pure water, and adjusting the pH to 9.5 with NaOH 1 N.

MH solutions

MH solutions were prepared in two different concentrations with ultra-pure water, 1 mg/mL and 2 mg/mL and different amounts of MH were incorporated into the TPP solutions. Ultra-pure

water was added in order to provide the same final volume in all groups, as well as the blank groups (nanoparticles without drug).

NPs were formed by adding TPP solutions, containing different amounts of MH and ultra-pure water, dropwise to the Chi solution, illustrated by Fig. 1. Three different proportions of Chi and TPP were used (2.5:1, 3:1 and 6:1), in the attempt to obtain the best formulation. All the formulations are shown in Table 1. The mentioned parameters of all samples that did not present clusters formation were measured and the best formulation was chosen accordingly.

For the scale up, the volume of the solutions were increased in 10 and 20 times, with the same initial proportion and the preparation of Chi and TPP was made following the procedure described above, with 24 mL of Chi solution + 0.8 mL of TPP + 2.2 mL of MH + 1 mL of H_2O as loaded NPs and 24 mL of chi solution + 0.8 mL of TPP + 3.2 mL of H_2O as blank NPs for the twenty fold scale up. TPP mixture was added slowly by dropwise into the Chi solution under vigorous magnetic stirring at room temperature for 25 min.

After, the solutions were centrifuged for 10 min, 15000 g at 6°C and the supernatant was discarded. Finally, a cryoprotectant solution was added (2.5 mL of 10% trehalose). Samples were freeze-dried for 12 h and then put in a desiccator for 24 h.

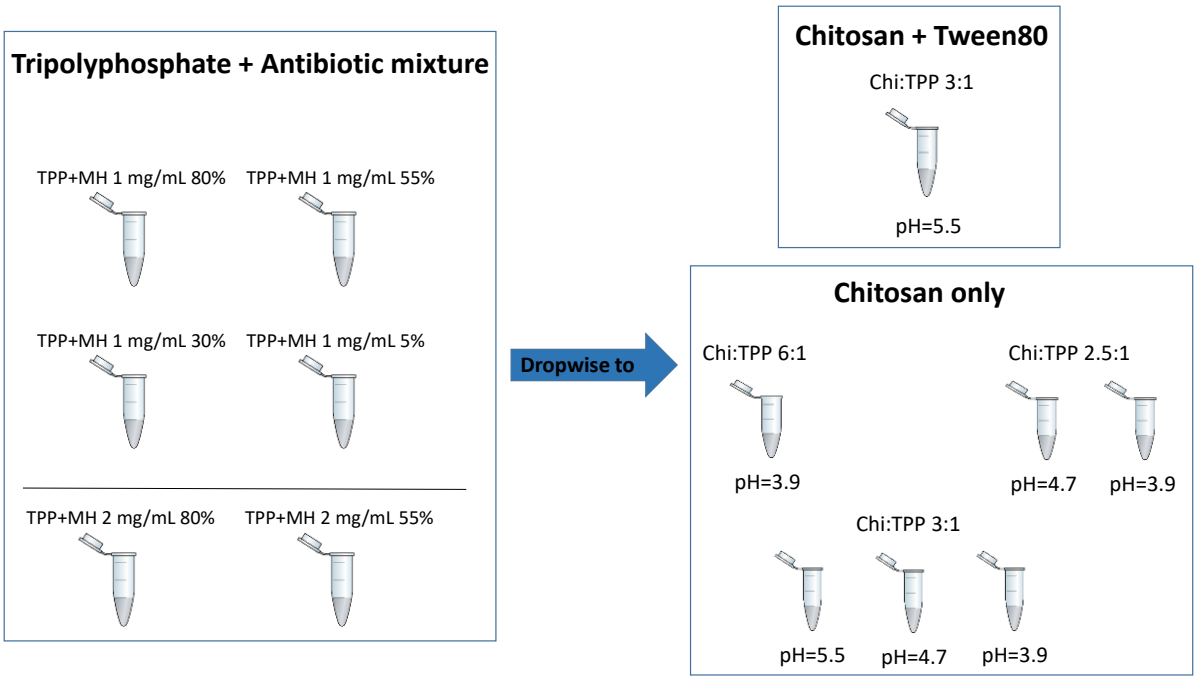

Figure 1. Illustration of the tested combinations for the NPs preparation. The concentration and the proportion of MH and water were varied in the TPP solutions. The pH and the final proportion of Chi:TPP concentration were also varied. Tween80 was mixed with Chi solution in order to increase the EE% of the NPs.

After analyzing the highest drug encapsulation efficiency (Table 1), values of size distribution between 250 and 400 nm and an adequate zeta potential value (to evaluate the stability of the nanoparticles), the formulation corresponding to batch 21 was chosen to scale up (Table 1).

This batch consists in a 1 mg/mL Chi solution + Tween80, pH 5.5, with a proportion of 3:1 Chi:TPP + MH (in a 2 mg/mL concentration) + H_2O in the proportions of 55% of MH and 25% of H_2O. The comparison of the EE% among all the batches, the average size, poly-dispersion index and zeta potential values are shown in Table 1. Each batch corresponds to three samples with the same formulation.

Table 1. Different formulations tested to achieve the stipulated parameters. Batch 21 presented the highest encapsulation efficiency value (EE%) with adequate average size, poly dispersion index and zeta potential values and consequently it was selected to the scale-up production. (n=9, average ± SD).

Formulation	Batch	Z-Ave (nm)	ZP (mV)	EE(%)
Chi:TPP 2.5:1. pH 3.9 Blanc	1	346.4 ± 7.5	34 ± 8	NA
Chi:TPP 3:1. pH 3.9 Blanc	2	313.6 ± 7.8	26 ± 8	NA
Chi:TPP 2.5:1. pH 4.7 Blanc	3	237.3 ± 9.6	22 ± 10	NA
Chi:TPP 3:1. pH 4.7 Blanc	4	312.1 ± 7.9	30 ± 8	NA
Chi:TPP 6:1. pH 3.9 Blanc	5	557.7 ± 3.1	42 ± 3	NA
Chi:TPP 3:1. pH 4.7. MH 1mg/mL 80%	6	379.3 ± 48.8	37 ± 2	12.6 ± 3.1
Chi:TPP 3:1. pH 4.7. MH 1mg/mL 55%	7	402.1 ± 73.3	36 ± 3	15.5 ± 0.4
Chi:TPP 3:1. pH 4.7. MH 1mg/mL 30%	8	419.5 ± 47.2	36 ±1	7.5 ± 4.8
Chi:TPP 3:1. pH 4.7. MH 1mg/mL 5%	9	432.3 ± 40.6	36 ± 2	7.3 ± 9.1
Chi:TPP 3:1. pH 4.7. Blanc	10	303.3 ± 82.7	35 ± 1	NA
Chi:TPP 3:1. pH 4.7. MH 2mg/mL 80%	11	339.1 ± 16.5	34 ± 1	1.6 ± 1.9
Chi:TPP 3:1. pH 4.7. Blanc	12	341.3 ± 22.4	34 ± 1	NA
Chi:TPP 3:1. pH 5.5. MH 1mg/mL 80%	13	406.7 ± 83.6	25 ± 1	13.4 ± 0.9
Chi:TPP 3:1. pH 5.5. MH 1mg/mL 55%	14	495.4 ± 79.4	26 ± 2	20.2 ± 3.3
Chi:TPP 3:1. pH 5.5. MH 2mg/mL 80%	15	350.2 ± 65.6	27 ± 1	1.7 ± 2.5
Chi:TPP 3:1. pH 5.5. Blanc	16	394.3 ± 87.8	26 ± 1	NA
Chi:TPP 3:1. pH 5.5 + Tween 80 Blanc	17	394.2 ± 146.2	20 ± 1	NA
Chi:TPP 3:1. pH 5.5 + Tween 80. MH 1mg/mL 80%	18	410.6 ± 49.3	24 ± 2	24.5 ± 2.4
Chi:TPP 3:1. pH 5.5 + Tween 80. MH 1mg/mL 55%	19	434.5 ± 103.3	22 ± 1	27.8 ± 1.7
Chi:TPP 3:1. pH 5.5 + Tween 80. MH 2mg/mL 80%	20	302.1 ± 21.6	22 ± 1	10.8 ± 0.4
Chi:TPP 3:1. pH 5.5 + Tween 80. MH 2mg/mL 55%	21	372.4 ± 55.5	23 ± 1	19.2 ± 3.6

NA: not applicable. Blanc: with no drug; Chi: chitosan; MH: minocycline hydrochloride.

2) Evaluation of the effect of freeze drying on NPs properties

The scale up samples were tested again after the freeze-drying procedure, in order to evaluate the effect of the process itself in the average size and zeta potential of the NPs. A small amount of the freeze-dried sample was re-suspended with 1 mL of ultra-pure water and then tested. Results showed that the freeze-drying procedure caused an increase of size and zeta potential in all samples (blank and loaded with MH), however it was not significantly different ($P<0.05$) (Fig. 2). Two different volumes of scale up were tested with the same initial proportion, in order to be sure about the maintenance of the NPs characteristics with different amounts. No differences were observed between the 10 and the 20 times volume, so the last one were used to produce the NPs.

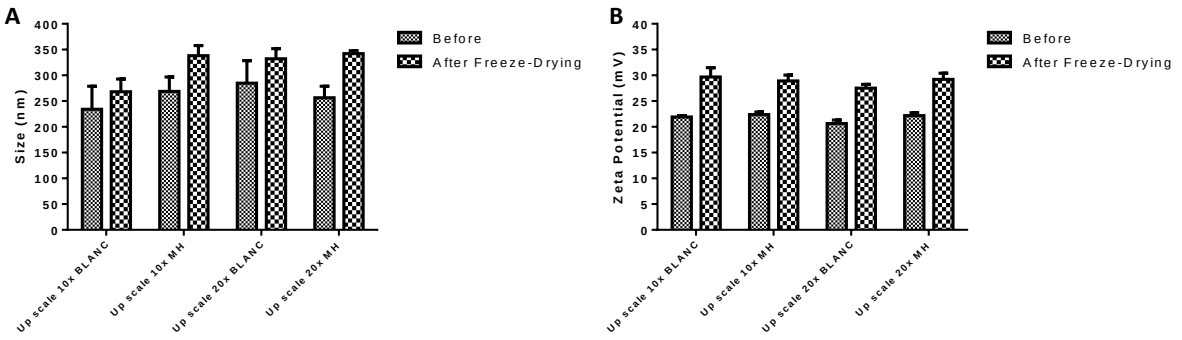

Figure 2. The effect of the freeze-drying procedure in A: size of the nanoparticles and B: zeta potential (n=3, average ±SD).